N°d'ordre NNT: 2020LYSEC49

THESE de DOCTORAT DE L'UNIVERSITE DE LYON
opérée au sein de
L'Ecole centrale de Lyon

Ecole Doctorale N°34
Ecole Doctorale Matériaux de Lyon

Spécialité/Discipline de doctorat: Matériaux

Soutenue publiquement le 18/12/2020, par:

Mingfa ZHANG

Composite patches for enhancing application on civil infrastructures

Devant le jury composé de :

Karim Benzarti,	Directeur de Recherche, Université Gustave Eiffel,	Rapporteur
Emmanuel Foltête,	Directeur de Recherche, ENSMM,	Rapporteur
Mohamed Ichchou,	Ecole Centrale de Lyon,	Examinateur
Laurence Curtil,	Université Claude Bernard Lyon 1,	Examinateur
Michelle Salvia,	Ecole Centrale de Lyon,	Directrice de thèse
Olivier Bareille,	Ecole Centrale de Lyon,	Co-directeur de thèse
Bruno Berthel,	Ecole Centrale de Lyon,	Co-directeur de thèse

Acknowledgement

At the very beginning, please let me give my deepest appreciation to every one of you, who has always been helping and supporting me during this Ph.D. study in France.

First of all, I would like to show my gratitude to Ph.D. jury members: Karim Benzarti, Emmanuel Foltête, Mohamed Ichchou, Laurence Curtil, Michelle Salvia, Olivier Bareille, Bruno Berthel who accept to report this manuscript, to examine this Ph.D. work and to participate in the jury.

I would like to express my sincerest gratefulness to my supervisors Michelle Salvia, Olivier Bareille, and Bruno Berthel, for their patience and motivation throughout this research project. I would also like to thank them for providing me this Ph.D. position in LTDS. Besides, discussion with them is always inspiring. I would also like to thank their care for my life in France since the first day I stepped on this gourmet land. Working with them, I am all gratitude.

I would like to thank Olivier Graton and Jean-Michel Vernet, who helped me and stayed with me through the last three years. Meanwhile, special thanks to Gaylord Guillonneau, who provided help for the mechanical test of composites; Bernard beaugiraud, who guided me in the operation of FTIR and SEM characterizations, as well as Dominique VINCENTELLI, who helped me a lot with the paper and reimbursement works.

I would like to thank professor Zhiqiang Su in Beijing University of Chemical and Technology, as well as professor Gang Wei in the College of Chemistry and Chemical Engineering, Qingdao University, for their care and guidance from the study and career aspects during the last years.

I would like to thank my beloved family. They are always behind my back and supporting me. During my study in Lyon, with my friends in France and China, we shared many unforgettable memories, stories and laughs, I love you all.

This work was financially supported by Chinese Scholarship Council (CSC). I am grateful.

I hope this paper will not be the end of academic thinking, and I hope the previous sentence is not just hoping.

Mingfa in écully,

November, 2020.

Heart is living in tomorrow;

Present is dejected here;

In a moment, passes sorrow;

That which passes will be dear.

Abstract

The civil infrastructure worldwide is extensive but often aged or damaged. Critical failures in those large infrastructures, beyond the risk of human-life losses, could also cause huge economic issues and, for sure, the loss of services. For those aged or damaged infrastructures, the complete demolition and reconstruction are not conceivable just because of the inherent waste of resources. Yet, in order to still guarantee a safe usage of these constructions, certain reinforcement strategies need to be adopted to extend the service life of damaged buildings, and to recover the requirements of bearing capacity for safe use. This would be undoubtedly a better deal. For that subject, fiber-reinforced thermosetting composites have received a lot of attention. They are usually bonded on the surface to protect the infrastructure from the inner stress and external erosion, and further to limit the micro-cracks growth.

As environmental problems worsen, as oil resources diminish, the advantages of environmentally friendly renewable resources become more prominent. The production and recycling process of natural fibers has less impact on the environment. What's more, due to photosynthesis, the cultivation of natural fibers can reduce the greenhouse effect by increasing the oxygen content and reducing the amount of carbon dioxide in the atmosphere. In this research, on the one hand, flax fiber was used as reinforcement. On the other hand, thermosetting bio-epoxy resin (CHS-EPOXY G-520), partly made from environmentally renewable resources, was adopted to fabricate the composites by hand lay-up method. Its curing mechanism was investigated via DSC measurements, whose results confirm that it is a typical dual-stage curing system with two different apparent activation energies.

The composite reinforcement system is attached to the surfaces of the unqualified infrastructures, whose service life span and enhancing efficiency partly depends on the environmental durability of composites as they might be exposed to harsh environments like extreme humidity or temperatures. To acknowledge this influence, the composite samples were undergone three kinds of accelerated ageing models: water immersion ageing, freeze-thaw cycles and wet-dry cycles. Both dynamic and quasi-static mechanical tests were adopted to testify the ageing degrees, and the AE and SEM have aided this analysis. It turns out that, water moisture content affects the composite the most, with a decrease of 37.5% in storage modulus (soaking for 7 months) and 40% in young's modulus (soaking for 24 weeks). For the

cyclic ageing tests, the shrinkage/swelling process destroys the effective bonding between fiber and resin, which further deteriorates the integrity of composites.

For infrastructure's strengthening, the composites enhancing system acts as a structural component, whose mechanical properties are directly in relation to the reinforcement and matrices type. And the moisture content is also a significant element to be taken into account due to the natural origin of the fibers. This aspect can imply specific sensitivity to damage or early ageing for the composites. Moreover, the external bonding reinforcement performance, or enhancing efficiency, mainly depends on whether the component interface can effectively transfer the stress. The bonding interface between composite reinforcement sheets and infrastructures is the weak link of the entire reinforced component, and the interfacial peeling is a brittle failure that occurs suddenly without obvious warning signs so far. Therefore, they must be tailored and monitored to ensure long-term structural performance. In this research, it was achieved through the application of an in-situ embedded piezoelectric sensor for continuous (in real-time) monitoring for the precise follow-up of the curing state as well as of their structural integrity (moisture ageing, damage extent).

At the last, the feasibility of the whole research thought, that composites serve as external enhancing support to the aged or damaged infrastructures, was testified by a single shear-lap test. The result indicates that the bonding interfacial is strong and sensitive enough to transfer the applied stress.

To obtain a comprehensive and profound acknowledgment about this research project, the curing mechanism of epoxy resin, the mechanical performance of flax fiber-reinforced epoxy resin composite (FFRC), the durability behaviors of FFRC, the curing and damage monitoring jobs, and the shear-lap test between FFRC and concrete were the exploration priorities.

Keywords: bio-sourced epoxy/flax fiber composite, curing kinetics, environment durability test, non-destructive monitoring, single shear-lap test

Résumé

L'infrastructure civile dans le monde est vaste mais souvent vieillie ou endommagée. Les défaillances critiques de ces grandes infrastructures, au-delà du risque de pertes en vies humaines, pourraient également entraîner d'énormes problèmes économiques et, bien sûr, la perte de services. Pour les infrastructures vieillies ou endommagées, la démolition et la reconstruction complètes ne sont pas envisageables uniquement en raison du gaspillage inhérent des ressources. Pourtant, afin de garantir toujours une utilisation sûre de ces constructions, certaines stratégies de renforcement doivent être adoptées pour prolonger la durée de vie des bâtiments endommagés, et pour récupérer les exigences de capacité portante et d'utilisation sûre. Ce serait sans aucun doute une meilleure affaire. Pour ce sujet, les composites thermodurcissables renforcés de fibres ont reçu beaucoup d'attention. Ils sont généralement collés en surface pour protéger l'infrastructure des contraintes internes et de l'érosion externe, et en outre pour limiter la croissance des micro-fissures.

À mesure que les problèmes environnementaux s'aggravent, à mesure que les ressources pétrolières diminuent, les avantages des ressources renouvelables respectueuses de l'environnement deviennent plus importants. Le processus de production et de recyclage des fibres naturelles a moins d'impact sur l'environnement. De plus, grâce à la photosynthèse, la culture de fibres naturelles peut réduire l'effet de serre en augmentant la teneur en oxygène et en réduisant la quantité de dioxyde de carbone dans l'atmosphère. Dans cette recherche, d'une part, la fibre de lin a été utilisée comme renfort. D'autre part, la résine bio-époxy thermodurcissable (CHS-EPOXY G-520), en partie fabriquée à partir de ressources renouvelables pour l'environnement, est adoptée pour fabriquer les composites à la main. Son mécanisme de durcissement a été étudié via des mesures DSC, dont les résultats confirment qu'il s'agit d'un système de durcissement à deux étages typique avec deux énergies d'activation apparentes différentes.

Le système de renforcement composite a été fixé aux surfaces des infrastructures non qualifiées, dont l'efficacité d'amélioration dépend en partie de la durabilité environnementale des composites, car ils pourraient être exposés à des environnements difficiles comme une humidité ou des températures extrêmes. Pour reconnaître cette influence, les échantillons composites ont été soumis à trois types de modèles de vieillissement accélérés : le vieillissement par immersion dans l'eau, les cycles de gel-dégel et les cycles humide-sec. Des

tests mécaniques dynamiques et quasi-statiques ont été adoptés pour témoigner des degrés de vieillissement, et l'AE et le SEM ont aidé à cette analyse. Il s'avère que la teneur en humidité de l'eau affecte le plus le composite, avec une diminution de 37,5% du module de stockage (trempage pendant 7 mois) et de 40% du module des jeunes (trempage pendant 24 semaines). Pour les tests de vieillissement cyclique, le processus de retrait / gonflement détruit la liaison efficace entre la fibre et la résine, ce qui détériore davantage l'intégrité des composites.

Pour le renforcement des infrastructures, le système d'enrichissement des composites agit comme un composant structurel dont les propriétés mécaniques sont directement liées au type de renfort et de matrices. Et la teneur en humidité est également un élément important à prendre en compte en raison de l'origine naturelle des fibres. Cet aspect peut impliquer une sensibilité spécifique aux dommages ou un vieillissement précoce pour les composites. De plus, l'effet de renforcement de la liaison externe, ou l'amélioration de l'efficacité, dépend principalement de la capacité de l'interface du composant à transférer efficacement la contrainte. L'interface de liaison entre la feuille de renforcement composite et l'infrastructure est le maillon faible de l'ensemble du composant renforcé, et le pelage interfacial est une rupture fragile qui se produit soudainement sans signes avant-coureurs évidents jusqu'à présent. Par conséquent, ils doivent être adaptés et surveillés pour garantir des performances structurelles à long terme. dans cette recherche, il a été réalisé grâce à l'application d'un capteur piézoélectrique embarqué in-situ pour une surveillance continue (en temps réel) pour le suivi précis de l'état de durcissement ainsi que de leur intégrité structurelle (vieillissement de l'humidité, étendue des dommages).

Enfin, la faisabilité de l'ensemble de la réflexion de recherche, que les composites servent de système de valorisation externe aux infrastructures vieillies ou endommagées, a été attestée par un seul essai de cisaillement. Le résultat indique que l'interface de liaison est suffisamment solide et sensible pour transférer la contrainte appliquée.

Pour obtenir une reconnaissance complète et profonde de cette recherche, du mécanisme de durcissement de la résine époxy, des performances mécaniques du composite de résine époxy renforcée de fibres de lin (FFRC), des comportements de durabilité du FFRC, des travaux de durcissement et de surveillance des dommages et du cisaillement Le test de recouvrement entre FFRC et le béton étaient les priorités d'exploration.

Mots clés: composite époxy / fibre de lin bio-sourcé, cinétique de durcissement, test de durabilité de l'environnement, contrôle non destructif, test de cisaillement unique.

Abbreviations

DSC	Differential scanning calorimetry
PLLA	Poly(l-lactide)
RTM	Resin transfer molding
FFRC	Flax fiber reinforced composite
PP	Polypropylene
CFRP	Carbon fibre reinforced polymer
GFRP	Glass fibre reinforced polymer
DMA	Dynamic mechanical analysis
TGA	Thermogravimetric analysis
TPS	Transient plane source
UT	Ultrasonic testing
AE	Acoustic emission
DCB	Double cantilever beam
IRT	Infra-Red Thermography
EMI	Electromechanical impedance
PZT	Piezoelectric sheet
Ea	Activation energy
3D	Three dimensional
Tg	α-relaxation associated to the glass transition temperature
β	Heating rates
Tp	Exothermic peak temperatures
F-T	Freeze-thaw cycles
W-D	Wet-dry cycles
SHM	Structural health monitoring

DIC	Digital Image Correlation
NDT	Non-destructive testing
SEM	Scanning electron microscope
RT	Room temperature
E′	Storage modulus
E′′	Loss modulus
tanδ	Loss factor
UD	Unidirectional
FSP	Fiber saturation point
ROI	Region of interest

Content

Chapter 1. General Introduction

1.1. Research background

During the last decades, there is a rapid demand for upgrading and repairing existing concrete structures. Due to the ageing and corrosion of infrastructures, the continuous deterioration of the world's civil concrete structures highlights the urgent requirement for low-cost, fast processing and effective repair technology that minimizes traffic interruption time [1,2]. Automotive infrastructure in France is extensive but often potentially aged. In particular, many French bridges have defects that need to be repaired in a more or less short term period to prevent the rapid development of structural disorders, and 7% of them have a risk of collapse in the short term. In some developing countries, the demand for replacement and reinforcement of concrete structures is soaring due to the substantial increase in traffic volume, exceeding the initial design limit [3]. The failure of materials involved in large infrastructure may cause a huge loss of life, economy or a loss of services. For those aged or potentially damaged infrastructures, the complete demolition and reconstruction will obviously cause a great waste of resources. On the contrary, by adopting certain reinforcement approaches to extend the service life of damaged structures and buildings, and to re-meet the requirements of bearing capacity and safe use, would be a better deal [4,5].

To solve this worldwide problem, high interest in scientific and industrial fields has been concentrated to explore the effective approaches to prevent the occurrence of infrastructure failure and increase their life-span [2,3,6]. Among these, an attractive solution is to use fiber-reinforced thermosetting composite reinforcement system (joints or patches) to strengthen the damaged structure and to extend their service life. Compared with other strengthening methods, this process of introducing polymers and advanced polymer composites into civil infrastructure is very rapid. In the past three decades, civil and structural engineers became more aware of the unique mechanical and use characteristics of these materials and their importance [1]. These patches are usually bonded on the surface to protect the infrastructure from inner stress and external erosion and to limit crack growth. They are mainly implemented using a wet lay-up process, which endows them with easy operation. Up now, the composites are mainly based on glass or carbon fibers and cold-curing epoxy resin made from fossil resources [2,3,6,7]. Their special manufacturing technology and extraordinary performance give designers greater confidence in the potential of the material, so it can be used more widely

to update civil infrastructure, including reinforced concrete, steel and cast iron, as well as bridges and columns Seismic retrofits for replacement bridge decks and new bridges and building structures.

As environmental problems worsen, as oil resources diminish, the advantages of environmentally friendly renewable resources become more prominent. The production and recycling process of natural fibers has little impact on the environment. Besides, due to photosynthesis, the cultivation of natural fibers can reduce the greenhouse effect by increasing the oxygen content in the atmosphere and reducing the amount of carbon dioxide in the atmosphere [8]. Compared to the traditional synthetic fibers, natural fibers present certain advantages as lightness, recyclability, abrasiveness with interesting specific properties and they are relatively cheap and abundant [9]. Therefore, high interests for civil engineering retrofitting applications are concentrated on environmentally friendly composites made from epoxy (thermosetting) resins derived from renewable resources and natural fiber as flax or hemp.

The composites patches act as a structural component, whose mechanical properties are directly in relation to reinforcement type but also to viscoelastic matrix properties and reinforcement/matrix interactions and thus are dependent on curing state or moisture content. During service, the patches may damage or age. Moreover, this external bonding reinforcement effect mainly depends on whether the component interface can effectively transfer stress [10,11]. Some researches indicated that the bonding interface between the composite reinforcement sheet and the infrastructure is the weak link of the entire reinforced component [12]. Interfacial peeling is a brittle failure that occurs suddenly without obvious warning signs. Therefore, the patches must be tailored to ensure long-term structural performance. This may be achieved through the use of an in-situ embedded sensor for continuously (in real-time) monitoring for precise observe of curing state of bonded patches and their structural integrity (moisture ageing, damage extent) and of self-healing constituent that will enable patch to slow down damage growth before catastrophic failure occurs.

Generally speaking, the reasons of infrastructure or composite failure are various, such as improper design or application of materials, improper processing or assembling of materials, poor service and maintenance conditions, correspondingly, the forms of damage mechanisms vary too [4,7]. As a result, the damage inspection (visual, conventional non-destructive inspection) of the cracks is often inconvenient or complex for composite materials. The crack

detectability is difficult for the hidden and random defects, and the assessment of the damage kinetics is not possible. Hence, there is a growing interest in utilizing multifunctional or "smart" materials or structures characterized by several functional properties: sensing function for health monitoring (curing level, stress exceed prescribed criteria, structural integrity), and actuator function for damage slowing or healing function [13-15].

In this paper, a novel piezoelectric intelligent composite made with bio epoxy and flax fibers was fabricated and bonded on the concrete for real-time fracture detection during the tensile test. The piezoelectric sheet not only performs the driving function but also performs the function of a sensor based on the electromechanical coupling effect. By comparing the coupling impedance spectrum measured under damage with no damage, the damage of the structure can be evaluated.

- Timeline about the whole research project

<table>
<tr><td>1-6 months</td><td>7-12 months</td><td>13-18 months</td><td>19-24 months</td><td>25-30 months</td><td>31-36 months</td></tr>
<tr><td colspan="2">Literature research</td><td></td><td></td><td></td><td></td></tr>
<tr><td></td><td colspan="2">The thermal analysis to the bio-epoxy resin</td><td></td><td></td><td></td></tr>
<tr><td></td><td colspan="3">Fabrication the composite, analyzing their mechanical properties</td><td></td><td></td></tr>
<tr><td></td><td></td><td colspan="4">The durability of the composite, as well as the corresponding characterizations</td></tr>
<tr><td></td><td></td><td colspan="3">Monitoring of the epoxy curing and the failure of composites</td><td></td></tr>
<tr><td></td><td></td><td></td><td colspan="3">Shear-lap test between composite and concrete matrix</td></tr>
<tr><td></td><td></td><td></td><td></td><td colspan="2">Writing the doctoral thesis</td></tr>
</table>

1.2. Flax fiber and its composite

1.2.1. Flax plants and the properties

Flax (Linum usitatissimum L.) is a member of the family Linaceae, which consists of 13 genera and 300 species. It is one of the ancient plants cultivating in temperate climate zones for its economic value, such as fibers and/or seeds. Currently, the main areas planting flax are concentrated in China, France, and Belarus [16,17]. In terms of botany, flax is an erect annual

plant with a height of 0.5-1.25m with a stem diameter of 16-32mm. Normally, the flax fiber is cut open when its outer stem turns yellow maturity, and this cutting period depends on both the sowing time and the growth cycle of the flax [18-20]. Besides, the influence of water content in the environment cannot be ignored as well, cause water deficit may inhibit the many crucial procedures for the growth, yield, and quality of the plants [20]. From the aspect of industry application, the major considerations associated with flax fibers from growing to harvesting are quantity and quality. Researches indicate that the highest quantity and quality harvest are gained obtained in drizzle weather with a moderate air temperature between 18 and 20℃ [21,22]. However, the phenomenon that the quality of flax fiber varies vastly according to the climate and weather needs to be valued. What's more, how to overcome the problem of meeting the industry requirement, and ensuring reliable supply at a competitive price is the priority.

The procedure of flax fibers extraction consists of two parts: retting and decortication, as shown in Figure 1.1. Retting means the process of extracting fibers from plants by microorganisms, which possess significant influence in enhancing the surface characteristics of fibers. The dry retting is one of the most commonly used methods, where the fibers are extracted from the plants by the frosts. Specifically, the mature plants are scattered and exposed in the open air for a fairly long time, during which they would be turned sides from time to time [23,24]. Subsequently, bacteria and fungi would grow on plants and degrade cell wall polysaccharides and interlayers, releasing fibers from the stem matrix. After that, the fibers are separated from the plant remains by the scotching process, and the chemical modifications could further complete this separation level and enhance the quality of fiber as well as its surface condition [25,26]. Besides the dry retting method, the dew or enzyme retting method is also applied to extract fibers from plants. This method obtains the plant stems by soaking plants in water or microbially treating by steam explosion [24,27,28]. After seed sacs harvesting and threshing, the stems are sprinkled on the ground for retting, which mainly by dew, rain, wind, and sunlight. Normally, dew retting is the process of the breakdown of the pectin compounds by micro-organisms, from the cambium layer to the phloem parenchyma. Decortication is a physical process that extracts fibers from flax straws, it is based on two techniques: (1) a hammer mill, which breaks straw by striking, and (2) a roller system, which involves crushing the straw. This process is also known as mechanical decortication which is applied to separate the coarse fibers out from the plant stems [28].

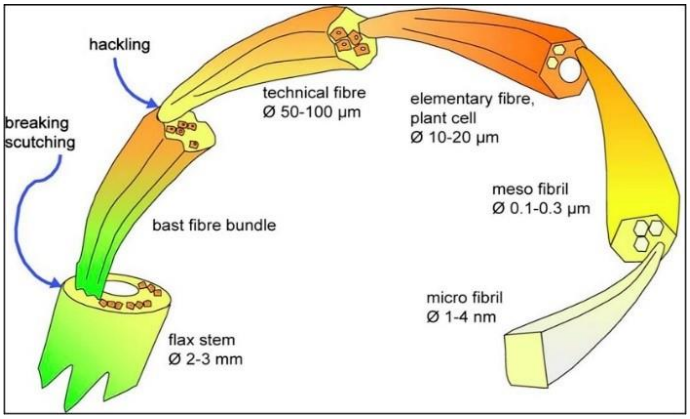

Figure 1.1 The structure of flax fiber (ref.28).

1.2.1.1. The structure and composition of flax fibers

Flax fiber is a typical original material for engineering fields, it consists of an abundance of ultimate or single-cell fibers bundled together. This kind of fiber possesses a wide range of application prospects for its excellent physic-chemical properties, mechanical properties, easy handling as well as its accessibility [29-34]. From the aspect of microstructure, flax fiber is mainly made of microfibrils of partially crystalline cellulose. It possesses an irregular polygonal cross-section and a hollow structure, and that is the reason that makes it crisp, strong, lightweight, stiff and easily wrinkled, as shown in Figure 1.2 [29,35]. As shown in Figure 1.2 (a, b), a non-constant transverse direction appears in the longitudinal view of fiber. The microstructure of flax fibers is very complex because of its nature of alloplast along the length and the influence of proportion variability in different flax parts. Figure 1.2c gives the optical images of the flax fiber cross-section part, more polygonal can be observed among individual fiber than circular cross-section. In addition, these bundles are gathered in the form of a central fiber surrounded by adjacent fibers. Each flax fiber has a typical hexagonal cross-section with a negligible lumen [36]. The cross-section image of the flax fiber is shown in Figure 1.2d. The sample slice comes from the base of the immature flaxseed variety and has been stained with toluidine blue. In this immature flax stem, the still-growing secondary xylem dominates the cross-sectional area.

From the outer to the inner, plant fiber consists of bark, phloem, xylem as well as central voids. 10-40 fibers can be observed in the cross-section part, which are bounded through pectin. The primary cell walls cover the secondary ones and bear the load-carrying capacity of the fiber as well as encloses the lumen. Flax fibers are composed of cellulose, hemi-cellulose, lignin, pectin, wax, etc. with varying proportions. The first three components are decisive because

they decide the basic mechanical strengths of one kind of flax. Among them, the cellulose is the major component, researches showed that cellulose represents between 65 and 75% of the total weight of flax fibers [35,37]. Besides, the cellulose is also the strongest and stiffest part of flax fibers. It possesses a semi-crystalline polysaccharide with abundant of hydroxyl groups, endowing the hydrophilic characteristic to fibers.

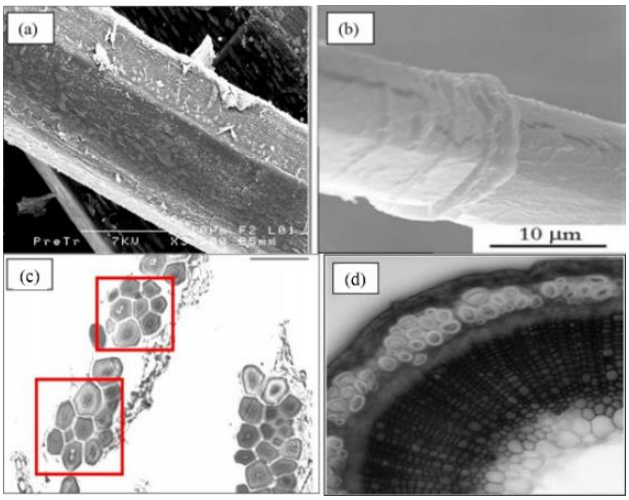

Figure 1.2 (a, b) Polygonal shape of flax fibres, (c) flax fibre cross-section and (d) stem cross-section (ref.29,36).

1.2.1.2. The Physico-chemical properties of flax fibers

Flax is a typical plant-based resource, which means its characteristics would vary with many factors, such as climatic conditions, soil quality, water supply [38]. As for the mechanical properties of flax fibers, they depend on the crystal structure, cellulose content, crystallinity, degree of polymerization, the angle of microfibers, porosity and size of lumens. Flax fiber strength decreases with the moisture uptake, and its stiffness decreases with increased water absorption in the fiber pores, which is due to the reduction of the cohesion of the fibrils. The tensile strength and modulus of elasticity would decrease as fiber diameter increases, and the inner cavity is responsible for moisture absorption [39,40]. Compared with synthesized fibers like glass fiber or carbon fiber, flax is a low density, cost-effective and biodegradable material but it does have competitive mechanical properties [38, 41].

Tensile performance

The tensile property of flax fibers is critical when used as reinforcements for polymer composites. Its deformation varies even if these fibers are planted in the same condition and are tested under the same parameters, which is affected by a series of comprehensive factors [24]. Generally speaking, fibers in the stem possess strong and stiffer tensile performance than

those at the mid-span or the tip. What's more, even though the flax fibers are extracted in the stem with different locations, their tensile strengths vary also, which is due to the fibers from different locations possess different chemical compositions and porosities [29]. The fluctuation in mechanical properties of flax fiber is its shortcoming compared with synthesized ones [42-44]. The specific properties comparison between flax, glass and carbon fiber is shown in table 1.1.

Table 1.1 the properties comparison between flax, glass and carbon fiber [42-44].

Fiber source (or type)	Density (g/cm^3)	Tensile strength (σ/MPa)	Tensile modulus (*E*/GPa)	Specific modulus (Approx.)	Elongation (%)
Flax	1.53	745–1145	44–61	35	2.07
E-glass	2.5–2.6	2000–3500	70–76	29	1.8–4.8
S-glass	2.5	4570	86	34	2.8
Carbon fiber	1.8	4330	231	129	1.8

Previous researches have explored the methods for the tensile test of flax fibers. Stuart *et al.* performed tensile testing of the flax fibers and their composite specimens by using an Instron universal testing machine model 1195 at a cross-head speed of 1 mm/min. The parameter of strain was measured by an attached extensometer on the specimen. To eliminate the errors, at least 10 replicates were tested for each type of sample [45]. Similar experiments were also conducted by Baley *et al*., they fixed the fiber specimens in a testing machine equipped with a 2N capacity sensor and load at a constant crosshead speed of 1 cross mm/min until it breaks [46]. This test has been carried out with NFT 25-704 standards. The length of the flax fiber is 150mm and handled in a manner to avoid any change in a twist. Similarly, this test was also repeated for 10 times and the average values were recorded.

The fiber-loaded in the testing setup is presented in Figure 1.3a and the failure of fiber breakage is shown in Figure 1.3b [47]. From those pictures, it can be observed that the tensile result of flax fiber is a combination of fiber slippage and breakage. The typical stress-strain curve of flax fiber tensile test is as shown in Figure 1.3c [48], it can be observed that this response curve has a clear 3-stage changing trend. The first stage corresponds to the change range of strain value from 0 to 0.3%, in this part, the deformation and the load of the fiber are

linearly correlated. The second stage is the strain ranged from 0.3% to 0.8%, this is a non-linear behavior that is interpreted as elastic-visco-plastic deformation, due to the alignment of the cellulose microfibers with the tensile axis resulted in an amorphous rearrangement. The part where the strain value is over 0.8% is the third stage, part of the wall is eventually cracked, which further lead to the elastic response of the aligned microfibers to the applied tensile strain. From the previous tests, it is can be found out that the tensile strength of the elementary fiber is about 1500MPa and the value of matured fiber is about 800Mpa [49]. The modulus of flax fibers is related to the diameter of flax fiber, whose value ranges from 39 to 78GPa with fibers diameter of 35–45μm [50].

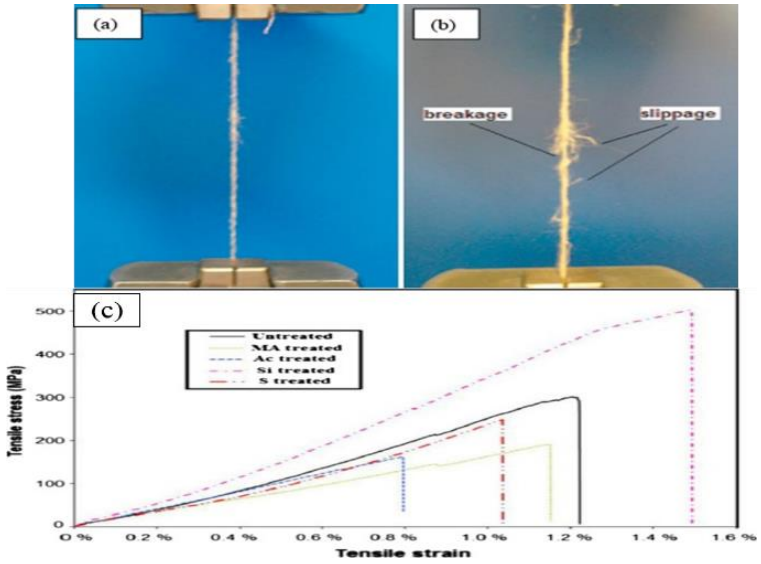

Figure 1.3 (a) tensile testing of flax fibre before loading and (b) after fracture, (c) typical tensile stress vs. strain plots of flax fibres (ref. 47, 48).

Moisture uptake

When considering the usage of plant fibers for construction reinforcement, the presence of absorbed water is often invoked. Most manufacturing processes of composite contain high-temperature steps, and the water content absorbed inside the fibers will evaporate eventually with the increasing temperature and exposure time. Therefore, serious consequences could be posed on the fiber/matrix bonding interface. At the same time, removing the moisture from flax fibers before manufacturing by increasing the storage temperature would cause their tensile strength to decrease [51]. Studies have shown that the strength of plant fibers increases with increasing moisture content and decreases with increasing temperature. On the other hand, the effect of moisture on plant fiber properties indicates that increasing moisture does not change the strength of the crystal region [52]. From a micro perspective, the cellulose

molecules of flax fibers contain a large number of hydroxyl groups that can form water molecules. Water molecules are directly absorbed onto these hydrophilic groups and fixed on the fiber structures. As more water molecules are absorbed, they may be attracted to other hydrophilic groups and further form more absorbing layers. Therefore, from a macro perspective, the hygroscopicity of flax fibers is initially linearly related to Fick's diffusion and then slows as the moisture content approaches its equilibrium [53]. According to previous experiences, at a relative humidity of 90% at room temperature, flax fibers can absorb more than 10% of moisture in less than an hour.

Thermal degradation and differential scanning calorimetry

A thorough understanding of the influence of processing temperature in relation to processing time is very important because there are always thermal stresses in the manufacture of natural fiber-reinforced materials. Wielage *et al.* conducted a series of experiments on the thermal stability of the natural fibers [54]. In their research, the degradation of the flax samples was observed by means of a thermogravimetric analysis (TGA) using a Perkin Elmer model TGA 7 with helium (flow rate 30 ml/min) and with air (flow rate 20 ml/min). Meanwhile, a differential scanning calorimetry (DSC) was applied for determining the enthalpies. A flow rate of 20 ml/min N_2 was realized. The sample was encapsulated in an aluminum pan (volume 30µl) with one hole in the top. They found that making use of air, the mass of natural fibers decreases slightly between 200 ℃ and 220 ℃, above this temperature irreversible degradation of the fibers would occur. Some other experiments pointed out that the thermal degradation of flax fibers is not having any effect for the first few minutes and at lower temperatures. It is proved that the raw flax fiber retains its actual strength after exposure at 170 ℃ for 120min, whereas at 210 ℃ the strength decreases almost by 50% in the same time interval. It is proved that flax fiber retains its original strength when stored in a convection oven at around 200 °C for half an hour [55,56].

1.2.2. Flax fiber reinforced composites (FFRCs)

The definition of a composite is the proper combination of two or more materials with unique properties then making a new material, whose characteristics are different from those conventional materials. In those years, environmental pressure has forced us to reevaluate those issues regarding bio-degradation, energy consumption, and the corresponding impact on the environment. The composite materials we currently use are made from conventional fibers and synthetic polymers, which are derivatives of petroleum, an unsustainable fossil fuel.

These are not easily degraded, so they cause serious problems during the disposal process at the end of their useful life and cannot be recycled or reused. On the contrary, biodegradable fibers reinforced with bio-based matrix materials have attracted extensive attention from researchers in recent years because of their availability, environmentally-neutral carbon neutrality, applicability to available processing machines, and good mechanical properties.

1.2.2.1 Processing of FFRCs

Compression molding

Generally, this process is very suitable for producing large parts, and the cost is lower than that of other methods. A conventional compression molding process can be performed either cold or hot, and a thermosetting matrix with sheets or block molding compound can be used. It consists of the usage of a thermoplastic matrix with glass mat thermoplastic as the molding compound. Cold compression molding uses only pressure due to the curing process takes place at room temperature, while hot molding involves the application of pressure and temperature (for curing and densification). Alternative stacking fibers are used between polymer matrix sheets, and careful control of viscosity is also necessary to achieve good adhesion and impregnation between the fibers and the matrix, especially for those thicker parts [57]. Meanwhile, it is also important to ensure that the fiber does not break or degrade under the excessive heat and pressure during hot compression molding. Therefore, with the temperature and pressure of the compression molding, there would always be a compromise between fiber degradation and good adhesion/wetting with the matrix, depending on the type of matrix and natural fibers used. In addition, part deformation is the main disadvantage of this process. A unique advantage of this process is that the fiber loading in the composite can reach up to 90% [58]. Zhang *et al*. conducted a series of experiments to study the mechanical behaviors of unidirectional flax and glass fiber reinforced hybrid composites and to investigate the hybrid effects of the composites made by natural and synthetic fibers by compression molding method [59]. In their research, the curing temperature is 140 ℃ for 1 hour to 100% cure the resin, and the curing pressure is maintained at 1.8MPa to minimize voids in the composite material.

Injection molding

In the injection molding process, natural fibers are usually cut into small pieces according to the critical fiber length. In this case, the applied stress will be effectively transferred from the matrix to the fiber, and the fiber can be fully loaded assuming that good interfacial adhesion

is achieved. Compared with other forming technologies, this method can produce relatively complex parts in large quantities. On the other hand, this method has its shortcomings as well. Due to the composition of flax fiber, the molding temperature requirement is usually below 200 ℃, which will bring about the problem of the fluidity of the polymer matrix, while providing short cycle time, low energy consumption, and damage/wear of the mold and screws. What's more, due to the hygroscopic nature of flax fibers, they would be dried before being fed to the machine. The matrices are heated, mixed, and then transported to the die using an extruder. Generally, during this mixing stage, natural fibers are damaged due to friction (between fibers, fiber matrix, fiber extruder). Then, the molten material is injected into the preheated mold to form a composite part. Maintain the pressure in the mold until the part solidifies and cools. Le Duigou *et al.* performed experiments to evaluate the capacity of flax/PLLA (poly(l-lactide)) biocomposite to be recycled. In their design, the polymer was dried under vacuum at 60 ℃ for 48 hours before extrusion. They were then extruded with flax fibers of different fiber content (20% and 30% by weight). The mixing was completed in a single screw extruder at 20 rpm and the nozzle temperature was around 180 ℃. The mixed pellets were also dried under vacuum at 60 ℃ for 48 hours [60].

Pultrusion

Pultrusion is a continuous process for the manufacture of spendere materials with constant cross-section, combining "pull" and "extrusion". This process is mainly used in some specific fields of composite material manufacturers for the purpose of producing long and uniform cross-section parts. Compared with other manufacturing processes, it possesses the possibility of continuous processing of composite materials. This method is specifically developed for thermosetting substrates. In recent years, thermoplastic substrates have shown rapid growth. From the aspect of applications, products fabricated by this method have many advantages, such as good chemical resistance, excellent recyclability and their post-forming ability, which can meet the requirements of the extrusion profile performance required by the construction industry at a lower cost. However, as the dilemma met in the injection molding, the reasonable temperature that flax fibers can bear limits the fluidity of the polymer matrix. On the contrary, the excessive pultrusion temperature may cause fiber damage, air entrapment. Besides, the bonding interface would be another barrier to hinder [61].

Resin transfer molding (RTM)

The RTM process is a closed mold forming technology improved by the hand lay-up process. Its basic principle is to place fibers and other reinforcing materials in the closed mold cavity, then use pressure to inject the resin glue into the mold cavity to penetrate the reinforced material, then cured and released from the molded product. This technology eliminates the need for prepreg and autoclave, which can effectively reduce equipment and molding costs. This method can produce composite products with high volume fraction and high strength to weight ratio. Fiber preforms are usually in the form of fabrics and mats. Generally, there is no limit to the size of composite materials with RTM and vacuum infusion process, which is very important for real-time industrial applications. In recent years, this technology has developed rapidly, and it has been widely used in the aircraft industry, automobile industry, shipbuilding industry and other fields [61].

Hand lay-up method

The hand lay-up method, also known as the manual pasting molding, is one of the molding processes for producing reinforced composite products. It is a classical labor-intensive manufacturing process that is easy to handle and cost-effective, and has been used to strengthen the engineering infrastructures by fiber-reinforced composite materials. This method is to apply resins to the mold coated with the release agent by hand while laying the reinforcing material until the required thickness is reached, and then obtain the product by curing and demolding. The synthetic resins used in hand lay-up molding are mainly epoxy resins and unsaturated polyester resins. A. Muralidhar *et al.* investigated the thermal, mechanical and thermomechanical properties of flax hybrid preform reinforced epoxy composites fabricated by hand lay-up method [62]. In their research, the fibers were cut to a size of 250 × 250 mm and stacked in sequence. Laminates were made using pressboards with fiber volume fractions of 23% and 34%. The epoxy resin used to impregnate the fiber is maintained until the complete impregnation of fabrics. Then the laminate is cured in a hot plate press at 50 ℃ and 3 bar for 2 hours.

1.2.2.2 Properties of FFRCs

The pressure of environmental problems and resources diminish has once again drawn our attention to renewable resources. Many scientists and engineers have been working on this issue for decades. However, the possibility of substitution from synthesis to natural resources depends on the mechanical properties of the latter. This pressure is not big enough to sacrifice

the properties of the products. Under no circumstances could it be done, because it is irresponsible.

Mechanical properties

A single polymer is difficult to meet the required properties in the modern industry. In order to improve the mechanical properties of the products, adding reinforcement is necessary in some cases. In general, the mechanical properties of composites mainly depend on the type of reinforcements as well as their distribution in matrices, the type of matrices and the interface quality. It seems that for plant fibers, the highest mechanical strength can be obtained along with the fiber orientation, and the fibers should be placed as straight as possible [45,60]. Some research indicates that the mechanical properties of the composites reinforced by plant fibers are comparable to those who reinforced by synthesized ones [38, 63].

Tensile test

The tensile test fixes the composite sample in the processing device, Instron machine, and then applies it to the force until it fails, the force is recorded as a function of the increase in gauge length [47,57]. The main contradiction here for composite samples is to obtain high tensile strength while also maintaining low-performance variability and relatively low cost. Generally speaking, the cross-head speed of the tensile test is 1-5 mm/min, the device is equipped with a 5-25 kN load cell to determine the specific experimental requirements.

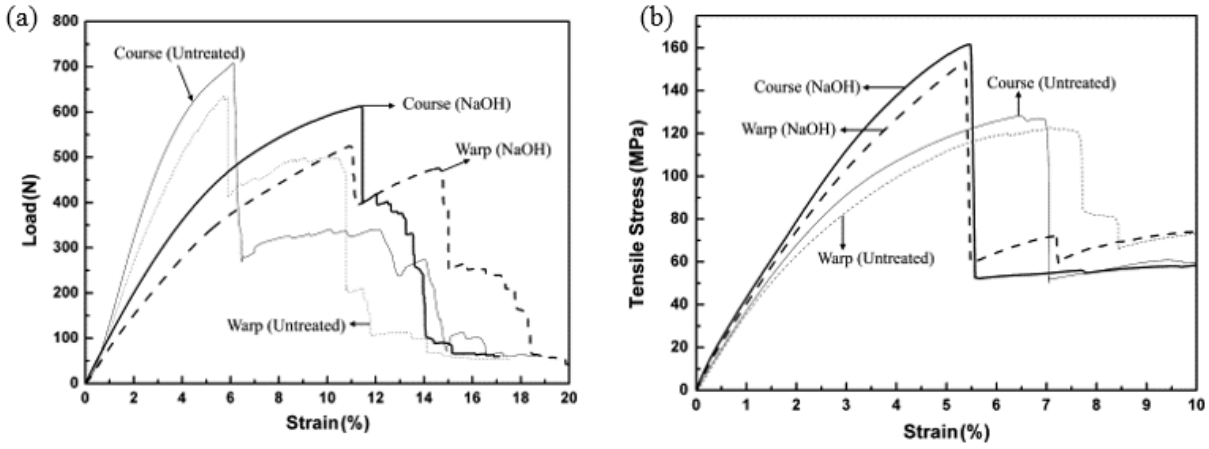

Figure 1.4 Typical (a) load vs. strain and (b) stress vs. strain curves of FFRCs (ref. 57).

Typical tensile stress versus strain curves are given (Figure 1.4). It can be seen from the figure that the nonlinear behavior of the first stage originates from the starting point to the maximum load point of the sample, where the fiber begins to break down. The shape of the curve is concave, which is the opposite of the fiber. The second stage is from the maximum load point

to the total fiber breakage. At this stage, a sharp drop in tensile strength is observed, because only the yarn is under tensile load. Many research indicates that chemical treatment may cause the tensile strength to decrease. The treatment of the fibers has a very significant positive effect on the tensile properties of the composite, and it is observed that the effects on the tensile properties after the treatment are almost the same. However, the increase in tensile strength is much greater than the increase in modulus.

Fatigue

Fatigue failure is a common phenomenon where a composite sample fails under cyclic loading. Even if the stress applied to the material is much lower than its static strength, this type of structural damage may occur. Especially, fatigue is one of the most common causes of mechanical structure failure of composite materials. The process of fatigue failure under repeated loads can be divided into three stages: (1) The material damage continues to develop at the micro-level until the formation of macro cracks under the action of multiple cycles. (2) In each cycle, the macro crack will continue to grow until it reaches a critical degree. (3) When a cracked component can no longer withstand peak loads, it will break [62]. Under the action of non-constant external stress, the state of the material will also change with time. The state of the material can be described by many corresponding variables (such as stress, strain, or energy dissipation). Usually, different cycles have different amplitudes. However, in the experimental research process, the variables that we can control the fatigue state have the same value at the beginning and end of each load cycle. Liang *et al*. investigated the properties evolution of flax/epoxy composites under fatigue loading [64]. The composites with different stacking sequences of $[0]_{12}$, $[90]_{12}$, $[0/90]_{3S}$ and $[\pm45]_{3S}$ were fabricated by hand lay-up method, and the probabilized Stress–Number of cycles curves have been determined for each laminate type. The tension–tension fatigue tests were conducted under load amplitude control mode on a servo-hydraulic MTS 809 machine with a capability of 100 kN, with a Servathin thermal chamber maintaining a constant temperature of 23 ℃. Tests were stopped at failure or after 2×106 cycles, whichever came first. Their research showed that the fatigue modulus exhibited a loss of 10–55%, depending on the loading level and the staking sequence. By the way, the damage (residual strain and fatigue modulus) correlated well with the crack density evolution for $[\pm45]_{3S}$ and $[0/90]_{3S}$.

Impact properties

The ability of absorbing energy during sudden stress is defined as the impact properties of materials. As for the FFRCs, the impact strength is related to the toughness, and fibers play a major role in the impact resistance of the material because they interact with cracks in the matrix and act as a transmission medium. The failure modes are strongly dependent on the fiber type, resin type, lay-up, thickness, loading velocity and projectile type. Bar *et al*. conducted some experiments concerning low-velocity impact response of flax/polypropylene (PP) hybrid roving based woven fabric composites [65]. They fabricated the laminates using thermally-bonded roving based woven fabrics and glass/PP sheets, and then tested for low-velocity impact properties. The typical drop-weight impact testing machine was applied at an impact velocity of 4.5 m/s with an impactor of 20 kg. The displacement sensor measures the displacement of the striker during loading, and the load cell measures the forced overtime. The impact test results revealed that the proportionate loss in flexural strength due to impact thrust is larger in the case of glass/PP composites than all flax-PP composites.

Interfacial shear strength

Interfacial shear stress refers to the stress caused by the sliding of the material patch between the interface layers, defined as the shear force divided by the shear area, which is a commonly used parameter characterizing the adhesion between the joints. As for the FFRCs, the value of interface shear strength reflects the load transfer efficiency between the fiber and the matrices, and it plays an important role in determining the mechanical properties as well as the applications of the composite material. Andersons *et al*. developed an indirect industry-friendly method for identification of the apparent interfacial shear strength of flax/starch acetate composites [66]. The tensile specimens were tested according to the ISO 527 standard on an Instron 4505 universal tensile tester with a 10kN load cell and a crosshead speed of 5 mm/min. The sliding gauge ($\pm$0.01mm) was used to measure the cross-sectional dimension of the gauge area, and Young's modulus was applied to evaluate as the slope of the experimental stress-strain diagram in the 0.1-0.3% strain range. Through the improved Bowyer and Bader technology, it was found that the apparent interfacial shear strength depends on the fiber load in the composite and decreases with increasing plasticizer content in the matrix.

Thermal properties

The thermal-physical properties of FFRCs are very important for both the processing part and applications. In the fabrication part, the influence of temperature on the FFRCs has been

discussed. High temperature treatment process is necessary for either eliminating the moisture content of flax fibers or increasing the flowability of the matrices. The resulting problems of thermal basic properties, heat transferability and heat resistance are discussed as followed.

Dynamic mechanical analysis (DMA)

The polymer matrix of the FFRCs is a typical viscoelastic material, whose mechanical behavior exhibits both solid and liquid performance. DMA is the most popular method for characterizing viscoelasticity, it measures the deformation of the material through sinusoidal or other periodic stress. The DMA results of the FFRCs depend on the type of fibers and matrices, the orientation and content of the fibers, as well as the quality of interfacial bonding. DMA is essential for establishing various temperature-related mechanical parameters of the materials. From the DMA test, two important parameters storage modulus and loss modulus. The storage modulus, or Young's modulus, is the real part of the complex modulus, it represents the springback of composites after deformation and indicates the material's ability to store elastic deformation energy. Loss modulus, also known as viscous modulus, refers to the amount of energy lost due to viscous deformation (irreversible) when the material is deformed, reflecting the viscosity of the material. It is the imaginary part of the complex modulus. The smaller the loss modulus, the smaller the damping loss factor of the material, and the closer the material is to the ideal elastic material [61]. Manral *et al*. investigated the dynamic mechanical properties of bio-composite with hybrid reinforcement of flax and jute by DMA test [67]. The DMA tests were performed on Anton Paar Rheometer (MCR-102), at cyclic frequency of 1Hz. Twisting load is applied on specimens with varying temperature range of 30-100 ℃. The experimental results showed that, compared with the developed hybrid composites, the non-hybrid composite flax/ polylactique has a higher glass transition temperature, storage modulus value and loss modulus value.

Thermogravimetric analysis

TGA refers to a thermal analysis technique that measures the relationship between the mass of a sample to be measured and temperature changes under programmed control. It can be used to study the thermal stability and composition of materials and can provide physical phenomena information, such as secondary phase transitions, including evaporation, sublimation, adsorption, and desorption. Similarly, it can also provide information about chemical phenomena, including chemical adsorption, decomposition, and solid-gas phase reactions, etc. Matykiewicz *et al*. conducted research on the impact of flax fibers as an internal

layer on the properties of basalt-epoxy composites modified with silanized basalt powder [68]. In their experiments, Netzsch equipment was used to evaluate the thermogravimetric properties of the composite in nitrogen and air, with a temperature range of 30 ℃ to 900 ℃ and a heating rate of 10 ℃/min. Approximately 10mg of sample was placed in a ceramic pot. The results showed that these composite materials can be recovered as ash during the combustion process without synthetic residues, such as glass fibers.

Thermal conductivity

Thermal conductivity is a measure of the thermal conductivity of a substance. It refers to a 1m thick material under stable heat transfer conditions. The temperature difference between the two sides of the surface is 1 degree. The heat transferred through 1 square meter in 1 second, the unit is watts per meter-kelvin. In addition, the thermal conductivity is for homogeneous materials. For composite materials, there are also porous, multilayer, multi-structure, anisotropic, etc. The thermal conductivity obtained by these materials is actually a comprehensive thermal conductivity performance is also called average thermal conductivity. Usually, the material with lower thermal conductivity is called insulation material. EI Hajj *et al.* measured the thermal conductivity of flax/PP composite by transient plane source (TPS) technique, which has proven to be a precise and convenient method for measuring the thermal transport properties of composites [69]. Firstly, the composite samples were placed in a drying cabinet at 50 ±2 ℃ until the weight loss does not exceed 1% within 24 days. Then, the samples were then polished until the surface is smooth to maintain proper contact between the TPS sensor and the sample. The experimental set-up is shown in Figure 1.5.

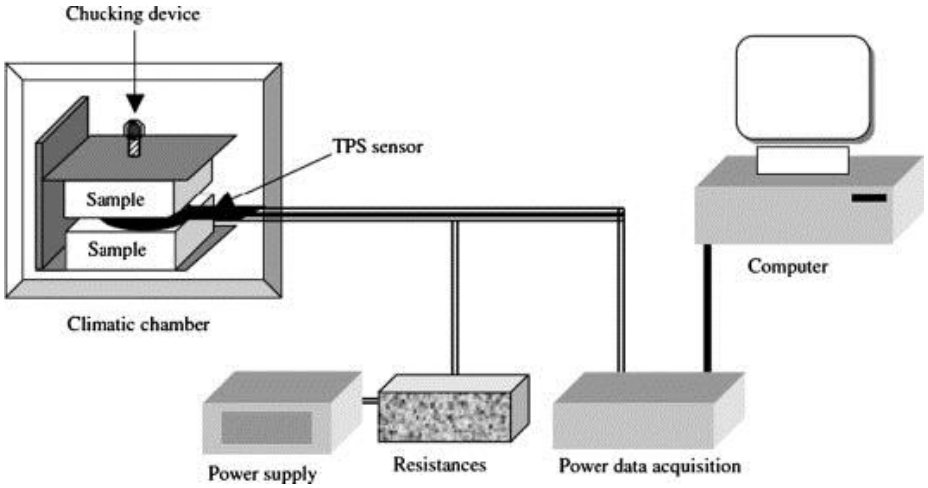

Figure 1.5 Experimental TPS-setup (ref.69).

1.2.3. Challenges in the field of FFRCs

Flax fiber is less harmful to the environment, which also ensures that the market potential of FFRCs increases. Nevertheless, challenges have always been with them, some problems still need to be solved. In the first place, the incompatibility between the hydrophobic matrix and the hydrophilic natural fibers is one of the biggest challenges to be overcome, it would lead to an unsatisfied stress transfer situation. Besides, flax fibers are hydrophilic, which means the durability, especially water content, of FFRCs is weak than the composites reinforced by synthesized fibers.

1.2.3.1 Interface between flax fiber and matrix

The final performance of the FFRCs is affected by factors such as fiber type, matrix selection, interface strength, fiber dispersion, fiber orientation, porosity, etc. Among which, the fiber type, matrix selection and fiber orientation are subjective factors, the porosity is a subjective controllable face, which determined by the manufacturing process. From an operational point of view, the formation of porosity is a known problem that occurs when poor impregnation occurs during composite processing. The interface strength is a non-subjective controllable factor. It is essential for transferring the load between flax fibers and matrices, which can be achieved by mechanical interlocking, electrostatic, chemical and inter-diffusion bonding. About the FFRCs, fibers act as the main load-bearing body, and the matrices serve as the load carrier between different fibers. In theory, the ultimate strength of FFRCs depends on the tensile strength at which the basic fiber breaks. However, limited by the interfacial bonding situation, the availability of fibers to the matrix is also a decisive factor. Therefore, cleaner, finer fibers with larger specific surface areas are more likely to bond the matrix, thereby increasing the strength of the composite.

Foulk *et al*. conducted a series of experiments of flax fiber modifications by enzyme-retting to investigate their effect on the interfacial bonding and composite performance [70]. They adopted four different degrees of gelation: no gelation (0h), minimum gelation (10h), moderate gelation (22h) and complete gelation (46h) to extract flax fiber bundles mechanically through bacterial pectate lyase at pH 8.5 and 42 ℃. Vinyl ester resins were used as matrix, and pull-out tests and interlayer shear strength tests were performed to test the interface strength between the fiber and the matrix. It was observed that the enzyme exposure time of 10h did lead to an increase in the interface strength, and when the enzyme exposure time added, the interface strength decreased. The researches assumed that the increase in the

interfacial adhesion strength was caused by the removal of impurities and wax on the fiber surface, but for a longer processing time, enzymatic treatment might affect the integrity of technical fibers through defibrillation.

1.2.3.2 Environmental impact

Flax fiber has gained increasing attention due to its environmentally friendly features. Intuitively, the production of flax fiber and its derivatives that do not require high-energy spinning operations is the key to reducing energy consumption [71]. However, the fact that processing requirements of FFRCs would consume even more energy makes their environmentally friendly properties are still questionable. Diener *et al*. used the life cycle assessment to comparatively study the flax fiber and glass fiber reinforced composite mats [72]. The main impact categories were global warming, soil acidification, eutrophication, ozone precursors, toxic air, toxic water, and non-renewable energy. Linen-reinforced panels score higher under all environmental conditions. This comparison reflects the fact that the production of flax fiber mats requires 80% less energy than glass fiber mats. However, the total energy savings of the entire assembly is smaller, because the overall environmental impact is mainly caused by resin input.

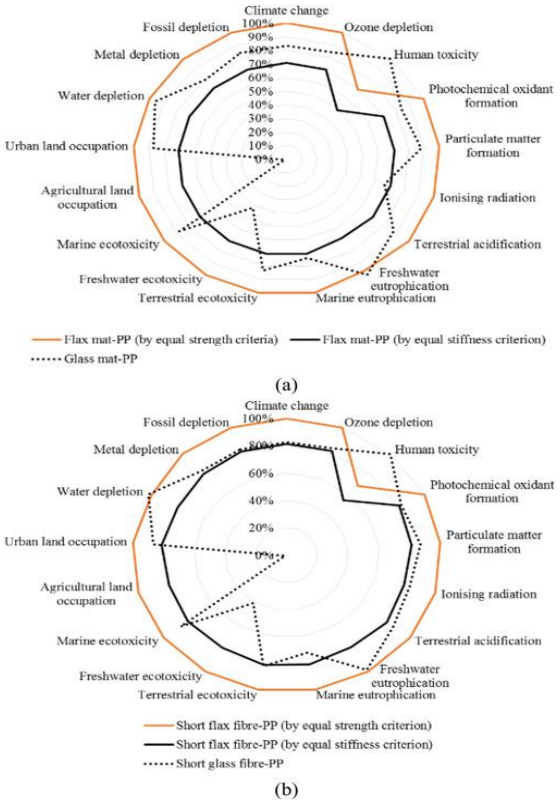

Figure 1.6 Life cycle impact comparison between FFRCs and glass fibre reinforced polymer (GFRPs) to equal stiffness and equal strength design criteria: (a) Flax mat-PP; (b) short flax-PP (ref. 73).

Guo *et al*. combined the Generalized Hybrid Rule model, the Ashby method, and applied the Life Cycle Assessment method to characterize the feasibility of FFRCs for automotive applications [73], as shown in Figure 1.6. The results showed that in most impact categories, the life cycle impact of flax-PP is lower than that of glass fiber with equal hardness standards. The advantage is the lower fuel consumption during usage, which can be attributed to the lightweight structure of the flax-PP under the same functional rigidity conditions. Nevertheless, the nutrients in fertilizers produce toxic pesticide compounds for marine and freshwater ecology. In addition, from the perspective of sustainable application of cultivated land, compared with the equivalent glass-PP composite material, flax-PP composite material has a much greater impact on agricultural land.

The environmental impact of FFCRs, as we discuss above, is a phenomenon that cannot be ignored when it comes to the advantages of natural or bio-based materials. Conversely, the impact on the FFRCs from the environment is also a non-negligible issue. Flax fiber is hydrophilic, which means its durability is more susceptible to environmental influence. FFRCs must withstand the combined effects of mechanical stress and the external environment. The external environment includes a series of factors that change with the rotation of the seasons, such as temperature changes (from high temperature in summer to negative temperature in winter), sunlight exposure, and corrosion caused by contact with alkaline solutions and so on.

Hallonet *et al*. investigated the durability and tensile performance of FFRCs for external strengthening application [74]. Composite materials of different weights of epoxy matrix and flax fabrics, and two-way glass fabric reinforced composite materials for control samples were prepared by hand lay-up method. About the ageing method, they adopted the accelerated ageing in the climatic chamber to reproduce as closely as possible the natural environment that the material will experience during its service life. The ageing cycle was 4 hours, including exposure to artificial rain for 30 minutes, cold exposure for 1 hour, exposure to heat and humidity for 1 hour, and exposure to dry heat and actinic radiation for 1 hour and 20 minutes. The ageing experiment results showed that the modulus value of the FFRCs was reduced by 50%, and the modulus value of the FFRCs was reduced by 20%. Observation of the internal structure by X-ray tomography showed that the flax/matrix interface was significantly degraded and cracks appeared, which may be due to the swelling of the flax fiber in water. A similar experiment concerning durability and mechanical performance of FFRCs was also conducted by Moudood *et al* [75]. They observed that the mechanical properties of

flax/bio-epoxy composites were significantly reduced due to water ageing compared to the "as manufactured" composites. Besides, the tensile strength and modulus of water aged (immersed in water until saturated) samples were also reduced by about 9% and 57%, respectively. In contrast, in the case of humidity-saturated (exposure to a humid environment until saturation) samples, the reduction rates were 0.8% and 3%, respectively. In addition, water exerts a more severe impact on the bending properties of the composites, with a value reduced by 64% and 70%, compared with the as manufactured samples. However, it was found that the mechanical properties partially restored after drying the water-aged composites. Warm and humid environments and freeze-thaw cycles have little effect on the composites.

Lu *et al*. tried to use non-drying flax fiber and polyester resin with low moisture sensitivity in the production of composite materials [76]. The basic hypothesis of this experiment is that since the fiber already contains some moisture and is therefore pre-swelled, the shrinkage and swelling of the compound due to moisture absorption can be restricted, slowing its degradation and thus improving its moisture resistance. They produced non-dried fibers by storing flax fibers in a conditioning room at 80% relative humidity until equilibrium was reached. Their results indicated that the composite material made of non-dry fiber has much lower moisture absorption and desorption performance, as well as the degree of swelling and shrinkage compared with the composite made of dry fiber. After the dry-wet cycle, the longitudinal and transverse bending properties of the composite material made of non-dry fibers are higher than the composite material made of dry fibers.

1.3. Overview of the composite reinforcement system

The composite patch is a rapidly developing emerging technology, which was initially studied as early as the 1970s by the Royal Australian Air Force [77]. They attempted the development and application of composite patches to repair aircraft parts, such as pillars, skins, and spars. Since then, various military and civilian aircraft manufacturers have been developing composite patch technology. Besides, composite repair technology is also used in other fields, such as shipbuilding and marine engineering maintenance, civil engineering structures and metal structures, etc.

The main purpose of composite reinforcement system repairing is to transfer the applied load from one side of the damaged structure to the other, bypassing the disordered area, thereby avoiding the expansion of the defect, as shown in Figure 1.7. Traditionally, such damage has been repaired by mechanical connections with pins or screws. However, these repairs result

in the formation of stress concentration around the fasteners (pins, screws), which further leads to other structural problems, such as reduced fatigue life. In theory, the type of strengthening materials, the thickness and local geometry of the composite patches and the damaged structure, the smoothness of the surface, and environmental factors all affect the reinforcement effect. The core issue of this technology is how to apply the existing materials to obtain the best strength of the composite patches. With the rapid development of various surface treatment technologies, such as sandpaper grinding, sandblasting, anodizing and plasma treatment, to a certain extent, sufficient interface strength between the adherend and the composite patch is ensured. Nonetheless, it should still be noted that due to the inherent discontinuity of the material in the bonded area, the stress concentration is still present between the patches and the adherend matrix. The carrying capacity of the overall reinforced structure is determined by its weakest part. The main stress existing between the composite patch and damaged matrix can be divided into shear stress and peeling stress, where the peeling stress directly loads the composite matrix in the unreinforced direction, which has a greater impact on the strength of the joint. Generally, higher stresses will appear at the edges of the junction area.

Figure 1.7 Application of composite patch for bridge strengthening.

1.3.1. Effectiveness of composite reinforcement system for enhancing application

In general, as a typical external bonding repair, composite patch is a powerful and effective method in civil repair. In this method, the patch can be cured directly on the potential damaged structures. Yang *et al.* studied the strengthening effectiveness of externally bonded carbon

fibre reinforced polymer (CFRP) composites on single-bolt timber joints [78]. In order to improve the bearing capacity of pin joints, the bearing strength of wood were increased. And the FRCs provide an effective and rapid modification and repair solution for joints. In their research, they presented a series of tests on 50 single-bolt timber joints that subjected tension test, of which, 25 joints were made of softwood and 25 joints were made of hardwood. Forty seams were reinforced with four different externally bonded CFRP panels. The fiber directions of these CFRP panels are 0 °, 0 °/90 °, ±45 ° and ±30 ° relative to the grain direction. In addition, ten joints were used as unreinforced controls. The basic diagram is as shown in Figure 1.8.

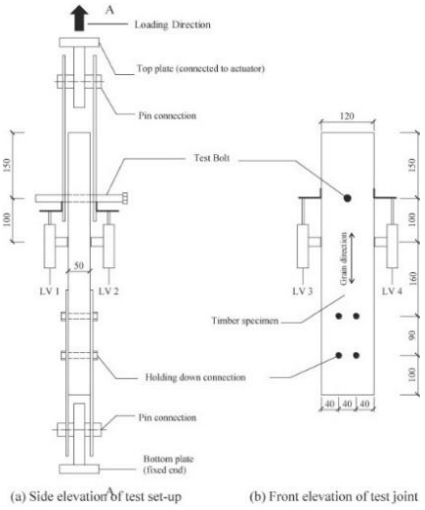

Figure 1.8 Schematic of test setup, instrumentation and test specimen (ref.78).

In addition to predicting the strength of the joint, they also reported the test details of all the tested joints as well as the failure mode, strength and ductility. Overall, it was found that the reinforcement schemes used can increase the strength of the wood joints, although their effects vary. With proper fiber orientation, it was observed that the strength of the joint was increased by 50% compared to the control joint. It has also been found in the case of reducing the failure of brittle wood by preventing premature splitting of wood.

Xu *et al.* analyzed the seismic behavior of CFRP-strengthened seismic-damaged composite steel-concrete frame joints [79]. They conducted a series of experimental studies to examine the seismic behavior of three seismically damaged composite steel-concrete frame nodes reinforced with CFRP panels and one original composite steel-concrete frame node. Besides, the effects of earthquake damage and CFRP reinforcement on shear capacity, ductility, energy dissipation and stiffness degradation were also strictly studied. The corresponding test set-up and loading system is given in Figure 1.9.

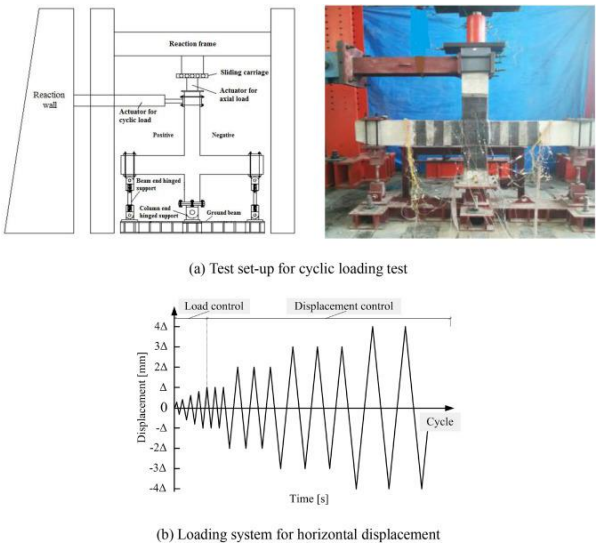

Figure 1.9 Test set-up and loading system (ref.79).

The research results showed that the reinforcing parches of CFRP plates can improve the ductility of infrastructures. And the greater the degree of earthquake damage is, the better the reinforcement effect. Some of the CFRP-reinforced specimens even reached the level of the original seismic state prior to the seismic damage up to a certain damage level. The stiffness of the sample reinforced with CFRP is lower than that of the control sample, which shows that CFRP effectively prevents damage to the sample and improves its seismic deformation resistance. For the CFRP-reinforced specimens, the bearing capacity and deformability of the severely damaged specimens are slightly better. To be specific, compared with the controlled samples, the average ultimate bearing capacity of the CFRP-enhanced sample increased by 15.58%, 13.27% and 10.35%, and the average ductility coefficient increased by 25.39%, 20.69% and 5.33%, respectively. The results show that the CFRP board effectively improves the ductility, carrying capacity and energy dissipation capacity of the sample. Besides, the prediction results of the shear strength model are in good agreement with the test results in terms of seismic damage and the amount of CFRP.

The usage of the FFRCs in the fields of concrete rehabilitation has been recognized as an innovative and effective technology. When the plate with high tensile strength properties bonds on the concrete surface, it can strengthen the structure with minimum changes of weight and dimension. Lau *et al.* investigated the mechanical performance of composite-strengthened concrete structures in their study [3]. They experimentally studied the structural performance of glass fiber composite reinforced concrete structures in uniaxial compression and 3-point bending tests. This study used different types of concrete structures, as shown in Figure 1.10.

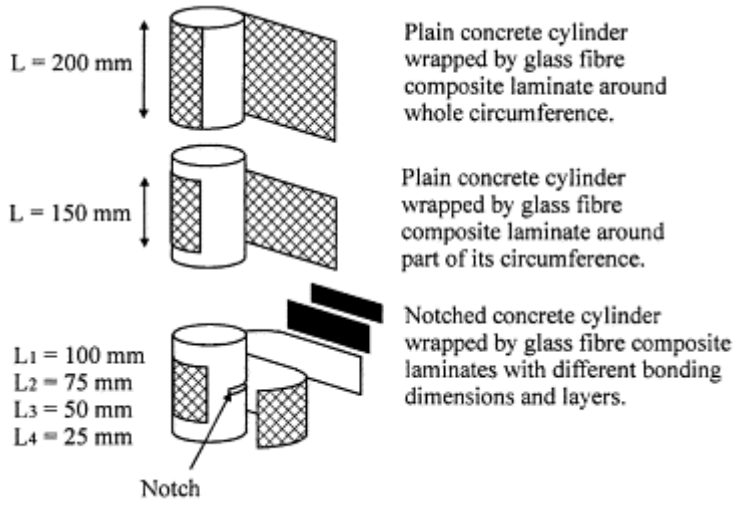

Figure 1.10 Schematic diagrams of the plain and notched concrete cylinders wrapped by glass–fibre composite (ref.3).

They analyzed the strengthened effectiveness of FRCs from both mechanical and chemical aspects. The exciting results showed that the glass fiber composite wraps can increase the bearing capacity of ordinary concrete cylinders with or without notches. By bonding three layers of glass fiber composite laminates on the tension surface of the beam, the flexural bearing capacity of the concrete beam is increased to more than 50%. Compared with the pre-cured board bonding technology, the direct manual laying method has better reinforcement performance in terms of ultimate bending load. At the same time, compared with unreinforced reinforced concrete beams, the flexural strength of composite reinforced concrete beams immersed in different chemical solutions for six months has increased.

Corrosion of steel bars caused by chloride ion intrusion is generally considered to be the most common cause of deterioration of reinforced concrete structures. Generally speaking, the corrosion of steel will be accompanied by the reduction of the cross-section of the corroded steel bar, the loss of the bonding force between the steel bar and the concrete, the volume expansion and the stress in the adjacent concrete cause many problems such as cracking and spalling of the concrete cover. Manalo *et al.* [80] indicated that simulating a 50% corrosion in a circular reinforced concrete column of 1 m height and 250 mm diameter resulted in a 56% reduction in the axial load capacity. Mohammed *et al.* designed a novel composite jacket in repairing damaged reinforced concrete structures subject to flexural loads, then evaluated the effectiveness of this repair system [81]. Their composite repair system consists of a prefabricated sheath, joints and grouting fillers, as shown following.

Figure 1.11 Novel glass fiber reinforced composite jacket with novel joining system (ref.81).

A full-scale beam was prepared and tested under four-point static load to evaluate the damage location in the concrete member, the joint location and the effect of the coating on the inner surface of the sheath. The experimental results indicated that the behavior of the repaired system was dominated by the tensile cracks of the grout and the destruction of the teeth at the joints. When the damage is at the top than bottom, it is found that the composite sheath is more effective in repairing concrete members under bending loads. This effect can be further improved by placing the composite sheath away from the compression zone. Compared with uncoated cement slurry, epoxy resin and coarse aggregate coating are provided inside the composite sheath surface, which can produce better stress distribution and crack propagation in the cement slurry. Due to the effect of the coating, the repair system components enhance the composite effect and increase their bending strength by 12% compared with the uncoated jacket sample. In addition, the provision of epoxy and coarse aggregate inside the sheath surface produces better stress distribution and crack propagation in grouting than unused epoxy and coarse aggregate.

Li *et al*. prepared a combination of carbon fiber reinforced polymer and steel jacket to enhance the corrosion resistance of reinforced concrete [82]. In this project, an external current technology was adopted to induce corrosion to the matrix specimen within a controlled period. The samples were placed in a water tank containing a 3.5% salt solution, the reinforced cage of each sample was used as an anode, a corrosion-resistant plate immersed in a bank was used as a cathode, and a constant current of 1.0 mA/cm^2 was applied. And the degree of corrosion is controlled by the integral current. For reinforced samples combined with CFRP sheets or the combination of CFRP sheets and steel sleeves, first, round the corners of each column to

a radius of 20 mm, and then apply a trowel to directly coat the epoxy resin on the prepared substrate, and finally CFRP was used to wrap the paper around the entire test area with an overlap of 200 mm in the circumferential direction. The results showed that reinforcing corroded concrete matrices with CFRP sheets can significantly improve ductility. The technology with CFRP plates and steel jacket or only steel jacket is very effective, which significantly improves the strength and ductility of the reinforced columns. However, compared with only the steel jacket reinforcement, the combination to strengthen the corroded concrete column is more effective in improving the strength and ductility, and the CFRP plate wrap significantly improves the seismic performance of the reinforced column.

Triantafyllou *et al.* studied the effect of composite patch repair and strengthening with External Bonding Reinforcement and Near Surface Mounted method for concrete beams with low, medium and heavy corrosion [83]. The rectangular cross-sections of all specimens are 150 mm wide, 300 mm deep, 2300 mm long, and the effective span is 2100 mm. The longitudinal steel bars consist of three ribbed steel bars with a tensile force of 12 mm and two ribbed steel bars with a tensile force of 10 mm. In order to prevent the shear failure of the beam, ribbed stirrups with a diameter of 8 mm are used, with a spacing of 150 mm (50 mm between the supports), and a 20 mm transparent concrete cover on all sides of the beam. The reinforcement scheme and test device are shown in Figure 1.12.

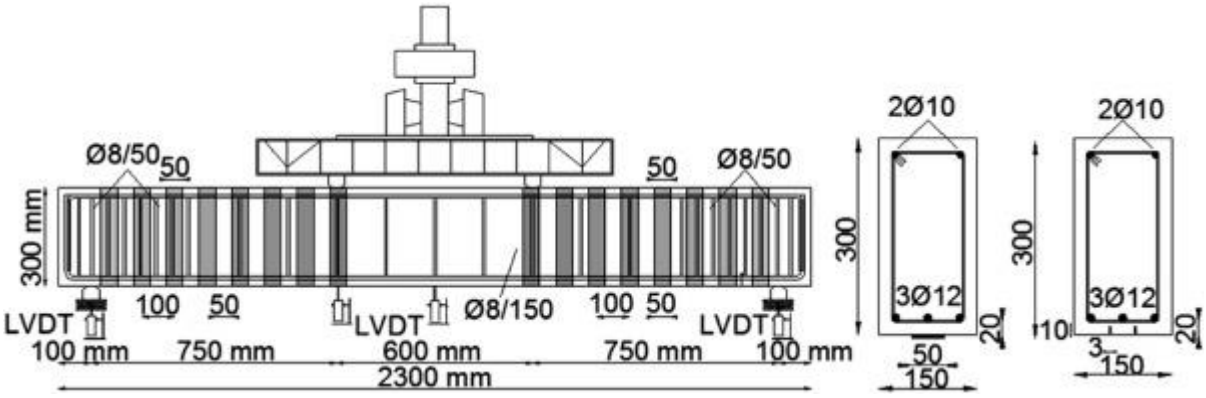

Figure 1.12 Geometry, loading conditions and reinforcement details of the tested beams (ref.83).

In order to accelerate the corrosion process, the beam is partially immersed in a tank containing a 3% industrial salt solution, and a constant current density is applied to it using a power source. The results implied that for all repaired and strengthened beams, it is necessary to ensure that all the force transmission mechanisms through the old repair mortar and the interface between the repair mortar and CFRP reinforcement. For low corrosion levels, the Near Surface Mounted strategy has a greater advantage, while for the medium and high

corrosion levels, the destructive contribution of External Bonding Reinforcement is significantly higher.

Belarbi and his research group evaluated the effects of environmental conditions on the long-term behavior of reinforced concrete columns strengthened with CFRP and GFRP sheets [84]. They manufactured the small concrete columns in the laboratory and processed the accelerated environmental cycling and steel corrosion. Then, a uniaxial compression failure test was performed to measure the changes in the mechanical properties of the concrete column with different environmental influences. The results showed that the concrete column system has changed due to environmental ageing and corrosion of steel bars, and the composite enhancing patches have the ability to slow down the damage propagation. Sen *et al.* fabricated the composite patches based woven jute and also heat treated woven jute, with epoxy resin as matrix and tested for its mechanical properties [85]. In addition, they also prepared and tested synthetic carbon fiber and glass fiber composite materials for retrofitting the reinforced concrete beams. For the purpose of clarifying the effectiveness of natural bio-based woven jute composite to enhance shear strength, fourteen reinforced concrete beams were designed to withstand shear failure. Then the heat-treated jute composite material, artificial CFRP and GFRP composite material are used to strengthen the beam to withstand shear failure. The tensile test showed that the tensile strength of the heat-treated sisal glass fiber reinforced composite material was 189.479 N/mm^2. What's more, this study also concluded that the woven jute glass fiber cloth reinforcement scheme had many advantages over the carbon and glass fiber cloth fiberglass reinforcement schemes, and it converted the brittle failure mode of the beam into a ductile failure mode. Unlike carbon fiber and glass fiber reinforced plastics, the beam did not suffer any sudden degumming, delamination or glass fiber reinforced fracture, and depicts a complete ductile failure mode with high deflection.

1.3.2. Methods for enhancing the adhesive strength

1.3.2.1. Graded adhesive

A joint patch that gradually changes in the direction of overlap is defined as a graded adhesive, as shown in Figure 1.13. This concept was first proposed by Raphael in 1966 [86]. This method obtains higher adhesive strength by minimizing the high-stress concentration at the overlapping ends. In general, the graded adhesive technique is usually studied in metal materials because they have conditions that provide simpler stress compared to composite

materials. Nowadays, with the development of lightweight construction methods, the application of gradient glue in compound joints is increasing.

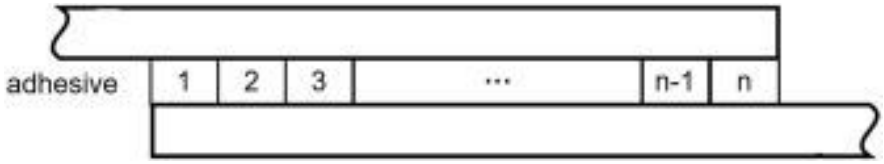

Figure 1.13 Mixed-adhesive bondline (ref. 86).

Mixed adhesive joints that combine two or more adhesives in a single joint can be considered as an alternative to one single flexible adhesive. This technique was originally used for metal joints to reduce stress concentration in the adhesive. Compared with the brittle adhesive used alone, the hybrid adhesive joint is easier to obtain a uniform stress distribution and higher bonding strength. As the composite patches developing, researches on mixed adhesive technique were later expanded to composite joint patches. Fitton *et al*. developed an approach of variable modulus adhesives to optimize joint performance [87]. They adopted hybrid bonded joint technology to analyze the performance of carbon fiber reinforced plastic lap joints. High-modulus adhesives and low-modulus adhesives were applied to the overlapping middle and ends, respectively. Their experimental results showed that this hybrid joint can not only effectively reduce stress concentration, increase joint strength and reduce experimental dispersion, but also change the failure mode of the material. At the same time, the study also pointed out that this technology does not significantly improve joints that almost reach the full shear strength of the adhesive. Therefore, in order to obtain higher strength in this case, a higher shear strength adhesive must be used in the center of the joint. De silva *et al*. obtained joint strength optimization by the mixed-adhesive technique [88]. They proposed a simple method to improve the bonding strength of the hybrid adhesive, that the usage of three different brittle and ductile adhesives in the manufacture of single-lap joints, as shown in Figure 1.14. Compared with the use of brittle adhesives alone, mixed adhesive technology can improve joint strength significantly, and by using different types of adhesives, mixed adhesive joints can provide the best combination of strength and ductility. The experiment tested the static failure of the single lap joint of the sample, it can be observed that in all cases studied, hybrid adhesive joints have higher joint strength than joints with only brittle adhesives. Besides, if the bonding strength of the ductile adhesive is lower than that of the brittle adhesive, the combined bonding strength of the mixed adhesive of both adhesives is

higher than that of the adhesive used alone. The authors explained this synergy by the shear stress distribution of the adhesive during failure.

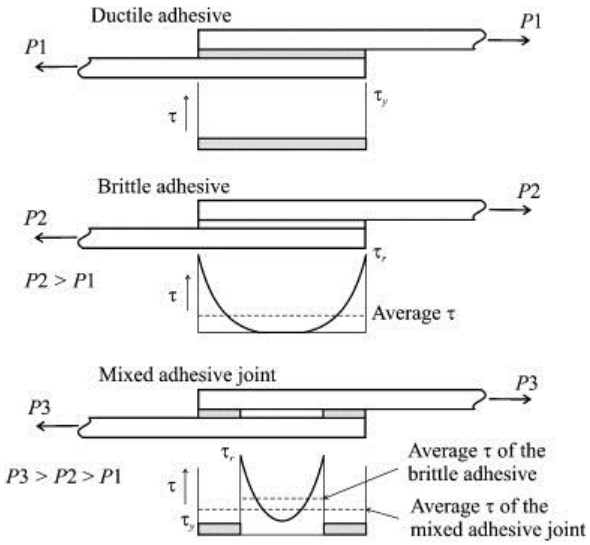

Figure 1.14 Schematic shear stress distribution at failure in mixed-adhesive joints (ref. 88).

The mixed adhesive or physical modification of the adhesive by incorporating other phase materials such as rubber particles or glass beads can be considered as a simple form of functionally graded adhesive. The ultimate goal of these methods is to obtain a functionally modified adhesive that gradually changes along the overlap, thereby achieving a truly uniform stress distribution. Similarly, this approach was also applied to metal materials in the first place, later studies on composite graded adhesive appeared. Compared with hybrid adhesive patches, graded joints with changing functions are more difficult to manufacture. Kumar *et al.* analyzed the tubular adhesive heads with functional modulus gradient bonding lines under axial load [89]. They found that by reducing the stress concentration at the lap ends and evenly distributing the stress across the bonding line, the strength and service life of the bonded joint can be significantly improved. Under the same axial load, the shear stress and peel stress concentration at the overlapping end of the graded adhesive head was much less than the shear stress and peel stress concentration of the mixed adhesive head.

Carbus *et al.* prepared the functionally graded adhesive joints by graded mixing of nanoparticles [90]. They used two different types of carbon black nanoparticles to reinforce the epoxy matrix. Then, cured by dielectric or thermal heating to obtain graded mechanical properties and the concentration of nanoparticles along the overlap. Their attempt made the stress distribution along the overlapping part even and allowed a stronger and more effective adhesive connection. The bonding stiffness changed along the overlapping part, the largest in

the middle of the overlapping and the smallest at the two ends of the overlapping. Compared with joints with homogeneous bonding wires, joints with graded bonding wires have the best mechanical performance. At present, although the research and development of functionally graded joints have obtained some encouraging theoretical analysis and experimental work, there is still a gap between the realization of its extensive and practical application in structural bonding. The specific experimental research in this field is still in its infancy, and there is still a long way to go to improve the practicality of gradient joints. One of the main problems of this technology is whether the increase in adhesive strength is worth increasing manufacturing complexity.

1.3.2.2. Graded adherend

Adhesive joints have become a common strategy for structural external enhancement due to their high efficiency and wide compatibility. Recently and previously, many researchers have been engaging in the studies of composite patch joints. Up to now, single lap joints and double lap joints have been successfully used in metal materials, as well as traditional composite materials. However, when these joints are subjected to tensile forces, they will undergo significant stress concentration near the edge of the bonding area, and even failures such as debonding along with the adhesive- adherents interface and eventually lead to joint bending or even destruction. How to alleviate this concentrated stress situation bot only affects the strengthen strength but determines the service life of composite patches and the matrix structure. The practical significance of the functionally graded adherends joints is to adjust the material composition, which would result in more uniform shear stress or peel stress distribution in the adherents and adhesive layers near the edge of the joint.

Guin *et al.* used a three-parameter elastic model adhesively bonded single lap joints with functionally graded adherents to study the stress distribution in composite patches [91]. They found that the peel stress is critical at the left edge of the upper adherend-adhesive interface and the right edge of the lower adherend-adhesive interface, which indicated that the joint is easily peeled along the upper layer. Besides, it was also observed that the modulus of the adherent varied along with the thickness, as shown in Figure 1.15. Compared to a softer layer near the adhesive, the peak peel stress in the adhesive is reduced by 27% when there is a harder layer near the adhesive.

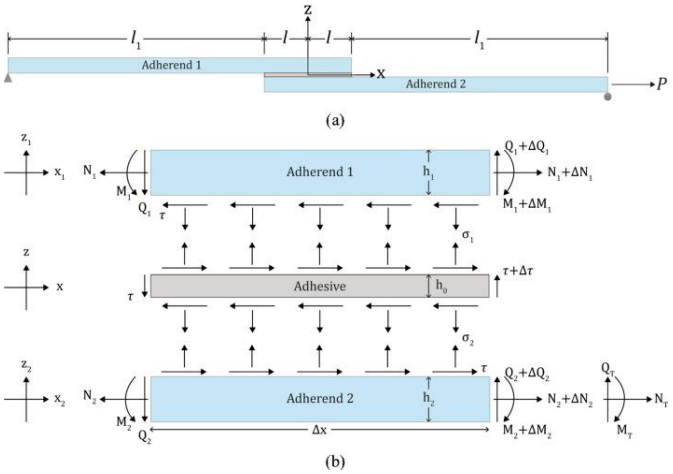

Figure 1.15 (a) Overall schematic of the adhesively bonded single lap joint, and (b) Free body diagram of the overlap region in the joint (ref.91).

Boss *et al*. investigated the behavior of single-lap bonded joints with adherends with modulus and geometrically graded adherends [92]. Modulus grading was made possible with the advent of the new fiber placement technology making it possible to fabricate composite material with spatially and continuously varying material properties. In their study, the grading modulus of the adherend was provided by continuously varying the braid angle, the geometrical grading provided by varying the adherend thickness in the overlap region. And the finite element method was applied to measure the peak stress distribution and lateral deformation at the thickness in the adhesive to compare the performance of modulus grading and geometric grading. It was observed that the controlled modulus grading could significantly affect the stress state and joint deformation in the adhesive. In some cases, material grading can reduce stress levels, and the reduction in shear stress makes modulus grading provide better performance.

Graded adhesives and graded adherends are two strategies based on the same theoretical foundation, that increasing the bonding strength as well as the servicing life by controlling the tensile and peel stress distribution. As we discussed before, the manufacturing job is a major obstacle for those methods. However, the practicality and operability of these two methods are different, especially for the subjects of civil infrastructures. By redecorating the surface shape of adherends is difficult, sometimes it is impossible for the subjects of civil infrastructures. Hence, this external strengthening strategy is more widely adopted in the areas of metal materials.

1.3.2.3. Transverse adherend toughening

In composite patch joints, the delamination of the composite patch adherend usually results in premature failure of the whole structure, thereby reducing joint strength. A simple method to reduce the delamination sensitivity of composite materials under lateral load is to increase the strength and toughness of the adherend in the lateral direction [93]. Considering that the stress is usually concentrated on the adherend patches surface, hence, high-toughness materials such as fiber metal laminates or tough surface composite materials on the outer surface of the laminate can play a role in toughening the surface of the composite adherend and improving the joint strength. Fiber metal laminate refers to the combination of metal and composite materials, which consists of layered structures of alternating metal and composite materials. It combines the characteristics of organic composite matrix and metal materials. It has shown gratifying performances in the field of aircraft fuselage structure, automobile panels and others. While increasing strength and reducing weight, it also reduces costs and improves its safety to a certain extent. From a practical point of view, fiber metal laminate can provide advantages such as high specific static performance, impact resistance, corrosion resistance, fatigue damage resistance, flame resistance, and lightweight. In addition, it is easy to manufacture. Due to the synergistic combination of merit performances of composite materials and metal alloys, the use of this type of material can significantly reduce weight, improve damage resistance and increase safety.

Lee and his teammates developed a simple adhesive connection technology through the carbon fiber reinforced plastic component structure [94]. They adopt the adhesive joint design of the carbon fiber fabric modified by electrophoretic deposition and the fiber metal laminate of the hydrothermally treated metal plate to improve the bonding strength. The preformed samples were then characterized for adhesive properties. They adopt the adhesive joint design of the carbon fiber fabric modified by electrophoretic deposition and the fiber metal laminate of the hydrothermally treated metal plate to improve the bonding strength. The preformed samples, as shown in Figure 1.16, were then characterized for adhesive properties. The results showed that the design of fiber metal laminates plays an important role in improving the adhesive strength and fatigue life. In addition, this laminate can effectively reduce the working space and simplify the shape of the mold to simplify the manufacturing process, thereby reducing production costs.

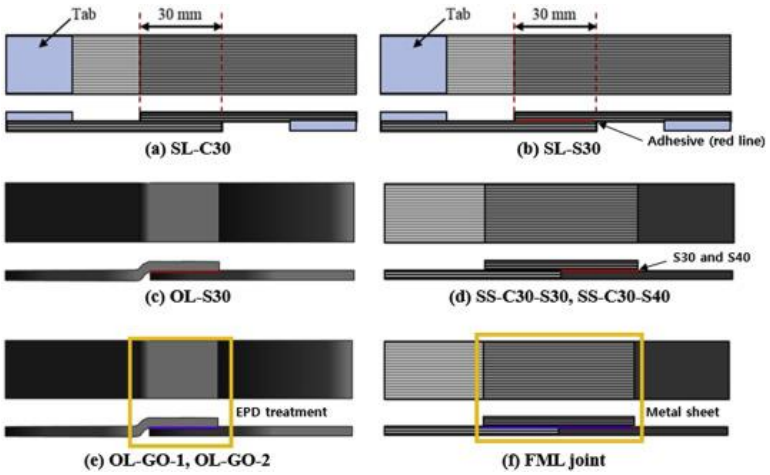

Figure 1.16 Prepared joint specimens (ref. 94).

Santo *et al.* adopted the fiber metal laminates to reinforce the CFRP joints [95]. They studied different layer configurations and the effect of adding an adhesive layer in the interface between the metal plate and the composite material to reinforce the basic carbon fiber reinforced polymer joint. Instead of aluminum, titanium was selected in this research as the metal material for enhancing CFRP adhesion due to its lower heating value, its expansion coefficient can also avoid the galvanic corrosion and thermal stress problems. The obtained experimental data and numerical analysis strongly indicated that the combination of additional interfacial adhesive layers can be used to significantly enhance CFRP joints using titanium layers. It can be observed that the failure load and peel strength of CFRP joints increase significantly without delamination.

Besides the fiber metal laminates, the currently available toughened thermoset plastics and thermoplastic composites can also significantly improve delamination resistance under static loads. That is tough surface composite materials, this concept was newly proposed by Shang *et al* [96]. This technology aims to reduce or avoid delamination of composite adhesive joints, and simultaneously bond fiber-reinforced high-toughness resin to both surfaces of the cured composite patches to form a new type of composite material with a tough surface, as shown in Figure 1.17a. Shang and his teammates found that compared with the sample reinforced by CFRP alone, 22% higher of the failure load of the sample using the new composite adherend appeared. Although a very brittle and hard adhesive was used, no delamination occurred on the new adherend. The lap shear strength was also close to the lap shear strength obtained when using high-strength steel adherends, which was considered to be the highest lap shear strength obtainable using the adhesive.

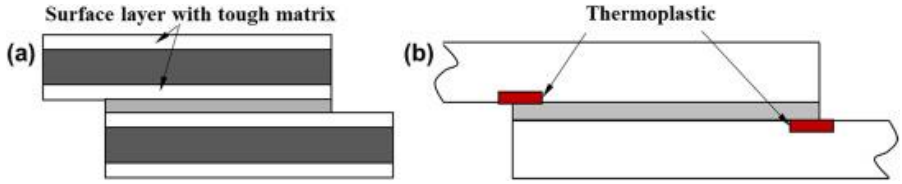

Figure 1.17 Schematic of surface toughening techniques (ref.96).

Since the stress of the bonded joint is usually transferred from the surface of the composite patches to the interior parts, the composite surface is normally under greater stress. Surface toughening technology can be used to manufacture laminates with higher load transfer capability in the lateral direction [90,93]. It is proved that composite materials with hard surfaces have a higher resistance to damage generation and propagation, which indicates that the application of these composite materials is not limited to conventional composite patch joints. About this adhesive technology, Schollerer and his group made a little improvement [97]. They did not toughen the entire surface of the adherend but chose to toughen only the local surface of the adherend, which also achieved the effect of enhancing the adhesive strength, as shown in Figure 1.17b. Specifically, two sheets of thermoplastic with a thickness of 0.1 mm were placed near the overlapping ends and co-cured with the stacked prepreg. The experimental results showed that the peel stress and shear stress of this configuration reduced by 38.2% and 33.7%, respectively, and the joint strength increased by 84% compared with the traditional composite patch joint.

1.3.2.4. Transverse joint reinforcement

Another method to improve the strength of the composite patch is to further strengthen the adherend in the lateral direction. This reinforcement method can be either continuous threads in stitched laminates, three Dimensional (3D) braiding and braiding, or discontinuous rods or pins, such as Z-reinforced materials, Z-inserted pins and inserts, etc. These techniques are very effective in preventing the delamination of composite materials. The reinforcement technology of transverse joints can generally be divided into the reinforcement of the adherend and the surface reinforcement, as shown in Figure 1.18. However, the transverse reinforcement joints will negatively affect the elastic modulus, strength and fatigue performance of the matrix material, and increase the complexity of the manufacturing process, which will increase the cost of the final product to a certain extent. At present, the application of laterally reinforced composite adherends in bonding heads can be basically divided into the following three types: hybrid joint, Z- pinning, and stitching.

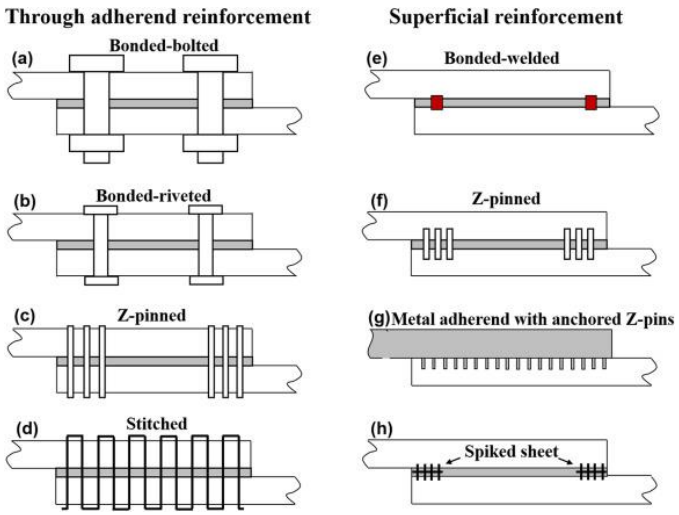

Figure 1.18 Schematic representation of transverse connection of adherends (ref.93).

Hybrid joint refers to the adhesive strategy that combines both the mechanical fastening and the adherend patches at the same time. According to the mechanical fastening in hybrid joints, this category can be divided into bonded bolt joints, bonded rivet joints and bonded welded joints. This method can not only reduce the stress concentration problem caused by a single joint, but also strengthen the adhesion performance of traditional patch reinforcement materials. Joesbury *et al*. prepared a resistance spot welded reinforced adhesive (weld-bonded) joint between 304 stainless steel to CFRP, where welds are made both with and without the reinforcing carbon fibers present [98], as shown in Figure 1.19. They found that the application of resistance spot welding before the adhesive bonding improves the connection performance; it not only improves the bonding strength, but also reduces the strength change obtained. In addition, resistance spot welding enhanced the strength of the adhesive joint to a large extent related to the presence of fibers before resistance spot welding, but for joints with fibers removed before welding, the fracture strain is much better.

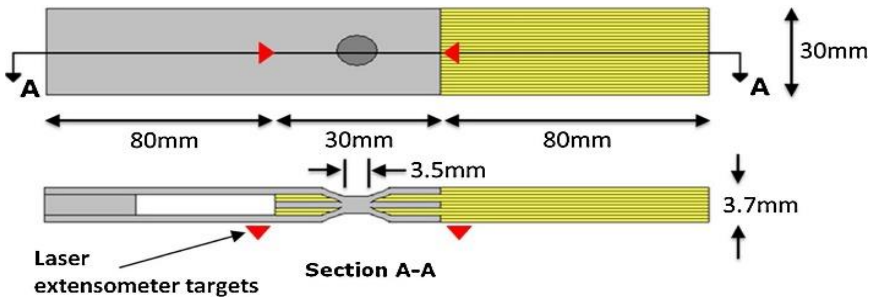

Figure 1.19 Diagram of the metal to carbon fibre spot weld-braze reinforced adhesive joint. Note: this diagram shows the preferred interleaved stacking sequence (ref.98).

Z pinning is a technique of inserting reinforcing fibers in the Z direction of continuous fiber-reinforced materials. The Z-shaped pins were made of metal materials in the first place [90]. Based on the metal "Z-shaped pin" anchored on the metal adherend, an improved Z-shaped pin technology for composite/metal connection was proposed. Anchored Z-shaped pins, either machined or welded or obtained, are inserted into the uncured prepreg adhered [93]. There is a large amount of experimental evidence that Z pinning can significantly improve the delamination resistance of the composite structure and significantly improve the adhesion performance of the composite patch. Chang and his teammates studied the properties and failure mechanisms of pinned composite lap joints in monotonic and cyclic tension [99], as shown in Figure 1.20. They found that pinning is very effective for increasing ultimate strength, elongation limit and fatigue life. The improvement of monotonic and fatigue properties is attributed to the transformation of the failure mechanism, from the degumming of unstable joints without pins to the stable degumming of pins, followed by pin pullout or shear fracture or tensile laminate fracture damage. The experimental results also showed that using the z pin to enhance the thickness of the co-cured single lap joint is an effective method to improve the ultimate tensile strength, elongation limit and fatigue life. For the lap processing method and laminate in their study, the z nail method can increase the static strength by 40%, the elongation at break by 55%, and the fatigue strength (at 106 cycles) by up to 40%.

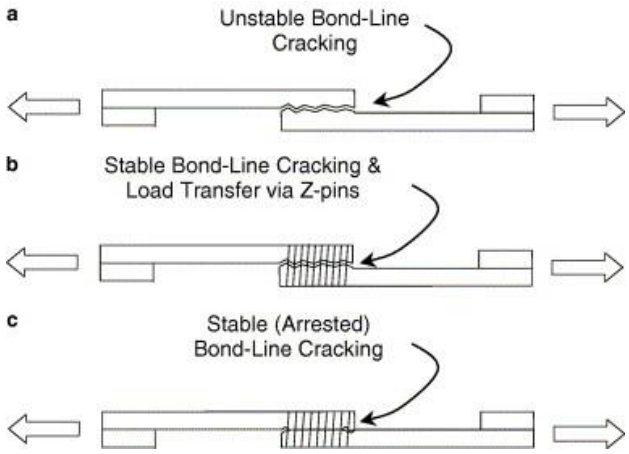

Figure 1.20 Schematic of the initial failure mode of the lap joints under static tensile loading: (a) unstable delamination fracture of the adhesive bond-line in the absence of z-pins; (b) stable delamination failure of the bond-line promoting crack bridging with the lowest volume content of thin z-pins; (c) small-scale delamination at the intermediate and highest volume content of z-pins (ref.99).

Stitching is an emerging strategy to enhance the bonding strength of the composite patch. It can enhance the thickness of the traditional 2-dimensional laminate, thereby improving its

resistance to delamination, as shown in Figure 1.21. Generally, this technique is applied to the entire bonding area, not limited to the adherend. The increase in joint strength is sensitive to a series of parameters, such as the thickness of the adherend, the overlap length, the number and density of stitches, the modulus of the stitches, the distance from the edge, and the thread pretension [90,93,100]. However, when it comes to the strengthening of civil infrastructure, the application of stitching is very limit. The drilling process during stitching would cause unavoidable stress concentration, which is obviously not a cost-effective option. Hence, this technology would not be presented in detail.

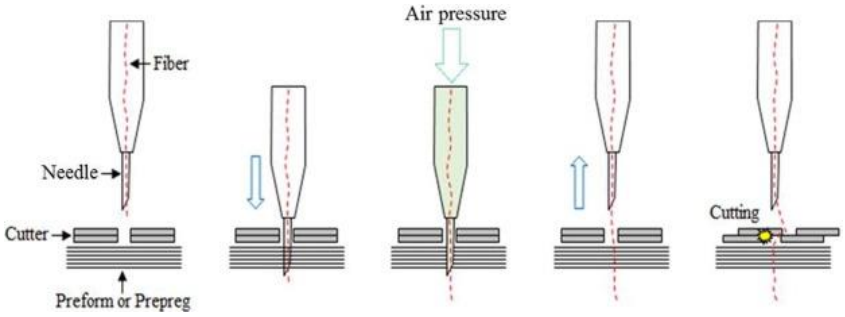

Figure 1.21 Proposed 1-thread stitching process (ref. 100).

1.3.2.5. Geometry design

In terms of improving the adhesion strength of composite joints, the geometric configuration is an important factor, which has a significant impact on the stress and the stress distribution acting on the adherend and the adhesive layer. During the design stage, it is necessary to ensure that the joint geometry is carefully selected to avoid undesirable stresses concentration that may lead to premature failure of the adhesive or adherend. After the overall configuration determined, the local joint geometry can be modified (including local modifications to the adherend, adhesive, and their combination) to further increase the joint strength. This technique is more efficient at the ends of joints where stress concentration is more severe.

Global configuration optimization

Shear lap joint is one of the most commonly used and most representative joint configurations for composite patches, where the joint overlaps and adheres to the matrix adherend. Due to the inherently unbalanced configuration, the stress transfer is uneven along the overlapping portion, resulting in stress concentration at the end of the overlapping portion. As a result, increasing the overlap length does not necessarily increase the fault load, many cases have indicated that the overlap length will reach a steady state when it reaches a certain value. The configuration optimization mentioned this part is another method. Shear stress and peel stress

concentration are common phenomena in almost all joint configurations, especially for the situation of shear lap joints. Focusing on its structure, the shape of the adherend near the overlapping area could be optimized to reduce stress concentration, as shown in Figure 1.22 [93].

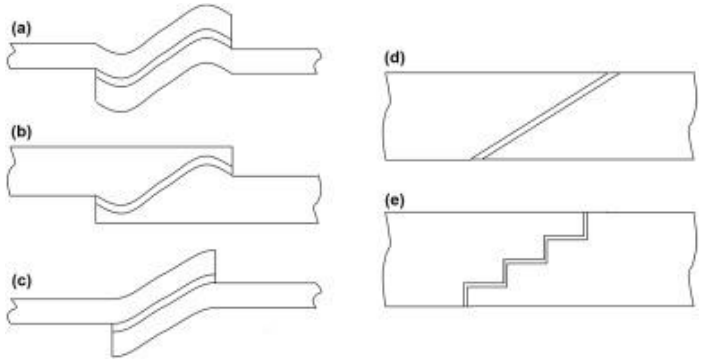

Figure 1.22 Schematic of joints with (a) wavy (b) single-side non-flat (c) reverse bent (d) scarf and (e) stepped adherends (ref.93).

Avila *et al*. presented an experimental and numerical study on adhesive joints for composites [101]. They studied an improved wave lap joint design and conducted finite element simulations to analyze the stress field inside the joint. In order to ensure the consistency of the data, not only the number of samples but also the statistical difference between the single-ring and wave-ring joints were considered when conducting statistical research. The experimental results showed that the average increase rate of failure loading is close to 41%. The authors attributed this increase to the compressive stress field generated inside the wavy lap joint. In addition, this stress field distribution might also be the cause of the observed adhesion delamination at the wave overlap. From the data analysis, the improved wave lap joint did make the joint stronger. Similarly, Ashrafi *et al*. prepared the adhesively bonded single lap joints with non-flat interfaces [102]. They manufactured a fiber-reinforced epoxy composite adherend with a sinusoidal bonding surface in a special mold. This construction method allowed the fiber to follow a sinusoidal curve, so that maximum strength can be obtained. Then, the sinusoidal surfaces are connected by an epoxy layer with a controlled thickness. A single lap joint with a flat interface was also manufactured using the same composite material and the same overall shape. The experimental results showed that there were considerable differences between the uniaxial force-displacement of bonded joints with different interface profiles. The finite element method was used to calculate the stress distribution in the bonded joint with the same configuration as the sample tested in our experiment, it showed that the failure of the specimen was mainly due to the peeling.

Bendamra *et al*. investigated the optimization study of the tapered scarf and stepped-lap joints in composite repair patches [103]. They studied the effect of joint parameters on the peak stress of adhesive bond lines in tapered scarf and stepped lap joints. Linear finite element analysis was carried out to conduct parameter research, focusing on six joint design parameters: layer thickness, adhesive thickness, cone angle, stacking order, overlapping placement and overlapping lap length. The experimental results showed that the stepped lap joint has a higher stress concentration than the equivalent tapered scarf joint, but this can be alleviated by introducing a sleeve and appropriately changing the joint design parameters to reduce the peak stress at the joint tip and step.

Local configuration optimization

Due to incoherence with the whole structure, composite patch joints are considered to be vulnerable areas, which reveals the weakness of this method. Global configuration optimization can further improve the joint strength, but the manufacturing difficulty and cost will also increase greatly. Therefore, choosing the most appropriate technology is a complex subject. If the configuration of the joint is limited by its application, local modification of the geometry of the adherend becomes more important. Adhesive molding is a good way to reduce the stress concentration at the overlapping ends because if the local stiffness of the joint is reduced, the concentrated load transfer can be more evenly distributed. At the same time, the taper of the adherend reduces the stiffness of the end of the adherend and also reduces the discontinuity at the edge of the bonded area. Figure 1.23 shows the different forming possibilities in terms of tapering and rounding of the adherend and their combination with the fillet of the adhesive.

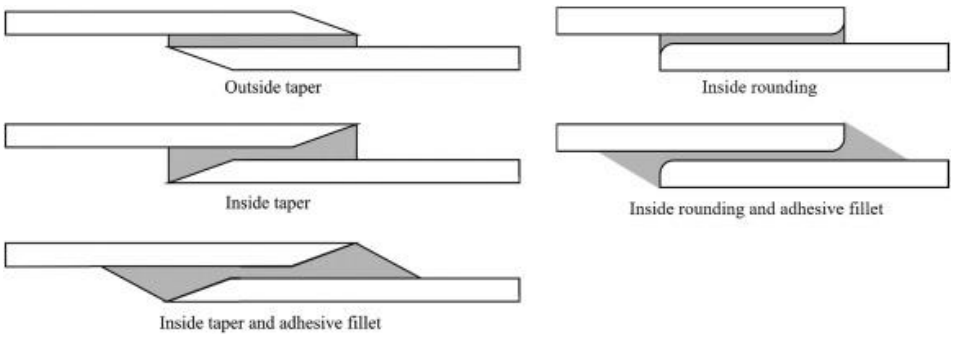

Figure 1.23 Different shaping possibilities of the adherends (ref.93).

Campilho *et al*. presented a two-dimensional numerical analysis to evaluate the effect of several geometric changes on the tensile residual strength of the repaired CFRP composite panel [104]. In their research, the geometric changes include chamfering the outer surface of

the patch, thickening the adhesive near the overlapping outer edges, filling the board gap with the adhesive (plug filling), using rounded corners of different shapes and sizes at the end of the patch, chamfering the inner and outer edges of the board, and a combination of these changes. The experimental results showed that with the correct joint configuration, the residual strength of a single knee joint can be increased by 27%, and the residual strength of a double knee joint can be increased by 12%. Besides, it has also been demonstrated that by using a lower Young's modulus for plug-in adhesives, an increase in joint strength can be obtained. Cui *et al.* studied the surface morphology and overlap zone parameters on the strength and failure analysis of viscous single-lap joints under material shear load [105]. They carried out a quasi-static shear test on the test piece to analyze the effect of different surface roughness, overlap length and thickness on the shear strength of the aluminum alloy adhesive joint. The dimensionless parameter δ was given to quantify the residual adhesive distribution of the damaged sample, which intuitively described the effect of overlap length on adhesive joints. It was observed that when the overlap length exceeded 40mm, the adhesive thickness had little effect on the joint shear strength. In addition, the joint strength increased by increasing the overlap length until δ is below 0.95.

1.3.3. Challenges and prospects

So far, all experiments and analysis works have shown that the use of composite patches can significantly reduce the end shear stress and peel stress of the joint. When the proper and optimized performance of the bonded joints used, the joint strength can be maximized. There is no doubt that the increase in adhesion strength helps to enhance the material's sustainability requirements, such as improving performance by reducing weight and reducing the environmental pollution. In addition, there is also a correlation between static strength and fatigue strength. Studies have shown that even if the failure strength is only increased by 10%, the increase in the number of failure cycles can also be increased by more than an order of magnitude [93]. In theory, composite patch joints with adherends of the same stiffness are the most effective, which has the potential to completely eliminate stress concentration. The main purpose of composite patch technology is to enhance the strength and stiffness of damaged matrices and to delay the rapid arrival of destruction. During the adhesive repair, the bonding between the matrix and the reinforcement material is an important factor, which mainly depends on the surface treatment and the type of adhesive. The adhesive strength of the joint design must be high enough to ensure that the stress is safely transferred between the two

adherends [75]. From the point of application, designs of composite patch joints should be designed to provide a shear-dominated stress state and cause minimal peel stress (i.e., normal stress throughout the thickness) in the adhesive layer to increase joint strength.

For now, there are certain challenges in the application and promotion of composite patch joints, mainly involving manufacturing jobs. In order to achieve sustainable and stable performance, the manufacture of composite joints involves many considerations, such as the choice of adhesives that take into account application and environmental factors, determining the optimal seam size, surface treatment, and jig processing to ensure all parts keep it in the desired position during the manufacturing process, correct curing conditions [77,87]. In any case, the adhesive properties of the composite patch are positively related to the difficulty of preparation. Such as graded adhesives, the insufficient benefit of functional grading would lead to ineffective stress dispersion. Conversely, if the grading numbers are too large, it will pose a great difficulty to the production process, and it may also lead to excessive sensitivity to conditions such as unexpected changes in load, size and direction. Other issues include the difficulty of surface pretreatment suitable for graded joints, but also the determination of an appropriate curing process.

The design of functionally graded joints and the study of related geometry design are still a challenge, and the development of easy-to-apply optimization methods has not yet attracted enough attention. Besides, attention should be paid to the development of methods for controlling the distribution of multiple adhesives with limited or no mixing. By leaving properly defined gaps between dispensing adhesives, the mixing of adhesives can be avoided. The plan can benefit from precision printing technology, and further progress in robot allocation and 3D printing has begun to appear. Computational fluid dynamics can be used to study flow patterns to determine their limits. The stress situation of the composite reinforced patch is complicated. Therefore, in addition to dealing with static mechanical testing, the research on the structural integrity and reliability of the material under dynamic load should also attract corresponding attention. It is expected that in the case of load fluctuations, the patch life and enhancement effects will be affected accordingly. Statistical sensitivity analysis can be performed to determine the effect of actual changes in composite patch parameters. The study of the single adhesive bond layer shows that the peel stress is more sensitive to the modulus change than the shear stress.

1.4. Non-destructive detection

Composite patches provide engineers with advantages over traditional mechanical repairs in terms of performance and cost. However, on the other hand, the monitoring and maintenance of composite materials in engineering should also be valued. Compared with metal and inorganic materials, the structural failure rules of advanced composite materials are not yet mature [93,101]. Generally, the damage of the composite laminates involves laminar damage (matrix cracking, fiber-matrix peeling, fiber breakage), laminate (delamination), or structural (extensive component damage), which may be due to machinery during repairs and environmental conditions. Importantly, impact loads usually cause considerable subsurface damage (within and between layers) in composite laminates, and visible surface damage is very limited.

Due to the crucial influence of the various damage to the performance of composite materials, it is necessary to accurately locate and quantify structural damage. However, positioning damage is not always that simple, as almost impact damage in composite laminates is invisible. Subsurface damage in composite materials can be in the form of matrix cracking, fiber-matrix peeling, fiber breakage, and delamination, which ranges in size from a few microns to a few centimeters. In addition, the damage mechanism of composite materials is usually very complex due to its inherent heterogeneous and anisotropic material behavior, destructive inspection poses several challenges for accurate and reliable damage assessment. To fully realize the potential for weight reduction and the excellent mechanical properties that composite materials provide in various applications, reliable non-destructive testing methods are needed to prevent catastrophic failure. Non-destructive detection technology consists of two methods: passive and active sensing. The former passively records continuous signals from sensors, such as optical fibers, to diagnose the health of the structure by analyzing the recorded signals. The purpose of passive non-destructive detection is to determine the early stage and location of the unknown input damage caused by a detectable change in sensor readings. Non-destructive testing does not directly measure the intensity, but measures the parameters that can be related to the intensity, which would exert no damage to the tested structures.

1.4.1. Ultrasonic testing (UT)

Ultrasound refers to a wave source with a longitudinal frequency of excitation greater than 20,000Hz, it can penetrate most materials and can be used to detect defects in and on materials.

Ultrasonic waves consist of longitudinal waves, transverse waves, surface waves, and plate waves. Among these, longitudinal waves are widely used in ultrasonic flaw detection because they are relatively easy to generate and receive. UT is a non-destructive detection method that uses differences in the acoustic performance of material matrix and their defects to check the internal defects of the material based on the energy changes in reflection and penetration time of ultrasonic wave propagation. Through the interaction of ultrasonic waves and the test piece, the reflected, transmitted and scattered waves can be analyzed, which would respond to the macro defects, geometric characteristics, changes in structure, and mechanical properties.

UT technology has been widely used to detect discontinuous defects in components, provide information on the position, and give data that can be used to evaluate defects. For example, detection of defects in welding seams, defects in transmission shafts, high-strength bolts and material interlayer. As the research progressed, its application gradually transitioned from metal to composite materials. UT inspection has many advantages, such as large thickness, high sensitivity, fast speed, low cost, harmless to the human body, etc. On the other hand, UT also has shortcomings. For example, it is not intuitive for flaw/damage display, easily affected by subject to objective factors, the data storage issues of flaw detection test. Besides, UT inspection requires a smooth working surface and requires an experienced inspector to determine the type of defect and suit the thickness. In addition, the inspection of larger parts makes UT detection have its limitations.

Jasiūnienė *et al.* developed an ultrasonic inspection technique suitable for defect detection in hybrid metal to composite joints where the metal part has pin arrays entangled with the composite part [106]. They used high-frequency focused transducers to study samples of innovative titanium/carbon fiber composite joints with artificial and natural defects, and proposed a special ultrasonic signal post-processing method to reconstruct the joint area and detect flaws inside the composite, as shown in Figure 1.24. The experimental results showed that the proposed UT nondestructive testing technique can detect and reconstruct the complex structure of the interface between the metal and the composite material even if the measurement was made from the side of the composite material. Besides, the location and approximate depth of the artificial defect was also determined.

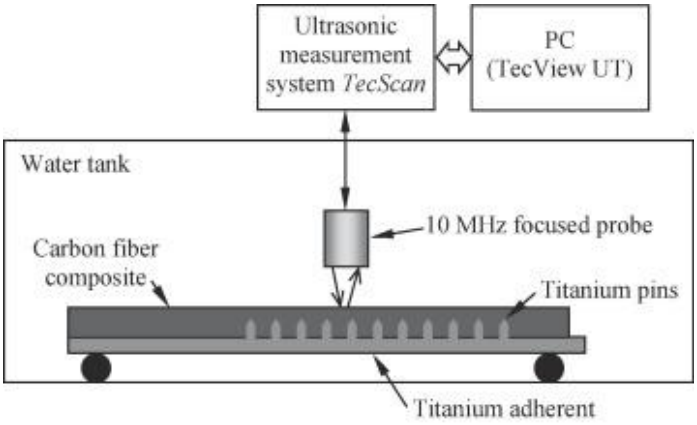

Figure 1.24 The experimental set-up for quality assessment of hybrid joint (ref.106).

Tamborrino *et al.* applied mix non-destructive methods to evaluate the effect of defects on the mechanical properties of bonded joints [107]. In their work, locking thermography and ultrasound methods were used to detect the defect size of bonded joints, and tensile tests were used to evaluate their strength and stiffness. The non-destructive testing methods provided an experimental basis for inspecting joints at a quality level. At the same time, a quantitative understanding of the shear behavior of the structure is obtained through mechanical property testing and statistical analysis of data. The analysis of statistical results showed that the strength and rigidity of the joint are affected by the percentage of degummed area. Similarly, Kumar and his group studied the adhesive joint degradation of the composite epoxy resin with different interfaces and cohesive characteristics using ultrasonic detection methods [108]. In their research, composite lap shear joints were prepared in the first place. Then, different degrees of degradation in the adhesive layer was achieved by mixing different amounts of polyvinyl alcohol during the connection process. Oblique incidence UT inspection was performed on the joints with mechanically load until the samples cannot be determined. It was observed that the degradation of adhesives could be measured by a significant change in the reflection amplitude and a change in the minimum value of the reflection spectrum. Besides, there is a correlation between the combined intensity and the frequency shift of the reflection minimum.

1.4.2. Acoustic emission (AE)

When the internal structure of the material changes, it will cause a sudden redistribution of the internal stress of the material. Meanwhile, the mechanical energy converts into acoustic energy, and thus an elastic wave is generated. The stress wave phenomenon caused by the rapid release of strain energy in the material due to crack propagation, plastic deformation, or

phase change is called AE, whose frequency is generally between 1KHz-1MHz. AE testing refers to a non-destructive testing method that assesses the performance or structural integrity of material by receiving and analyzing the AE signal of the material [109].

So far, AE technology has been widely used in different research studies to monitor the propagation of the microcracks in composite structures under different load types in real-time. This technique is one of the most advanced and effective methods for non-destructive assessment of damage development to study the damage mechanism of composite materials. Many objectives could be finally obtained through the analysis of AE signals, such as determining the location of the AE source; analyzing the nature of the AE source; determining the time or load at which the AE occurs, and assessing the severity of the AE source [109, 110]. In the cases of composite materials, the clustering effect was studied to understand what damage occurred in the laminate, such as matrix cracking, fiber-matrix interface peeling, delamination, fiber pullout, and fiber breakage defects. Using this method requires a reasonable understanding of the relationship between the damage process and the recorded signal. Different AE signal analysis methods were used previously, such as frequency band, AE count, amplitude range, AE energy, or a combination of several AE parameters.

AE signals are generated under the influence of external conditions, they are extremely sensitive to changes in defects/damage, which can detect micro-crack changes in the order of micrometers. Due to the low requirement for access to the inspected parts, AE inspection is suitable for detection under other methods that are difficult or inaccessible to the environment, such as high and low temperatures, nuclear radiation, flammable, explosive and extremely toxic environments. In addition, AE testing is not limited by materials, and it can continuously monitor the safety of defects and overrun alarms for a long time.

Saidane *et al.* adopted AE analysis to evaluate the failure mechanism of braided composites [110]. In their research, the I-type interlayer fracture toughness of flax, glass and flax fiber-glass fiber hybrid composites was studied through the double cantilever beam (DCB) test. AE technology was used to monitor DCB tests to determine the different failure mechanisms of these composites, as shown in Figure 1.25. In order to evaluate the damage mechanism in the samples studied during the DCB test, the AE signal was recorded and analyzed by considering the statistical multivariate analysis using Noesis software. It was found that the damage mechanism in type I stratification could be determined by multivariate statistical analysis based on the AE method. The combination of the two types of fibers caused the deviation of

the crack path, it was not observed in other composite materials, which may start when there is a large resistance. In addition, compared to mixed linen glass and glass laminates, flax fiber laminates require more energy for crack initiation.

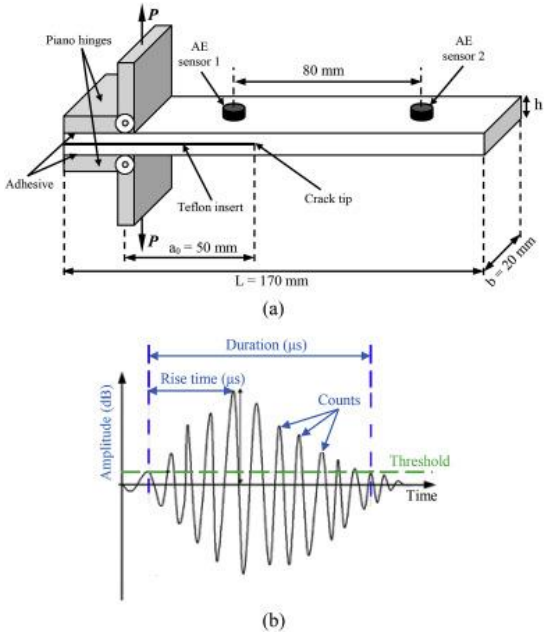

Figure 1.25 (a) Geometry and nominal dimensions of specimen for mode-I DCB test, (b) AE waveform (ref.110).

Maleki *et al.* used AE technology combined with tomographic images to study the failure of cracked aluminum plates repaired by single-sided composite materials under fatigue load [111]. The authors repaired rectangular samples made of 6061 aluminum alloy with a central through-thickness pre-crack by using glass/epoxy laminate patches. After that, the samples were fatigue loaded, and AE technology was used to monitor the impact of the repair patch on the damage progress, the AE signals of matrix cracking and adhesive layer destruction were distinguished according to their energy. As a result, it was found that the cracking of aluminum would produce an AE signal with an energy of less than 8aJ, while the cracking of the adhesive layer was more than 8aJ. In addition, it has been found that the best functionality is for 8-layer patches, which increase the fatigue life of cracked aluminum by 197%. Similarly, Andrew *et al*. used AE monitoring to study the effect of hybrid patch repair on the tensile properties of glass/epoxy composite laminates [112]. In their research, Kevlar woven fabrics based on glass and hybrid external patches bonded to both sides of the damaged matrix laminate were fabricated. The virgin and damaged specimens were taken as the reference specimens for comparison of residual mechanical properties and damage mechanisms. Simultaneously, the real-time AE monitoring technology was adopted to monitor the damage evolution and destruction progress of repaired glass/epoxy samples. The different damage

curves depicted by the AE results connected with the mechanical test results reveal the effect of the mechanical load on the change of the destruction mechanism. Besides, the AE results have a good correlation with the photographic images of the fractured specimens.

1.4.3. Infra-Red Thermography (IRT)

Thermal imaging technology refers to the application of infrared detectors and optical imaging objectives to receive the infrared radiation energy distribution pattern of the measured target reflected on the photosensitive element of the infrared detector, thereby obtaining an infrared thermal image. It is the integration of many high technologies such as thermal imaging technology, infrared calibration technology, image processing technology, and image compression and recovery technology [113]. Thermal imaging technology is based on the fact that all things heat up. Although many objects can't see anything from the outside, there are still hot and cold points on it. IRT allows humans to surpass visual obstacles so that people can "see" the temperature distribution on the surface of objects, as shown in Figure 1.26. Popularly speaking, the infrared camera is to convert the invisible infrared energy emitted by the object into a visible thermal image. The different colors on the thermal image represent the different temperatures of the measured objects.

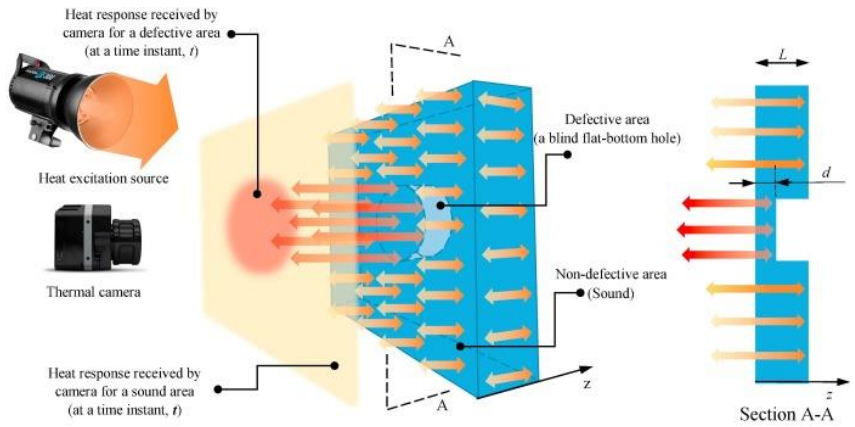

Figure 1.26 Schematic of heat diffusion and response of Infra-Red Thermography through a defective material (ref.113).

IRT inspections can be divided into two methods: passive thermal and active thermal imaging. Passive thermography measures thermal variations of materials by an infrared vision device without external thermal sources. In passive thermography, the features of interest are naturally at a higher or lower temperature than the background. On the contrary, active thermal imaging requires external heat sources to stimulate the material being tested. The original heat sources can be a hot air gun, hot water nozzle, hot air nozzle or hot water bottle [114]. Generally, the destruction of composite materials in mechanical testing, the monitoring

of the health of composite structures and other thermomechanical behaviors can be achieved using passive thermal imaging technology. IRT imaging possesses many advantages that make its applications wide. In the first place, it is an online method for non-destructive testing, which means it can eliminate the time delay of receiving results. Then, it is a non-invasive measurement, which means that there will be no non-subjective interruption and downtime during the experiments or monitoring process. Besides, this is also a non-contact method that can mitigate the occurrence of danger and the need for experienced personnel, workers can safely monitor extremely high temperatures or dangerous objects. Compared with other monitoring technologies, IRT does not apply harmful radiation. Therefore, it is suitable for long-term repeated use [113, 114].

Swiderski *et al*. investigated the possibilities for detecting defects in multilayer carbon reinforced epoxy composites through laser-excited thermography [115]. They used IRT imaging technology with laser thermal stimulation to conduct non-destructive testing on composite samples with intentionally introduced defects, and performed corresponding computer numerical simulations. In the experimental test, the semiconductor laser with a wavelength of 808 nm and a maximum power of 32W for thermal stimulation were adopted. The thermal imaging camera FLIR 7600SC was used to record the temperature field changes on the surface of the test sample. The author suggested that lasers can be used as the heating source in the thermal imaging non-destructive testing of composite materials.

One-sided thermal non-destructive testing is one application form of IRTs, which is of vital importance in composites fields to monitor structural degradation, as well as to detect subsurface defects [116]. Vavilov and his teammates characterized defects in carbon fiber reinforced polymer composites and studied the behaviors of low-speed impact damages with this method. This experiment proved the effectiveness of one-sided thermal inspection in composite material defect detection and inspection. However, this technology is still mainly qualitative. On this basis, the author validated this technology on the numerical 3D model of impact damage. Even if the quantitative characteristics of the technology were to be further explored, it also showed the feasibility of "slicing" the test samples at the depth of the defect, thereby realizing the reference-free dynamic thermal imaging technology.

Locking thermal imaging technology is also a type of thermal imaging technology, which is based on the application of periodic thermal energy input to the surface of an object. When the generated heat wave encounters defects, some of it is reflected, resulting in a phase shift

relative to the input heat wave. The depth range of defect detection depends on the thermal diffusion length. Palumbo *et al.* used locking thermal imaging technology combined with ultrasonic analysis to evaluate the debonding of composite bonded joints [117]. Glass fiber reinforced thermosetting plastic bonded joints were fabricated and exerted to the static tensile mechanical testing and accelerated ageing cycles. Locking thermal imaging technology was applied to determine the ability and reliability of the non-destructive tests. The experimental results showed that the lock-in thermal imaging technology can provide information about the "correctness" of the manufacturing process and can indicate where the process could be improved. The author also believed that the lock-in thermal imaging technology itself had become an excellent non-destructive testing tool for evaluating the condition of initially manufactured bonded composite components and an effective tool for tracking the performance of parts under various environmental conditions.

Eddy current thermography is another form of IRT, which is also known as induction thermal imaging. It is a combination of eddy current and thermal imaging that based on electromagnetic induction and Joule effect heating. This method has many advantages, such as non-contact, fast, full-field and high resolution. Xu *et al*. explored the feasibility of eddy current pulsed thermal imaging for detecting surface defects in glass fiber reinforced polymer composites, a typical non-conductive material [118]. They introduced metal parts as heat-generating parts to generate induced heat under the eddy current excitation. The generated heat is then effectively transferred to the composite material, so that the IR temperature record can be used to detect surface defects in the composite material, as shown in Figure 1.27. Theoretical analysis showed that the best heating element selection of the proposed method was metal parts with higher magnetic permeability, lower electrical conductivity, lower thermal conductivity and smaller thickness. From the recorded thermal analysis chart and thermal response data, it could be proved that the proposed detection method can effectively detect and characterize the defects of flat-bottom back-drilled holes. Besides, this method can well detect the corresponding delamination caused by surface damage and impact.

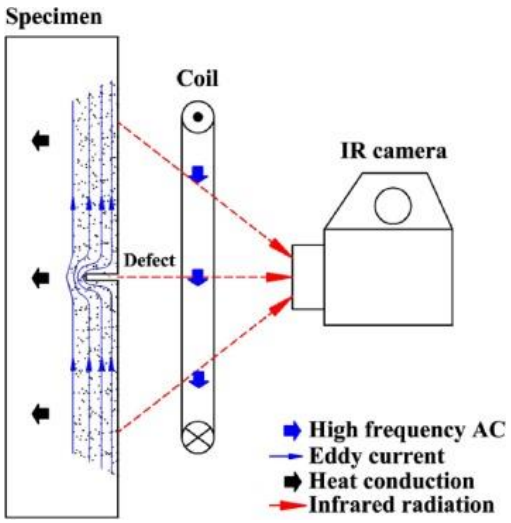

Figure 1.27 Fundamentals of eddy current pulsed thermal to detect defect (ref.118).

Microwave thermography is a new heating IRT based on dielectric loss, which is a process in a series of electromagnetic heating technologies (such as induction, radio frequency, direct resistance, or IR heating). This method possesses many advantages such as fast heat transfer, relatively uniform heating mode, volume and selective heating, compact equipment, fast switching speed and no combustion. In industry, the frequency of microwave thermography is close to 900MHz or 2450MHz, whose main purpose is to minimize interference with communication services [114].

French Bethune University Institute of Technology has developed microwave pulse thermal imaging technology for defect detection in composite materials [119]. In their experiments, commercial magnetrons generated microwaves with a frequency of 2.45GHz. A tapered horn antenna with an opening of 40 °was used to direct the microbeam onto the test sample. The infrared sensor was sensitive enough to medium waves in the range of 3-5μm and a 320 × 256 matrix detector was used in InSb, which is placed 1.5m away from the sample in the direction of 55 °to detect the entire area of the microwave-heated beam. The antenna was placed in a 45 ° direction. Thermograms were recorded at 1Hz by a computer, synchronized to the IR camera, using the ALTAIR program. The CFRP specimen was heated with a power of 360W for 150s. The tests on defect and virgin samples had the same procedure. The experimental results are shown in the Figure 1.28. Obviously, defects can be found in the middle of the sample. Lack of adhesive makes it hotter than other areas without defects. The authors believed that microwave excitation is a large amount of heat source and is suitable for deep defects in materials. The CO_2 laser excitation is a powerful surface heating source, which can provide excellent performance for defects near the surface of the material.

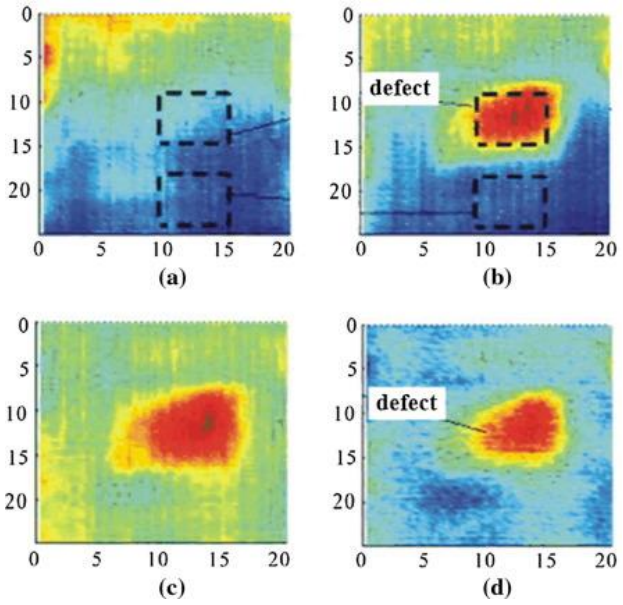

Figure 1.28 (a) Specimen without defect, (b) specimen with defect, (c) subtraction between the sample with defect and the sound sample, and (d) the subtraction of thermogram (ref.119).

1.4.4. Electromechanical impedance

Electromechanical impedance (EMI) technology is a new non-destructive testing method that combines the characteristics of piezoelectric materials with mechanical wave theory. The piezoelectric sheet (PZT) is attached to the surface or inserted inside of the structure for the detection or monitoring works. When an alternating voltage with a certain frequency is applied to the PZT, a certain force will be generated on the surface of the structure, which causes the external structure to vibrate, and the vibration causes the piezoelectric element to deform. EMI is an application of self-sensing characteristics. That is, under the effect of positive and negative piezoelectric effects, the mechanical impedance of the structure and the electrical impedance of the piezoelectric sheet are coupled to each other, as shown in Figure 1.29. When the structure is damaged, the mechanical impedance changes, which would reflect in the coupled electrical impedance. By comparing the electrical impedance spectrum of the piezoelectric sheet when the structure is free of defects, it is possible to determine the internal damage development of the structure, which can be used for health monitoring and damage diagnosis of the structure. This technology was initially applied to the development of cutting-edge weapon delivery vehicles with great success. It has been widely used in various industrial sectors and gradually developed into a conventional non-destructive method [120, 121].

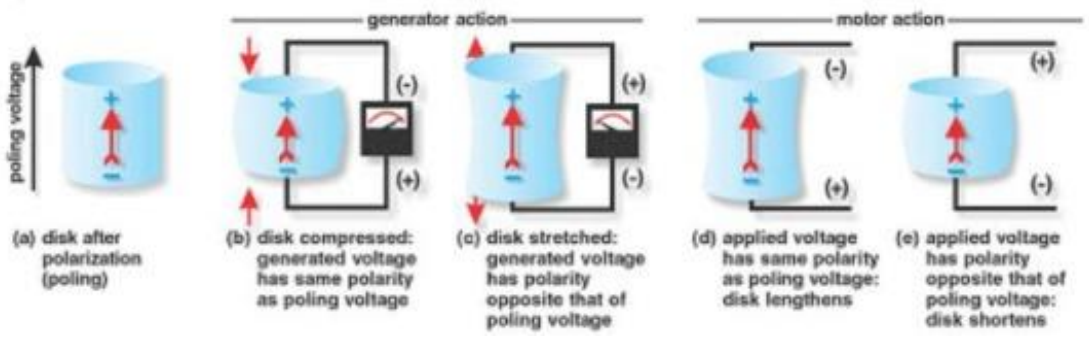

Figure 1.29 Direct and reverse piezoelectric effects (ref.121).

This method has many advantages. Firstly, its working frequency used is very high (10kHz~2MHz), so it is very sensitive to damage in the initial stage and small changes in the overall structure, which is conducive to timely and effective measures. Next, due to the sensitive range is limited to a certain area near the PZT sensors, the far-field effect will be isolated so that it can accurately identify the location of the damage. Besides, the PZT sensors exhibit good properties under normal operating conditions: large linear range, fast response, light weight, high cost-efficiency ratio and good long-term stability [121,122].

Saint-Pierre *et al*. used the EMI method to monitor the resin curing during the glass fiber/epoxy material manufacturing process and the hydrolytic degradation during the service life [122]. They inserted the PZT disc into glass fiber reinforced epoxy composite material. The measurement of PZT used in passive mode during the manufacturing process enables the author to calculate the velocity and attenuation of the waves propagating in the medium around the PZT, thereby providing them with information about the structure of the resin matrix. In addition, the author also hydrolyzed the composite material sample and monitored the experiment by impedance method. The results indicated that water absorption causes an increase in electrical impedance. This increase is due to the diffusion of water into the polymer network of the resin, thereby increasing its modulus. Based on these results, the author suggested that the EMI technique has been proven to be suitable for structure health monitoring. Zhu *et al*. used a real-time EMI method to monitor and detect composite patch repair structures [123]. In their experiments, a thin titanium plate was used to simulate the metal structure. The high-strength epoxy resin was used to bond the T800 composite patch to the substrate, and the same epoxy resin mounted the 3×3 PZT array on the top surface of the patch to detect the patch-titanium substrate interface peeling off. By coupling sensitive components in the constitutive, usable signatures were extracted from the measured raw signals to utilize quantitative degumming identification. Then the extracted signature was

applied to calculate the damage index. The experimental results showed that the real-time active monitoring scheme proposed in this paper can accurately identify the degumming location and severity.

Hwang *et al.* used the EMI technique to investigate the effect of the crack length on the piezoelectric damage monitoring of glass fiber epoxy composite DCB specimens [124], as shown in Figure 1.30. He used a DCB specimen to perform the dynamic test of mode I, and analyzed the relationship between the crack length and the charge signal measured from the electrode on the DCB specimen. It is observed that when the crack tip approaches the electrode, the amplitude of the charge signal increases very slowly; when the crack tip passes through the electrode, the amplitude of the charge signal rises sharply; then, when the crack tip approaches the electrode, the amplitude of the charge signal decreases rapidly and keep it at a relatively low level. The study of mechanical behavior by finite element analysis during the dynamic test showed that the trend of the charge signal is very similar to the strain change trend of the glass fiber epoxy composite material near the electrode. Based on the obtained experimental results and finite element analysis, the author concluded that piezoelectric damage monitoring can detect crack propagation.

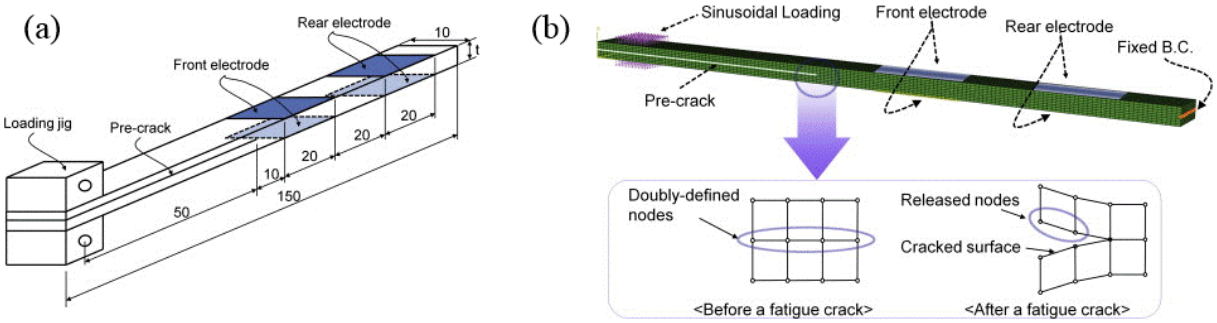

Figure 1.30 (a) DCB specimens of unidirectional glass fiber epoxy composites. (b) The finite-element model of the DCB specimens (ref.124).

1.5. Main research topics

1. Epoxy curing mechanism optimization.

The bio-epoxy curing reaction is a typical dual-stage curing system, given by the evidence of two exothermic peaks and dramatic variation of the apparent activation energy. The dual-stage curing system was separated by controlling the curing conditions, then both isothermal and dynamic DSC tests were used to study these two curing stages.

2. Preparation of flax reinforced epoxy composite, as well as smart composite patches.

In this part, the flax fiber reinforced bio-epoxy composites were manufactured by hand lay-up method. The ratio of epoxy resin and hardener has been optimized in previous studies, and the curing condition was determined by epoxy curing kinetic study. In addition, the smart composite was fabricated by introducing the piezoelectric sensors, which also through hand lay-up method.

3. Mechanical properties and failure study of flax reinforced epoxy composite.

The purpose of this part is to study the mechanical properties of flax fiber-reinforced bio-epoxy composites and to explore its feasibility as external reinforcement for building components. The mechanical characterization was performed using the DMA test, tensile test. Besides, the tensile failure and fracture performance of unidirectional flax fiber reinforced epoxy composites were studied by non-destructive detection techniques: acoustic emissions and electromechanical impedance test.

4. Durability research on composite materials.

Fiber-reinforced epoxy composites have received a lot of attention on enhancing the damaged structures. They are usually bonded on the surface to protect the infrastructure from the inner stress and external erosion and to limit crack growth, which poses another question of durability. In this part, the durability of composites when exposed to different environmental conditions, water immersion, freeze-thaw cycles, and wet-dry cycles were mentioned.

5. Shear lap test of composites bonded concrete material.

The bonding interface between the composite reinforcement sheet and the infrastructure is regarded as the weak link of the entire reinforced component. Interfacial peeling is a brittle failure that occurs suddenly without obvious warning signs. This part is the application of all this thesis, smart composite reinforcement system was bonded on the surface of concrete, then the interfacial strength was measured by single shear-lap test.

1.6. References

1. Zollo R F. Fiber-reinforced concrete: an overview after 30 years of development[J]. Cement and concrete composites, 1997, 19(2): 107-122.
2. Kim S B, Yi N H, Kim H Y, et al. Material and structural performance evaluation of recycled PET fiber reinforced concrete[J]. Cement and concrete composites, 2010, 32(3): 232-240.
3. Lau K, Zhou L. Mechanical performance of composite-strengthened concrete structures[J]. Composites Part B: Engineering, 2001, 32(1): 21-31.
4. Hollaway L C. The evolution of and the way forward for advanced polymer composites in the civil infrastructure[J]. Construction and Building Materials, 2003, 17(6-7): 365-378.

5. Pendhari S S, Kant T, Desai Y M. Application of polymer composites in civil construction: A general review[J]. Composite structures, 2008, 84(2): 114-124.
6. Mase L Z, Likitlersuang S, Tobita T. Analysis of seismic ground response caused during strong earthquake in Northern Thailand[J]. Soil Dynamics and Earthquake Engineering, 2018, 114: 113-126.
7. Baggio D, Soudki K, Noel M. Strengthening of shear critical RC beams with various FRP systems[J]. Construction and Building Materials, 2014, 66: 634-644.
8. Goudenhooft C, Bourmaud A, Baley C. Conventional or greenhouse cultivation of flax: What influence on the number and quality of flax fibers?[J]. Industrial crops and products, 2018, 123: 111-117.
9. Kerni L, Singh S, Patnaik A, et al. A review on natural fiber reinforced composites[J]. Materials Today: Proceedings, 2020.
10. Abdy A I, Hashemi M J, Al-Mahaidi R. Fatigue life improvement of steel structures using self-prestressing CFRP/SMA hybrid composite patches[J]. Engineering Structures, 2018, 174: 358-372.
11. Jirawattanasomkul T, Likitlersuang S, Wuttiwannasak N, et al. Behaviour of Pre-damaged Reinforced Concrete Beams Strengthened with Natural Fibre Reinforced Polymer Composites[J]. Composite Structures, 2020: 112309.
12. Zhuang B, Liu Y, Wang D. Shear mechanism of Rubber-Sleeved Stud (RSS) connectors in the steel-concrete interface of cable-pylon composite anchorage[J]. Engineering Structures, 2020, 223: 111183.
13. Teguedy M C, Joly-Lapalice C, Sorelli L, et al. Optical fiber sensors implementation for monitoring the early-age behavior of full-scale Timber-Concrete Composite slabs[J]. Construction and Building Materials, 2019, 226: 564-578.
14. Jin M, Jiang Y, Jiang L, et al. Fabrication and characterization of pseudo reference electrode based on graphene-cement composites for corrosion monitoring in reinforced concrete structure[J]. Construction and Building Materials, 2019, 204: 144-157.
15. Ding S, Ruan Y, Yu X, et al. Self-monitoring of smart concrete column incorporating CNT/NCB composite fillers modified cementitious sensors[J]. Construction and Building Materials, 2019, 201: 127-137.
16. Neves R M, Ornaghi Jr H L, Zattera A J, et al. Recent Studies on Modified Cellulose/Nanocellulose Epoxy Composites: A Systematic Review[J]. Carbohydrate Polymers, 2020: 117366.
17. Properties and performance of natural-fibre composites[M]. Elsevier, 2008.
18. Heller K, Woznica Z, Byczynska M, et al. The efficacy of Salicylic and Acetylsalicylic Acids in the protection of fibrous flax against drought stress[J]. Journal of natural fibers, 2013, 10(1): 29-39.
19. Nilsson D. Dynamic simulation of the harvest operations of flax straw for short fibre production—part 1: model description[J]. Journal of natural fibers, 2006, 3(1): 23-34.
20. Vigneshwaran S, Sundarakannan R, John K M, et al. Recent advancement in the natural fiber polymer composites: a comprehensive review[J]. Journal of Cleaner Production, 2020: 124109.
21. Rolski S, Heller K. Yielding capacity of different flax cultivars in varied environmental condition[J]. Natural fibres, 1998, 2: 84-88.
22. Heller K, Konczewicz W, Byczyńska M, et al. The effect of fibre flax growing technologies on ontogenesis and cultivars yielding capacity[C]//Conference on Flax and other Bast Plants. 2008: 315-25.
23. Pasila A. The effect of frost on fibre plants and their processing[J]. Molecular Crystals and Liquid Crystals Science and Technology. Section A. Molecular Crystals and Liquid Crystals, 2000, 353(1): 11-22.

24. Archibald L B. Quality in Flax Fibre, in “The Biology and Processing of Flax,” HSS Sharma and CF Van Sumere[J]. 1992.
25. Baley C, Busnel F, Grohens Y, et al. Influence of chemical treatments on surface properties and adhesion of flax fibre–polyester resin[J]. Composites Part A: Applied Science and Manufacturing, 2006, 37(10): 1626-1637.
26. Alkbir M F M, Sapuan S M, Nuraini A A, et al. Fibre properties and crashworthiness parameters of natural fibre-reinforced composite structure: A literature review[J]. Composite Structures, 2016, 148: 59-73.
27. Kessler R W, Becker U, Kohler R, et al. Steam explosion of flax—a superior technique for upgrading fibre value[J]. Biomass and Bioenergy, 1998, 14(3): 237-249.
28. Bos H L, Müssig J, van den Oever M J A. Mechanical properties of short-flax-fibre reinforced compounds[J]. Composites Part A: Applied Science and Manufacturing, 2006, 37(10): 1591-1604.
29. Charlet K, Baley C, Morvan C, et al. Characteristics of Hermès flax fibres as a function of their location in the stem and properties of the derived unidirectional composites[J]. Composites Part A: Applied Science and Manufacturing, 2007, 38(8): 1912-1921.
30. Stamboulis A, Baillie C A, Peijs T. Effects of environmental conditions on mechanical and physical properties of flax fibers[J]. Composites Part A: Applied Science and Manufacturing, 2001, 32(8): 1105-1115.
31. Jia Y, Fiedler B. Tensile creep behaviour of unidirectional flax fibre reinforced bio-based epoxy composites[J]. Composites Communications, 2020, 18: 5-12.
32. Andersons J, Poriķe E, Spārniņš E. The effect of mechanical defects on the strength distribution of elementary flax fibres[J]. Composites Science and Technology, 2009, 69(13): 2152-2157.
33. Gouanvé F, Marais S, Bessadok A, et al. Kinetics of water sorption in flax and PET fibers[J]. European Polymer Journal, 2007, 43(2): 586-598.
34. Bergfjord C, Holst B. A procedure for identifying textile bast fibres using microscopy: flax, nettle/ramie, hemp and jute[J]. Ultramicroscopy, 2010, 110(9): 1192-1197.
35. Huang X, Netravali A. Characterization of flax fiber reinforced soy protein resin based green composites modified with nano-clay particles[J]. Composites Science and Technology, 2007, 67(10): 2005-2014.
36. Charlet K, Béakou A. Mechanical properties of interfaces within a flax bundle–Part I: Experimental analysis[J]. International journal of adhesion and adhesives, 2011, 31(8): 875-881.
37. Altaner C M, Jarvis M C. Modelling polymer interactions of the ‘molecular Velcro’type in wood under mechanical stress[J]. Journal of Theoretical Biology, 2008, 253(3): 434-445.
38. Saheb D N, Jog J P. Natural fiber polymer composites: a review[J]. Advances in Polymer Technology: Journal of the Polymer Processing Institute, 1999, 18(4): 351-363.
39. Baley C. Analysis of the flax fibres tensile behaviour and analysis of the tensile stiffness increase[J]. Composites Part A: Applied Science and Manufacturing, 2002, 33(7): 939-948.
40. Bodros E, Baley C. Study of the tensile properties of stinging nettle fibres (Urtica dioica) [J]. Materials Letters, 2008, 62(14): 2143-2145.
41. Snoeck D, De Belie N. Mechanical and self-healing properties of cementitious composites reinforced with flax and cottonised flax, and compared with polyvinyl alcohol fibres[J]. Biosystems Engineering, 2012, 111(4): 325-335.

42. Li M, Pu Y, Thomas V M, et al. Recent advancements of plant-based natural fiber–reinforced composites and their applications[J]. Composites Part B: Engineering, 2020: 108254.
43. Khandai S, Nayak R K, Kumar A, et al. Assessment of Mechanical and Tribological Properties of Flax/Kenaf/Glass/Carbon Fiber Reinforced Polymer Composites[J]. Materials Today: Proceedings, 2019, 18: 3835-3841.
44. De Fazio D, Boccarusso L, Durante M. Tribological Behaviour of Hemp, Glass and Carbon Fibre Composites[J]. Biotribology, 2020, 21: 100113.
45. Stuart T, Liu Q, Hughes M, et al. Structural biocomposites from flax—Part I: Effect of bio-technical fibre modification on composite properties[J]. Composites Part A: Applied Science and Manufacturing, 2006, 37(3): 393-404.
46. Baley C, Le Duigou A, Bourmaud A, et al. Influence of drying on the mechanical behaviour of flax fibres and their unidirectional composites[J]. Composites Part A: Applied Science and Manufacturing, 2012, 43(8): 1226-1233.
47. Yan L, Chouw N, Yuan X. Improving the mechanical properties of natural fibre fabric reinforced epoxy composites by alkali treatment[J]. Journal of Reinforced Plastics and Composites, 2012, 31(6): 425-437.
48. Alix S, Philippe E, Bessadok A, et al. Effect of chemical treatments on water sorption and mechanical properties of flax fibres[J]. Bioresource technology, 2009, 100(20): 4742-4749.
49. Bos H L, Van Den Oever M J A, Peters O. Tensile and compressive properties of flax fibres for natural fibre reinforced composites[J]. Journal of Materials Science, 2002, 37(8): 1683-1692.
50. Martin N, Mouret N, Davies P, et al. Influence of the degree of retting of flax fibers on the tensile properties of single fibers and short fiber/polypropylene composites[J]. Industrial crops and products, 2013, 49: 755-767.
51. Herrmann A S, Nickel J, Riedel U. Construction materials based upon biologically renewable resources—from components to finished parts[J]. Polymer Degradation and Stability, 1998, 59(1-3): 251-261.
52. Hearle J W S. The fine structure of fibers and crystalline polymers. III. Interpretation of the mechanical properties of fibers[J]. Journal of applied polymer science, 1963, 7(4): 1207-1223.
53. Zhang D, Milanovic N R, Zhang Y, et al. Effects of humidity conditions at fabrication on the interfacial shear strength of flax/unsaturated polyester composites[J]. Composites Part B: Engineering, 2014, 60: 186-192.
54. Wielage B, Lampke T, Marx G, et al. Thermogravimetric and differential scanning calorimetric analysis of natural fibres and polypropylene[J]. Thermochimica Acta, 1999, 337(1-2): 169-177.
55. Gassan J, Bledzki A K. Thermal degradation of flax and jute fibers[J]. Journal of Applied Polymer Science, 2001, 82(6): 1417-1422.
56. Kohler R, Wedler M. Nichttextile Anwendungen von Flachs[C]//Proc Techtextil-Symposium. 1994, 6: 1-8.
57. A, Daoshun Xue , and H. H. B . "Mechanical properties of biaxial weft-knitted flax composites. "Materials & Design 46.1(2013):264-269.
58. Balla V K, Kate K H, Satyavolu J, et al. Additive manufacturing of natural fiber reinforced polymer composites: Processing and prospects[J]. Composites Part B: Engineering, 2019: 106956.
59. Zhang Y, Li Y, Ma H, et al. Tensile and interfacial properties of unidirectional flax/glass fiber reinforced hybrid composites[J]. Composites Science and Technology, 2013, 88: 172-177.

60. Le Duigou A, Pillin I, Bourmaud A, et al. Effect of recycling on mechanical behaviour of biocompostable flax/poly (l-lactide) composites[J]. Composites Part A: Applied Science and Manufacturing, 2008, 39(9): 1471-1478.
61. Ramesh M. Flax (Linum usitatissimum L.) fibre reinforced polymer composite materials: A review on preparation, properties and prospects[J]. Progress in Materials Science, 2019, 102: 109-166.
62. Muralidhar B A. Study of flax hybrid preforms reinforced epoxy composites[J]. Materials & Design (1980-2015), 2013, 52: 835-840.
63. Shah D U, Schubel P J, Clifford M J, et al. Fatigue life evaluation of aligned plant fibre composites through S–N curves and constant-life diagrams[J]. Composites Science and Technology, 2013, 74: 139-149.
64. Liang S, Gning P B, Guillaumat L. Properties evolution of flax/epoxy composites under fatigue loading[J]. International Journal of Fatigue, 2014, 63: 36-45.
65. Bar M, Alagirusamy R, Das A, et al. Low velocity impact response of flax/polypropylene hybrid roving based woven fabric composites: Where does it stand with respect to GRPC?[J]. Polymer Testing, 2020: 106565.
66. Andersons J, Modniks J, Joffe R, et al. Apparent interfacial shear strength of short-flax-fiber/starch acetate composites[J]. International Journal of Adhesion and Adhesives, 2016, 64: 78-85.
67. Manral A, Ahmad F, Chaudhary V. Static and dynamic mechanical properties of PLA bio-composite with hybrid reinforcement of flax and jute[J]. Materials Today: Proceedings, 2019.
68. Matykiewicz D, Barczewski M. On the impact of flax fibers as an internal layer on the properties of basalt-epoxy composites modified with silanized basalt powder[J]. Composites Communications, 2020: 100360.
69. El Hajj N, Dheilly R M, Goullieux A, et al. Innovant agromaterials formulated with flax shaves and proteinic binder: Process and characterization[J]. Composites Part B: Engineering, 2012, 43(2): 381-390.
70. Foulk J A, Rho D, Alcock M M, et al. Modifications caused by enzyme-retting and their effect on composite performance[J]. Advances in Materials Science and Engineering, 2011, 2011.
71. Liang S, Gning P B, Guillaumat L. A comparative study of fatigue behaviour of flax/epoxy and glass/epoxy composites[J]. Composites Science and Technology, 2012, 72(5): 535-543.
72. Diener J, Siehler U. Ökologischer Vergleich von NMT‐und GMT‐Bauteilen[J]. Die Angewandte Makromolekulare Chemie, 1999, 272(1): 1-4.
73. Guo Y, Deng Y. Recycling of Flax Fiber Towards Developing Biocomposites for Automotive Application from a Life Cycle Assessment Perspective[J]. 2019.
74. Hallonet A, Ferrier E, Michel L, et al. Durability and tensile characterization of wet lay-up flax/epoxy composites used for external strengthening of RC structures[J]. Construction and Building Materials, 2019, 205: 679-698.
75. Moudood A, Rahman A, Khanlou H M, et al. Environmental effects on the durability and the mechanical performance of flax fiber/bio-epoxy composites[J]. Composites Part B: Engineering, 2019, 171: 284-293.
76. Lu M M, Van Vuure A W. Improving moisture durability of flax fibre composites by using non-dry fibres[J]. Composites Part A: Applied Science and Manufacturing, 2019, 123: 301-309.
77. Moropoulou A, Kouloumbi N, Marioli-Riga Z P, et al. Damage detectability on aluminum alloy panels under composite patching by various NDT techniques[J]. MRS Online Proceedings Library Archive, 2001, 699.

78. Yang J Q, Smith S T, Wu Y F, et al. Strengthening single-bolt timber joints with externally bonded CFRP composites[C]//Structures. Elsevier, 2020, 28: 2671-2685.
79. Xu C, Peng S, Liu X, et al. Analysis of the seismic behavior of CFRP-strengthened seismic-damaged composite steel-concrete frame joints[J]. Journal of Building Engineering, 2020, 28: 101057.
80. Manalo A C, Mohammed A A, Maranan G B. Novel Composites Jacket for Repair of Concrete Structures, Proceedings of the 13th Fiber Reinforced Polymer for Reinforced Concrete Structures (FRPRCS13)[J]. 2017.
81. Mohammed A A, Manalo A C, Maranan G B, et al. Effectiveness of a novel composite jacket in repairing damaged reinforced concrete structures subject to flexural loads[J]. Composite Structures, 2020, 233: 111634.
82. Li J, Gong J, Wang L. Seismic behavior of corrosion-damaged reinforced concrete columns strengthened using combined carbon fiber-reinforced polymer and steel jacket[J]. Construction and Building Materials, 2009, 23(7): 2653-2663.
83. Triantafyllou G G, Rousakis T C, Karabinis A I. Effect of patch repair and strengthening with EBR and NSM CFRP laminates for RC beams with low, medium and heavy corrosion[J]. Composites Part B: Engineering, 2018, 133: 101-111.
84. Belarbi A, Bae S W. An experimental study on the effect of environmental exposures and corrosion on RC columns with FRP composite jackets[J]. Composites Part B: Engineering, 2007, 38(5-6): 674-684.
85. Sen T, Reddy H N J. Efficacy of bio derived jute FRP composite based technique for shear strength retrofitting of reinforced concrete beams and its comparative analysis with carbon and glass FRP shear retrofitting schemes[J]. sustainable cities and society, 2014, 13: 105-124.
86. Raphael C. Variable-adhesive bonded joints(Stresses in ordinary lap joint compared to variable adhesive joint)[C]//STRUCTURAL ADHESIVES BONDING, SYMPOSIUM, STEVENS INST. OF TECH, HOBOKEN, N. J. 1966: 99-108.
87. Fitton M D, Broughton J G. Variable modulus adhesives: an approach to optimised joint performance[J]. International journal of adhesion and adhesives, 2005, 25(4): 329-336.
88. Da Silva L F M, Lopes M J C Q. Joint strength optimization by the mixed-adhesive technique[J]. International Journal of Adhesion and Adhesives, 2009, 29(5): 509-514.
89. Kumar S. Analysis of tubular adhesive joints with a functionally modulus graded bondline subjected to axial loads[J]. International Journal of Adhesion and Adhesives, 2009, 29(8): 785-795.
90. Carbas R J C, Da Silva L F M, Andrés L F S. Functionally graded adhesive joints by graded mixing of nanoparticles[J]. International Journal of Adhesion and Adhesives, 2017, 76: 30-37.
91. Guin W E, Wang J. Theoretical model of adhesively bonded single lap joints with functionally graded adherends[J]. Engineering Structures, 2016, 124: 316-332.
92. Boss J N, Ganesh V K, Lim C T. Modulus grading versus geometrical grading of composite adherends in single-lap bonded joints[J]. Composite Structures, 2003, 62(1): 113-121.
93. Shang X, Marques E A S, Machado J J M, et al. Review on techniques to improve the strength of adhesive joints with composite adherends[J]. Composites Part B: Engineering, 2019, 177: 107363.
94. Lee D W, Song J I. Research on simple joint method using fiber-metal laminate design for improved mechanical properties of CFRP assembly structure[J]. Composites Part B: Engineering, 2019, 164: 358-367.

95. dos Santos D G, Carbas R J C, Marques E A S, et al. Reinforcement of CFRP joints with fibre metal laminates and additional adhesive layers[J]. Composites Part B: Engineering, 2019, 165: 386-396.
96. Shang X, Marques E A S, Machado J J M, et al. A strategy to reduce delamination of adhesive joints with composite substrates[J]. Proceedings of the Institution of Mechanical Engineers, Part L: Journal of Materials: Design and Applications, 2019, 233(3): 521-530.
97. Schollerer M J, Kosmann J, Völkerink O, et al. Surface toughening–a concept to decrease stress peaks in bonded joints[J]. The Journal of Adhesion, 2019, 95(5-7): 495-514.
98. Joesbury A M, Colegrove P A, Van Rymenant P, et al. Weld-bonded stainless steel to carbon fibre-reinforced plastic joints[J]. Journal of Materials Processing Technology, 2018, 251: 241-250.
99. Chang P, Mouritz A P, Cox B N. Properties and failure mechanisms of pinned composite lap joints in monotonic and cyclic tension[J]. Composites Science and Technology, 2006, 66(13): 2163-2176.
100. Kim C H, Jo D H, Choi J H. Failure strength of composite T-joints prepared using a new 1-thread stitching process[J]. Composite Structures, 2017, 178: 225-231.
101. Avila A F, Bueno P O. An experimental and numerical study on adhesive joints for composites[J]. Composite structures, 2004, 64(3-4): 531-537.
102. Ashrafi M, Ajdari A, Rahbar N, et al. Adhesively bonded single lap joints with non-flat interfaces[J]. International journal of adhesion and adhesives, 2012, 32: 46-52.
103. Bendemra H, Compston P, Crothers P J. Optimisation study of tapered scarf and stepped-lap joints in composite repair patches[J]. Composite Structures, 2015, 130: 1-8.
104. Campilho R D S G, De Moura M, Domingues J. Numerical prediction on the tensile residual strength of repaired CFRP under different geometric changes[J]. International Journal of Adhesion and Adhesives, 2009, 29(2): 195-205.
105. Cui J, Wang S, Wang S, et al. Strength and failure analysis of adhesive single-lap joints under shear loading: Effects of surface morphologies and overlap zone parameters[J]. Journal of Manufacturing Processes, 2020, 56: 238-247.
106. Jasiūnienė E, Mažeika L, Samaitis V, et al. Ultrasonic non-destructive testing of complex titanium/carbon fibre composite joints[J]. Ultrasonics, 2019, 95: 13-21.
107. Tamborrino R, Palumbo D, Galietti U, et al. Assessment of the effect of defects on mechanical properties of adhesive bonded joints by using non destructive methods[J]. Composites Part B: Engineering, 2016, 91: 337-345.
108. Kumar R L V, Bhat M R, Murthy C R L. Some studies on evaluation of degradation in composite adhesive joints using ultrasonic techniques[J]. Ultrasonics, 2013, 53(6): 1150-1162.
109. Saeedifar M, Zarouchas D. Damage characterization of laminated composites using acoustic emission: A review[J]. Composites Part B: Engineering, 2020: 108039.
110. Saidane E H, Scida D, Pac M J, et al. Mode-I interlaminar fracture toughness of flax, glass and hybrid flax-glass fibre woven composites: Failure mechanism evaluation using acoustic emission analysis[J]. Polymer Testing, 2019, 75: 246-253.
111. Maleki A, Saeedifar M, Najafabadi M A, et al. The fatigue failure study of repaired aluminum plates by composite patches using Acoustic Emission[J]. Engineering Fracture Mechanics, 2019, 210: 300-311.

112. Andrew J J, Arumugam V. Effect of patch hybridization on the tensile behavior of patch repaired glass/epoxy composite laminates using acoustic emission monitoring[J]. International Journal of Adhesion and Adhesives, 2017, 74: 155-166.
113. Doshvarpassand S, Wu C, Wang X. An overview of corrosion defect characterization using active infrared thermography[J]. Infrared Physics & Technology, 2019, 96: 366-389.
114. Yang R, He Y. Optically and non-optically excited thermography for composites: A review[J]. Infrared Physics & Technology, 2016, 75: 26-50.
115. Swiderski W. Non-destructive testing of CFRP by laser excited thermography[J]. Composite Structures, 2019, 209: 710-714.
116. Vavilov V P, Pawar S S. A novel approach for one-sided thermal nondestructive testing of composites by using infrared thermography[J]. Polymer testing, 2015, 44: 224-233.
117. Palumbo D, Tamborrino R, Galietti U, et al. Ultrasonic analysis and lock-in thermography for debonding evaluation of composite adhesive joints[J]. Ndt & E International, 2016, 78: 1-9.
118. Xu C, Zhang W, Wu C, et al. An improved method of eddy current pulsed thermography to detect subsurface defects in glass fiber reinforced polymer composites[J]. Composite Structures, 2020: 112145.
119. Sam-Ang K, Didier D, Florin B, et al. Comparison between microwave infrared thermography and CO 2 laser infrared thermography in defect detection in applications with CFRP[J]. Materials Sciences and Applications, 2013, 2013.
120. Tuloup C, Harizi W, Aboura Z, et al. On the use of in-situ piezoelectric sensors for the manufacturing and structural health monitoring of polymer-matrix composites: A literature review[J]. Composite Structures, 2019, 215: 127-149.
121. https://www.americanpiezo.com/knowledge-center/piezo-theory/piezoelectricity.html.
122. Saint-Pierre N, Perrissin-Fabert I, Jayet Y, et al. Monitoring the hydrolytic degradation of polyester-based composites by a piezoelectric method[J]. Journal of reinforced plastics and composites, 1996, 15(7): 663-672.
123. Zhu J, Wang Y, Qing X. A real-time electromechanical impedance-based active monitoring for composite patch bonded repair structure[J]. Composite Structures, 2019, 212: 513-523.
124. Hwang H Y. Effect of the crack length on the piezoelectric damage monitoring of glass fiber epoxy composite DCB specimens[J]. Composites science and technology, 2012, 72(8): 902-907.

Chapter 2. Kinetic studies on a dual-stage curing epoxy resin system

A low molecular weight "green" epoxy resin that made from bio-based epichlorhydrine epoxy resin (CHS-EPOXY G-520) and a solvent-free, low viscosity phenalkamine hardener (Cardolite NX5619) blends were prepared by mechanical mixing, then the curing kinetics of this system was investigated with several kinetic methods by means of differential scanning calorimetry (DSC). The exothermic curves show that this is a typical dual-stage curing system. Both isothermal and dynamic DSC tests were adopted to analyze the first and second curing stage, respectively. The classical isoconversional methods were used to determine the apparent and real-time activation energies (Ea), and the results indicate that the value of Ea decreases slightly until the range of two exothermic peaks overlapped, then increases as the second curing period proceeds. The particular model-fitting methods were used to demonstrate the kinetics equations, whose results ascertain the transition from Kamal autocatalytic model to autocatalytic model of the whole reaction. Good confidence was observed between the calculated data and the experimental data.

2.1. Introduction

Epoxy resin is a high performance industrial thermosetting that has wide applications in various fields for its many excellent properties, such as high mechanical strength and adhesion, low cure shrinkage, superior chemical resistance and thermostability [1-3]. On the other hand, the higher quality epoxy resin is always expected. Generally speaking, the polymerization of epoxy resin is the forming process of a 3 dimensional (3D) crosslinking network, whose degree directly determines the properties and the applications of the materials. The other way round, the final quality of epoxy products not only depends on the original materials but equally on the fabrication procedures related to the curing mechanism [4,5]. To select the ideal curing conditions and obtain the best performance materials, the importance of curing kinetics is self-evident. Of which, comprehensive understanding and reasonable applying of the curing kinetics are instructive for optimizing the curing parameters and further getting the ideal properties of materials.

The curing reaction of epoxy is a typical exothermic process, which gives the DSC technique more applicability to do the kinetics investigation. Over the past decades, scientists have been studying and exploring many curing kinetics of epoxy resin by isothermal and dynamic DSC measurements for various applications, and many kinetic models have been proposed. [4-7]. With years of exploration, three types of kinetic models about the thermoset resins have been gradually formed, (1) the *n*th-order model, (2) the autocatalytic model and (3) the Kamal autocatalytic model. The main differences of those classifications are based on whether the maximum rate of the cross-linking reaction occurs at zero conversion or at a certain conversion rate [8-10].

With those kinetic models, researchers usually regard the apparent Ea, a constant data that deduced from isoconversional method, as the fixed Ea of the whole curing reaction [11]. However, the mechanism of curing process is very complex. It contains so many correlated physical and chemical reaction steps, such as the transitions from the linear growth of the molecular chain to gelation to vitrification, or the shift from chemical reaction control to diffusion control [12,13]. All those different reaction courses possess various energy barriers, the apparent Ea is far from precisely reflecting the real value during the whole reaction period. Hence, simply taking the apparent Ea as the desired energy of the whole curing process may not be totally appropriate, analysis with more accurate Ea is still needed.

The curing mechanism and kinetics of epoxy resin have been the subject for many studies. However, the specific research is still less abundant about curing of epoxy with more than one curing stage, in particular, accompanying the dramatic change of the Ea. In this section, the dual-stage curing system was separated by controlling the curing conditions, then both isothermal and dynamic DSC tests were conducted to study the curing kinetics with different models. By means of those analyzing methods, a more comprehensive and in-depth perceive about our certain system was given.

2.2. Experiments

2.2.1. Materials

In this work, the thermoset resin system is designed for ambient and low-temperature cure. The Bisphenol A diglycidyl ether (DGEBA) prepolymer is a low molecular weight “green” epoxy resin that made from bio-based epichlorhydrine. The hardener is a solvent-free, low viscosity phenalkamine curing agent that made through the Mannich reaction of cardanol from

cashewnuts, formaldehyde, and amines. The structural formulas are given in scheme 2.1. The epoxy resin was prepared by blending the DGEBA and the hardener at a weight ratio of 1.8;1, whose stoichiometric ratio between epoxy groups and amidogen is 1:1.

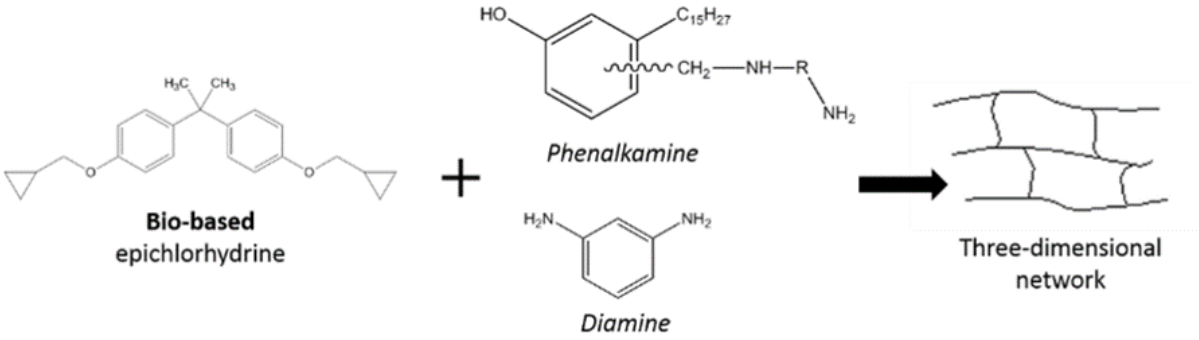

Scheme 2.1 Crosslinking reaction between epoxy monomers and bi-component hardener.

2.2.2. DSC measurement

The DSC analyses of this epoxy resin were carried out with a METTLER DSC822e thermal analyzer to measure either the heat of reaction for uncured system or the glass transition temperature (Tg) and the curing degree for cured systems. Based on our specific multiple curing system, we adopted both isothermal and dynamic tests. During the DSC test, the epoxy resin was placed in the DSC cell for a very short time to eliminate the heat history, with an ambient temperature of 40 ℃ and a nitrogen gas at a flow rate of 100 cc/min. Then, the whole system was heated up to the experimental temperature at very high rates. By that, we can minimize the improper reaction heat during the initial stage before the data analyzing process was started.

As for the test of the whole curing period, the prepared resin samples of 5-10mg were placed in aluminum pans and scanned from -80 ℃ to 300 ℃ with four different heating rates 5, 10, 15 and 20 ℃/min. The particular researches of the first curing stage were studied by isothermal test at 80, 90, 100, 110 and 120 ℃. Each isothermal test was followed by a dynamic run from -80 ℃ to 300 ℃ with 10 ℃/min to identify the final degree of conversion at that temperature. About the samples for analyzing the second curing stage, the fabrication process is a little tricky. Several patches of epoxy resin with 5 to 10mg were placed in the aluminum pans and cured at room temperature for 1 day, then samples were transferred to the oven at 90℃ for 2 hours. Subsequently, those samples were scanned with a dynamic process as mentioned above.

2.3. Theoretical foundation

Like other solid matters, the reaction rate equation of epoxy curing is given in the form that the reaction rate is proportional to some function of the amount of reactant [14], as shown in eq1:

$$\frac{d\alpha}{dt} = k(T) * f(\alpha) \qquad \text{e(1)}$$

Where dα/dt is the reaction rate, α is the amount of conversion, f(α) is the "some-function of α". The particular expression form of f(α) is known as the "kinetic model" [15], and k(T) is the reaction rate constant, the proportionality factor at absolute temperature T. In isothermal computation, it is a constant, while in non-isothermal computation, it is a function of temperature and expressed by Arrhenius equation:

$$\mathrm{k(T)} = \mathrm{A} * e^{(-Ea/RT)} \qquad \text{e(2)}$$

where A is the pre-exponential factor, Ea is the activation energy, R is the universal gas constant (8.314 J/mol*K) and T is the absolute temperature.

For further analyzation of the DSC results by isoconversional method, there are two important hypotheses: (1) the total area of the exothermic curve is in direct proportion to the whole reaction heat, as shown in the equation:

$$\mathrm{H(t)}=\int_{t0}^{t1} Q(t)dt \qquad \text{e(3)}$$

(2) the reaction rate of the functional groups is assumed to be proportional to the heat flow [16]. Hence, the conversion at time *t*, *α*(*t*), can be determined from the equation:

$$\alpha(\mathrm{t})= \frac{H(t)}{\delta H} \qquad \text{e(4)}$$

where H(t) is the enthalpy change, Q(t) is the reaction heat, t is reaction time and δH is the total enthalpy change of the whole reaction. With those hypotheses, we can regard that the heat accumulated at any time is proportional to the overall content that the reactive material has been consumed. About the model-fitting methods of epoxy curing reactions, there are some equations that have been widely used [8-10,17].

In case of the *n*-th order reaction model, the reaction rate equation is followed:

$$\frac{d\alpha}{dt} = A * \exp(\frac{-Ea}{RT}) * (1-\alpha)^2 \qquad \text{e(5)}$$

In case of the autocatalytic reaction model, the reaction rate equation is followed:

$$\frac{d\alpha}{dt} = A * \exp(\frac{-Ea}{RT}) * \alpha^m * (1-\alpha)^2 \quad \text{e(6)}$$

In case of the Kamal autocatalytic reaction model, the reaction rate equation is followed:

$$\frac{d\alpha}{dt} = (\mathrm{k1} + \mathrm{k2} * \alpha^m) * (1-\alpha)^n \quad \text{e(7)}$$

Where m and n are reaction orders, k1 and k2 are reaction rate constants. In the form of the expression, the Kamal autocatalytic reaction model is the combination of the other two models, and it assumes that the curing process involves two steps. The first one is the uncatalyzed epoxy ring-opening reaction, and it produces hydroxyl groups that initiate the second step, which is the catalyzed epoxy ring-opening reaction. The rate constants k1 and k2 represent respectively the uncatalyzed and catalyzed steps [18]. If the value of k1 is zero, which means there is no uncatalyzed step, then the Kamal reaction model turns into the autocatalytic reaction model, as shown in eq6. If the value of k2 is zero, then the Kamal reaction model becomes the *n*-th order reaction model.

The apparent Ea is an important kinetics parameter because it is representative of the main energy barrier in each reaction. Its value can be used to confirm the rate-determining step and further to control the whole reaction system. There are several isoconversional methods to calculate the apparent Ea, such as Friedman method, Kissinger method, and Ozawa method [19-21]. More often than not, those methods are also known as model-free methods. This kind of method does not make hypothesizing models, it usually performs a series of DSC experiments in which small milligram quantities of the reacting material are heated at different heating rates (β) and yields the corresponding values of the Ea as a function of conversion [22]. The final expressions of the equations are different based on each method.

In case of the Friedman method:

$$\ln(\beta * \frac{d\alpha}{dT}) = \ln[A * f(\alpha)] - \frac{Ea}{RT} \quad \text{e(8)}$$

In case of the Kissinger method:

$$\ln\left(\frac{\beta}{T^2}\right) = -\frac{Ea}{RT} + ln\frac{AR}{Ea} \quad \text{e(9)}$$

In case of the Ozawa method:

$$\ln\beta = \mathrm{const} - 1.052 * \frac{Ea}{RT} \quad \text{e(10)}$$

2.4. Results and discussions

The typical DSC thermograms of the whole curing process by non-isothermal scan are shown in Figure 2.1a. It can be observed that there are two broad and relative independent exothermic peaks, which is a characteristic of this two-stage epoxy crosslinking reaction. The percentage of the second peak increases with higher heating rates due to the thermal hysteresis, and it gets more prominent with heavier tested sample. Besides, the heating rates have little influence on the total reaction enthalpy change: $\Delta H_{total} = 321 \pm 6$ J/g. Usually, the curing reaction of the epoxy resin can be divided into several different stages. In the initial stage or the induction period, the curing rate is very slow and the test sample gradually changes from liquid to the gel. In the middle stage, the curing rate begins to increase rapidly and reaches a maximum at peak conversion. In the final termination phase, the crosslinking degree of the network structure increases further, the resin gradually turns to a glassy state and the cure rate reduces significantly. Correspondingly, during the whole curing period, curve of conversion rate versus temperature is a standard sigmoidal shape. However, for this special curing system, the situation is a little different, instead of the standard sigmoidal shape, it can be observed that a stranded region of conversion degree who appears around 80%, as shown in Figure 2.1b. This phenomenon results from the two stages curing and the backwater area corresponds to the transition period from the first curing stage to the second curing stage.

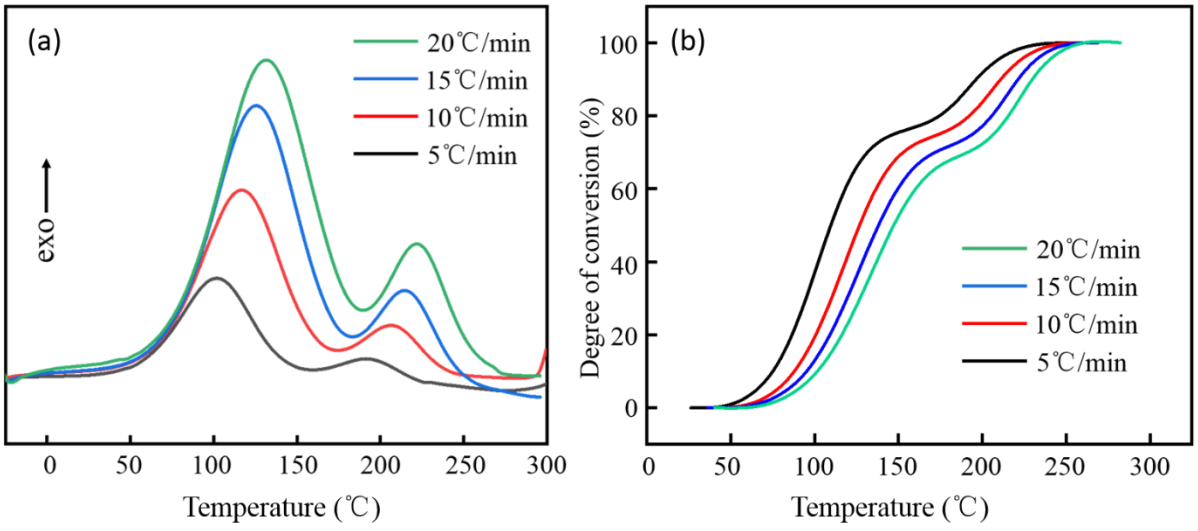

Figure 2.1 (a) Dynamic DSC curves in 4 different heating rates. (b) Degree of conversion as a function of temperatures in 4 different heating rates.

2.4.1. The evolution of Ea with isoconversional method

Ea is representative of the energy barrier of a reaction, it is an important kinetic parameter for better understanding the whole reaction system. Its value can be obtained by the isoconversional method as mentioned above. This section, the Kissinger method was applied to do the calculation. The Kissinger method is known as one of the most extensive used approaches to obtain kinetic parameters by DSC thermal analysis, its mechanism is based on a series of DSC tests in which minuteness quality of samples are scanned at different heating rates (β) [19]. The exothermic peak temperatures (Tp) are recorded during each scan. By the derivation and corresponding deformation and simplification, eq9 can be obtained. As shown in Figure 2.2a and 2.2b, plots of $\ln(\beta/Tp^2)$ versus 1000/Tp are displayed and straight lines are fitted to the data. From these two fitting lines, we can obtain that the value of apparent Ea in the first and second curing stage are 51.65 KJ/mol and 76.78 KJ/mol, respectively. What's more, instead of Tp, we can also obtain the specific temperature at each certain value of α, then repeating this same procedure and get the specific Ea at different α, as shown in Figure 2.2c. These results show that the values of Ea decrease a little with the increasing of α from 0.05 to almost 0.8 then sours to the end of the reaction.

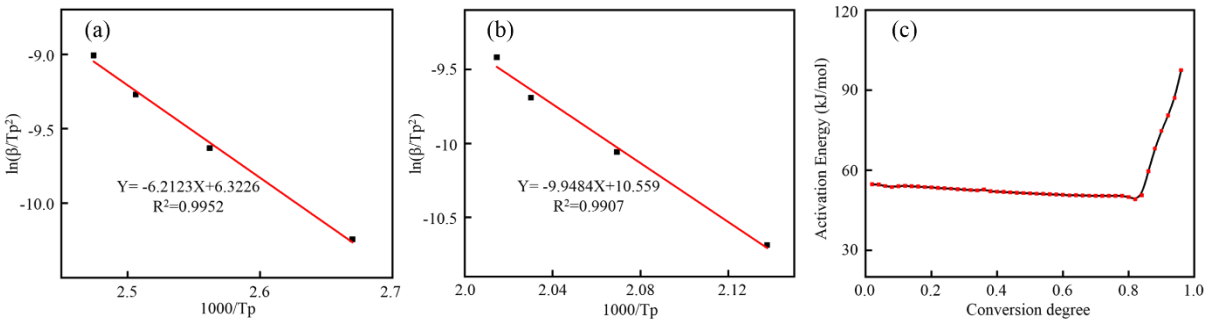

Figure 2.2 (a, b) Kissinger method plot between $\ln(\beta/Tp^2)$ and 1000/Tp based on the first and second exothermic peak temperatures. (c) Values of Ea obtained at different degree of conversion.

Normally, the value of Ea fluctuates in a narrow range as the curing process goes, that's because of the influence of the propagation of polymer segments and the heat history of the whole system. However, when the variation, as well as its tendency, changes dramatically, we cannot simply assume Ea as a constant. To the contrary, this variation trend must be valued, it is an intuitional presentation of the two-stage curing system. To solve that, we separated the whole curing process into two relatively individual curing stages and adopted both isothermal and dynamic DSC tests to analyze the kinetics of the first and the second curing stage, the resulting two reaction rate equations would avoid the problem of the dramatic variation of Ea.

2.4.2. Isothermal tests for analyzing the first curing stage

For curing reactions, the mobility of reactive moieties has a significant influence on the reaction rate. In theory, the curing reaction of epoxy resin is a cross-linking process of 3D networks, the viscosity of the whole system increases along with the higher curing level. Correspondingly, at a high degree of crosslinking, the reaction rate usually slows down or even freezes. Hence, in order to obtain higher crosslinking density, more energy is required for endowing mobility of the segments. Therefore, that means for isothermal tests, the curing process cannot be totally complete [18], especially for the two-stage curing system. In this part, 5 different temperatures were selected for the isothermal test, each one was followed by a non-isothermal test to evaluate the heat residual as well as the Tg value. By comparing the total heat enthalpy obtained by non-isothermal test, the final α at this certain temperature can be calculated. Besides, we can also get the final α by the theoretical equation of Dibenedetto equation [22]:

$$\frac{Tg(\alpha)-Tg0}{Tg\infty-Tg0}=\frac{\lambda\alpha}{1-(1-\lambda)\alpha} \qquad \text{e(11)}$$

Where Tg0 is the glass transition temperature of the pure uncured resin (α=0), Tg∞ is the glass transition temperature of the totally cured resin (α=1), and λ is the structure-dependent parameter with an empirical data of 0.52±0.02. Both methods may have some inevitable errors, hence, we adopted the average of these two values, as shown in Table 2.1.

Table 2.1 the value of residual enthalpy and final conversion degree in each temperature.

Tempe-rature	Total enthalpy	Residual enthalpy (J/g)	α (mathematical)	Tg (angle middle point)	α (Dibenedetto equation)	α (first curing)
80℃		37.97	88.166%	66.67℃	88.17%	88.317
90℃		30.75	90.416%	66.67℃	90.66%	90.538%
100℃	321±4	24.21	92.454%	73.45℃	93.54%	92.997%
110℃		16.95	94.717%	75.43℃	94.76%	94.7385%
120℃		15.27	95.241%	76.65℃	96%	95.6205%

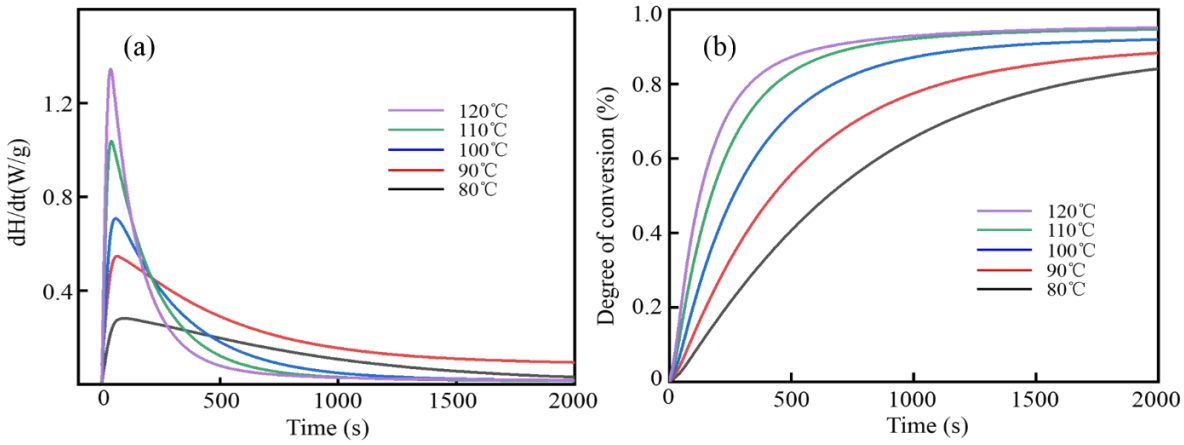

Figure 2.3 (a) Isothermal DSC curves in 5 different temperatures. (b) Degree of conversion as a function of time of the system in 5 different temperatures.

The typical isothermal DSC curves of the first curing stage are given in Figure 2.3a, it can be observed that the reaction rate culminates in a short time, then decreases gradually to almost zero. This is a remarkable feature of autocatalytic reaction, that the existence of an induction period at the beginning of the reaction. To compare vertically, with higher temperature, the induction period shortens and the phenomenon of centralized heat release gets more obvious. This is due to the higher the temperature, the more active the thermal motion of molecular segments. Besides, thermal expansion of the system allows more free volume, which also increases the effective collision between functional groups. As a result, the reaction rate surges. The reaction rate at 120℃ is much higher than the others and the curing time at that temperature is correspondingly the shortest. However, in practical operation, it might cause explosive polymerization, and further lead stress concentration or other defects to the products. Figure 2.3b gives the results of conversion degree versus time, it can be observed that the higher curing temperature, the steeper the lines, and the methods to access final conversion level at each temperature are mentioned above and given in Table 2.1. In order to obtain the kinetics equation of the first curing stage, the Kamal autocatalytic model was applied. We made some adjustments to this model: the reaction rate at a certain temperature $d\alpha/dt$ is defined as Y, α is defined as X, then $1-\alpha$ is shown as 1-X. The simplified equation of the Kamal model is given in Table 2.2, as well as the different kinetic models and parameters.

Table 2.2 Fitting parameters describing the curing kinetics

Reaction model	equation	Kinetic parameter	Fitting equation
Kamal model	$\frac{d\alpha}{dt} = (k_1 + k_2\alpha^m) * (1-\alpha)^n$	k_1, k_2, m, n	$Y= [k_1+k_2*X^m](1-X)^n$

By analyzing the data of the DSC curves, a series of the corresponding value of X and Y are obtained. Then those organized data were fitted by mathematical software, and the kinetic parameters were obtained, as shown in Table 2.3. The non-linear regression method results indicate that all the correlation coefficients are over 0.99, which confirm this curing system is a Kamal autocatalytic reaction. Taking the Arrhenius equation (eq2) as the natural logarithm gives 1nk=lnA-Ea/RT. The reaction rate constants at each temperature in Table 2.3 were logarithmically plotted against the reciprocal of the temperature, and the results are shown in Figure 2.4. It can be seen that the value of ln(k) and 1000/T of the system have a very good linear relationship. Further, the curing reaction activation energies Ea and pre-exponential factors A can be derived by linear fitting: Ea_1=45.48KJ/mol, A_1=133, Ea_2=33.23KJ/mol, A_2=3249.

Table 2.3 The kinetics parameters and regression parameters of the 1st curing stage.

Temperature	**k_1**	**k_2**	**m**	**n**	**R^2**
80℃	0.0005952	0.001651	0.3503	1.232	0.9904
90℃	0.0009567	0.002238	0.338	1.211	0.9936
100℃	0.001329	0.002736	0.3026	1.236	0.9962
110℃	0.002305	0.004053	0.3635	1.251	0.9928
120℃	0.002739	0.005184	0.3459	1.35	0.9917

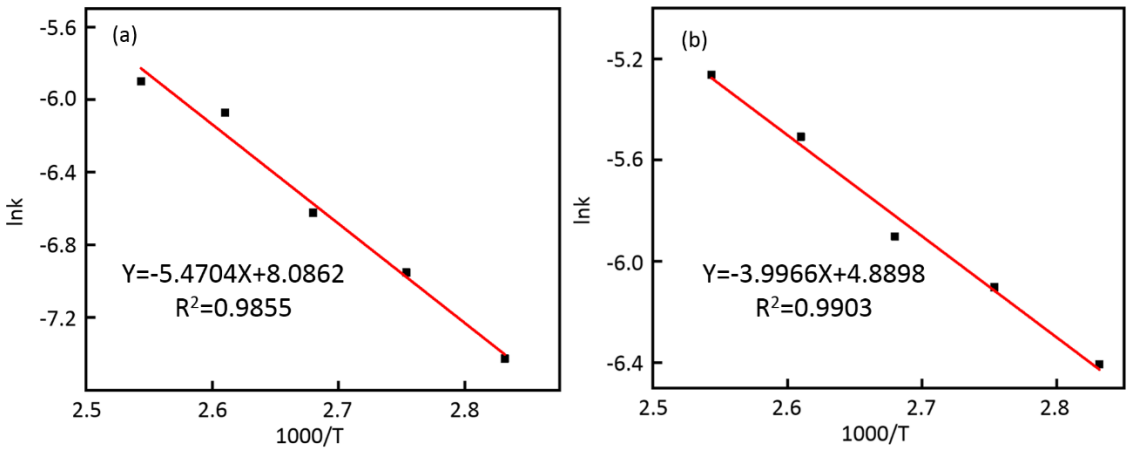

Figure 2.4 (a) $\ln k_1$ vs. 1000/T and (b) $\ln k_2$ vs. 1000/T.

Based on all the analysis and calculation, the kinetics equation of the first curing stage is followed:

$$\frac{d\alpha}{dt} = 3349 * e^{-\frac{5470.4}{T}} * (1-\alpha)^{1.26} + 133 * e^{-\frac{3996.6}{T}} * \alpha^{0.34} * (1-\alpha)^{1.26}$$

Whether a model can reasonably reflect the experimental phenomenon requires the necessary verification [23]. Generally speaking, this verification can be confirmed by directly comparing the theoretically calculated and experimentally obtained dα/dt versus temperature curves, and the correlations of these two curves can be regarded as the main basis for the validity of model fitting. Figure 2.5 shows the comparison between experimental and simulated curves, it is obviously that the Kamal autocatalytic model can well describe the kinetics of the first curing stage and the fitting lines have good calculation accuracy.

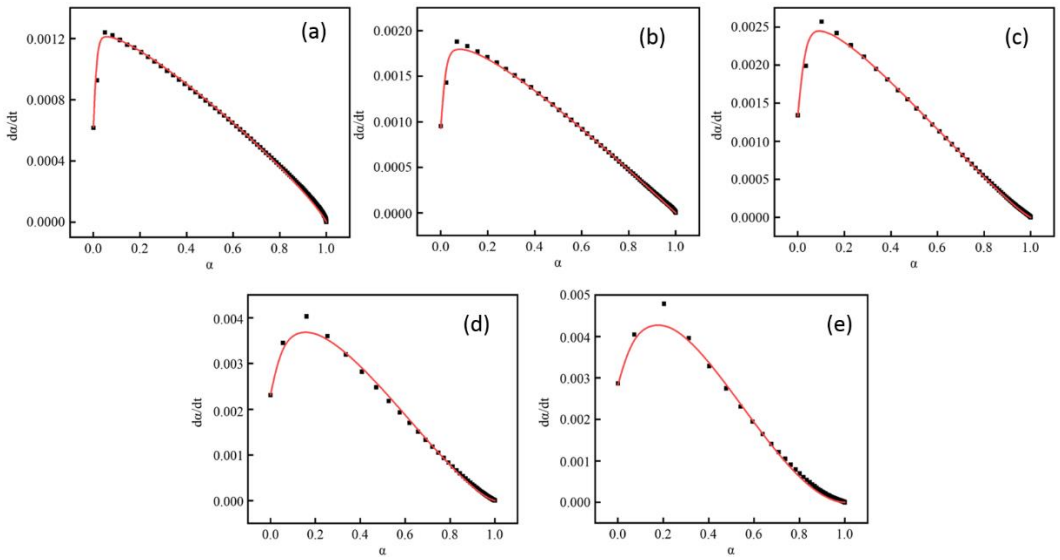

Figure 2.5 Comparison of experimental values (symbols) and calculated values (lines) by Kamal autocatalytic model, (a-e): temperature 80 to 120℃.

2.4.3. Non-isothermal tests for analyzing the second curing stage

The typical non-isothermal DSC thermograms for the second curing stage are shown in Figure 2.6a. It can be found that there is only one single exothermic peak in each scan. The first exothermic peak has disappeared and the Tg value increases correspondingly. The curves of conversion versus temperature are shown in Figure 2.6b, we can find these curves are standard sigmoidal shapes, except the induction period is shorter than that of the first curing stage, that is because of the differences in temperature. At the terminal part, the conversion rate turns slow too.

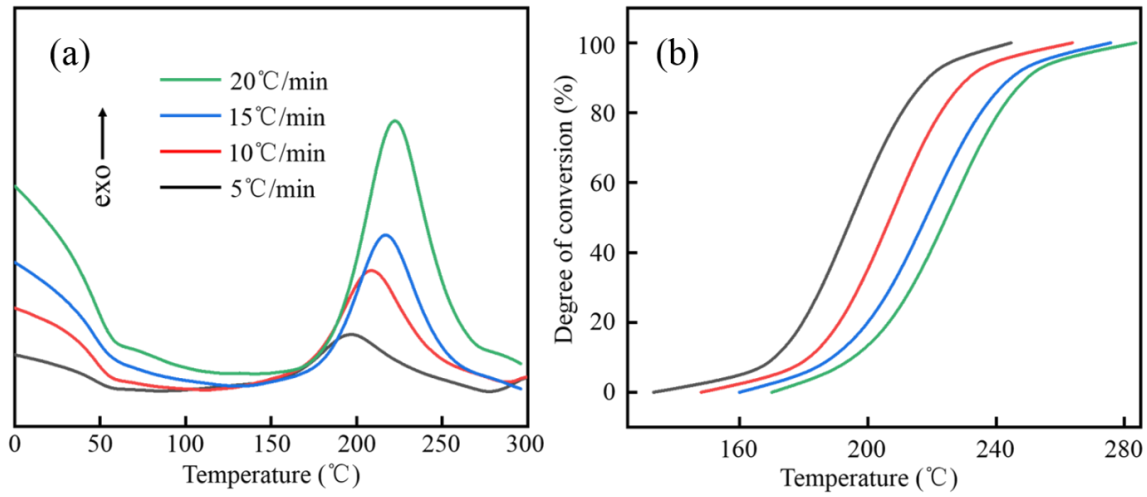

Figure 2.6 (a) Dynamic DSC curves of the second curing stage. (b) Degree of conversion as a function of temperatures.

The biggest difference between the isothermal and non-isothermal analytical methods is the parameter k, that the reaction rate constant. It is a constant in isothermal tests, which can be obtained by data fitting. However, in non-isothermal tests, k is a function of temperature and the other kinetics parameters like A, Ea, and reaction orders are the coefficients of the function. The analyzation method of the second curing stage was conducted with the Málek equations [24]. This analysis method introduces two new functions, y(α) and z(α), whose value can be obtained via the experimental data, for non-isothermal experiments the special functions are defined as follows:

$$y(\alpha)=\beta * \frac{d\alpha}{dT} * \exp(x) \qquad \text{eq(12)}$$

$$Z(\alpha)=\pi(x) * \frac{d\alpha}{dT} T \qquad \text{eq(13)}$$

Where x is the reduced activation energy, known as Ea /RT, β is the heating rate, T is the absolute temperature as mentioned before, π (x) is the function of x that can be approximated by the 4th rational expression of Senum-Yang [25] showed in equation:

$$\pi(x) = \frac{x^3+18x^2+88x+96}{x^4+20x^3+120x^2+240x+120} \quad \text{eq(14)}$$

According to the Málek method as well as the corresponding function equation of eq5 and eq6, two parameters of α_M and α_∞ can be calculated, which are the maximum values of y(α) and z(α) respectively. To further study the kinetic parameters like m, n as well as A, another special parameter p (the value of m/n) was introduced. And this value can also be presented from the equation of y(α) function:

$$p = \frac{m}{n} = \frac{\alpha_M}{1-\alpha_M} \quad \text{eq(15)}$$

with the specific data of p that obtained from equation above, we can further deform and deduce the equation as follow:

$$\ln\left(\frac{d\alpha}{dt} * \exp\left(\frac{E_a}{RT}\right)\right) = \ln A + n * \ln[\alpha^p(1-\alpha)] \quad \text{eq(16)}$$

The relationship between $\ln\left(\frac{d\alpha}{dt} * \exp\left(\frac{E_a}{RT}\right)\right)$ and $\ln[\alpha^p * (1-\alpha)]$ was linearly fitted, and the kinetic parameters n and A can be obtained from the slope and intercept of the line, respectively. The other kinetic parameter m was calculated from equation ep15. In this study, we use four different heating rates (5 to 20 ℃/min) as previously for the non-isothermal curing study, the obtained results were listed in Table 2.4, and the average value were determined as the kinetics parameters (Figure 2.7).

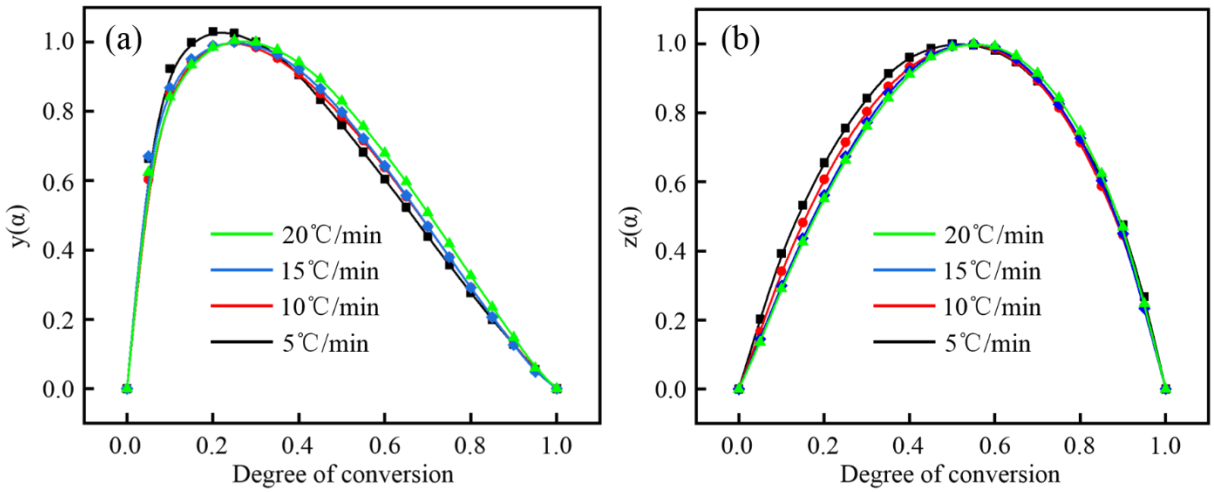

Figure 2.7 Normalized y(α) (a) and z(α), (b) versus conversion of the reaction system.

Table 2.4 The kinetics parameters of the 2nd curing stage based on Málek's method.

β(℃/min)	α_m	α∞	p	n	m	lnA
5	0.2303	0.5170	0.2992	1.2737	0.3811	18.673
10	0.2474	0.5404	0.3287	1.2902	0.4241	18.889
15	0.2510	0.5452	0.3551	1.3289	0.4453	18.811
20	0.2687	0.5539	0.3674	1.2626	0.4639	18.85

Based on the parameters above, the obtained kinetics reaction equation is written as follow:

$$\frac{d\alpha}{dt} = \exp(18.673) * e^{\frac{-9235}{T}} * (1-\alpha)^{1.2727} * \alpha^{0.3818}$$

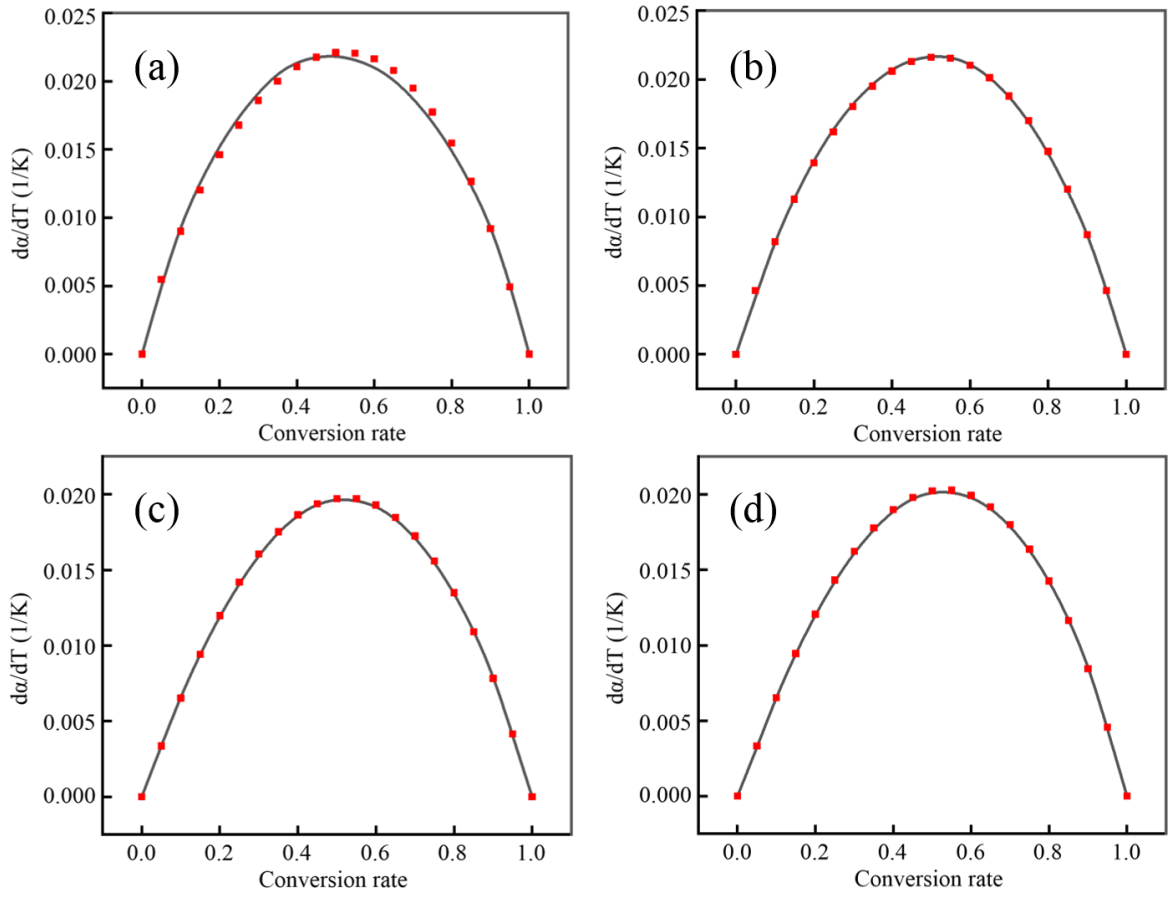

Figure 2.8 Comparison of experimental values (symbols) and calculated values (lines) by autocatalytic model, (a-d): heating rates from 5, 10, 15, 20℃/min.

Figure 2.8 shows the verification results between experimental data and simulation data. It can be observed that, despite some discrepancy exists, the fitting value still has a good

calculation accuracy to the experimental data. This result also indicates that the kinetics model deduced from the Málek's function method can well reflect the general tendency of the reaction kinetics during the second crosslinking reaction process, which also proves conversely the correctness of the model selection of this part.

2.5. Conclusion

This epoxy curing reaction is a typical dual-stage curing system, given by the evidence of two exothermic peaks and dramatic variation of the apparent activation energy. Both isothermal DSC experiments and dynamic DSC tests were used to study these two curing stages. The results show that the first stage is Kamal autocatalytic model and the activation energies in this part are 45.48KJ/mol and 33.23KJ/mol, which correspond, respectively, the uncatalyzed and catalyzed reactions in the system. The overall reaction order is 1.6. The second obeys the autocatalytic mechanism, the apparent activation energy and overall reaction order in this period are 76.78 KJ/mol and 1.66. The theoretically stimulated curves showed excellent agreement with the experimental data, which verifies the correctness of model selections.

2.6. References

1. Jin F L, Li X, Park S J. Synthesis and application of epoxy resins: A review[J]. Journal of Industrial and Engineering Chemistry, 2015, 29: 1-11.
2. Jayan J S, Saritha A, Joseph K. Innovative materials of this era for toughening the epoxy matrix: A review[J]. Polymer Composites, 2018, 39(S4): E1959-E1986.
3. Ahmadi Z. Epoxy in nanotechnology: A short review[J]. Progress in Organic Coatings, 2019, 132: 445-448.
4. Zhao X, Huang Z, Song P, et al. Curing kinetics and mechanical properties of fast curing epoxy resins with isophorone diamine and N‐(3‐aminopropyl)‐imidazole[J]. Journal of Applied Polymer Science, 2019: 47950.
5. Bello R H, Coelho L F. Curing kinetics of chemically recyclable thermoset and their nanocomposites[J]. Thermochimica Acta, 2019, 679: 178317.
6. Bratasyuk N A, Zuev V V. The study of the curing mechanism, kinetic and mechanical performance of polyurethane/epoxy composites using aliphatic and aromatic amines as curing agents[J]. Thermochimica Acta, 2020: 178598.
7. Ren R, Xiong X, Ma X, et al. Isothermal curing kinetics and mechanism of DGEBA epoxy resin with phthalide-containing aromatic diamine[J]. Thermochimica acta, 2016, 623: 15-21.
8. Granado L, Kempa S, Gregoriades L J, et al. Kinetic regimes in the curing process of epoxy-phenol composites[J]. Thermochimica acta, 2018, 667: 185-192.
9. Šimon P. Fourty years of the Šesták–Berggren equation[J]. Thermochimica acta, 2011, 520(1-2): 156-157.

10. Kamal M R, Sourour S. Kinetics and thermal characterization of thermoset cure[J]. Polymer Engineering & Science, 1973, 13(1): 59-64.
11. Vafayan M, Beheshty M H, Ghoreishy M H R, et al. Advanced integral isoconversional analysis for evaluating and predicting the kinetic parameters of the curing reaction of epoxy prepreg[J]. Thermochimica acta, 2013, 557: 37-43.
12. Pin J M, Mija A, Sbirrazzuoli N. Stereodynamic control of star-epoxy/anhydride crosslinking actuated by liquid-crystalline phase transitions[J]. Soft matter, 2017, 13(10): 1956-1965.
13. Gillham J K. Formation and properties of thermosetting and high Tg polymeric materials[J]. Polymer Engineering & Science, 1986, 26(20): 1429-1433.
14. Vyazovkin S. Kinetic concepts of thermally stimulated reactions in solids: a view from a historical perspective[J]. International Reviews in Physical Chemistry, 2000, 19(1): 45-60.
15. Brown M E. Introduction to thermal analysis: techniques and applications[M]. Springer Science & Business Media, 2001.
16. Javdanitehran M, Berg D C, Duemichen E, et al. An iterative approach for isothermal curing kinetics modelling of an epoxy resin system[J]. Thermochimica acta, 2016, 623: 72-79.
17. Xiong X, Guo X, Ren R, et al. A novel multifunctional glycidylamine epoxy resin containing phthalide cardo structure: Synthesis, curing kinetics and dynamic mechanical analysis[J]. Polymer Testing, 2019, 77: 105917.
18. Vyazovkin S. Isoconversional kinetics of polymers: The decade past[J]. Macromolecular rapid communications, 2017, 38(3): 1600615.
19. Friedman H L. Kinetics of thermal degradation of char‐forming plastics from thermogravimetry. Application to a phenolic plastic[C]//Journal of Polymer Science Part C: Polymer Symposia. New York: Wiley Subscription Services, Inc., A Wiley Company, 1964, 6(1): 183-195.
20. Kissinger H E. Reaction kinetics in differential thermal analysis[J]. Analytical chemistry, 1957, 29(11): 1702-1706.
21. Ozawa T. A new method of analyzing thermogravimetric data[J]. Bulletin of the chemical society of Japan, 1965, 38(11): 1881-1886.
22. DiBenedetto A T. Prediction of the glass transition temperature of polymers: a model based on the principle of corresponding states[J]. Journal of Polymer Science Part B: Polymer Physics, 1987, 25(9): 1949-1969.
23. Vyazovkin S, Burnham A K, Criado J M, et al. ICTAC Kinetics Committee recommendations for performing kinetic computations on thermal analysis data[J]. Thermochimica acta, 2011, 520(1-2): 1-19.
24. J. Málek. Thermochim. Acta, 200 (1992), p.257-269
25. G.I. Senum, R.T. Yang, Rational approximations of the integral of the Arrhenius function, J. Therm. Anal. Calorim. 11 (1977) 445–447.

Chapter 3. Fabrication procedure, mechanical properties and environmental durability of flax fiber/epoxy composite

This section gives the fabrication procedure of the flax fiber-reinforced bio-epoxy composite (FFRC), investigates both the dynamic and quasi-static mechanical properties of FFRC, which gives the comparison of demonstrating its feasibility as external strengthening materials. The hand lay-up method was used to fabricate the composite laminates, after totally cured they were subjected to the durability test like water immersion, freeze-thaw cycles, and wet-dry cycles in order to study the ageing effect on their mechanical performances and failure evolution. The dynamic and quasi-static mechanical characterization of the composite was conducted by using dynamic mechanical analysis (DMA) and tensile tests for assessing the viscoelastic performance on both pristine and potentially aged specimens. During the tensile test, the acoustic emission (AE) was applied to monitor the damage evolution. Water ageing was performed by immersing composite specimens into tap water at room temperature until saturation, it was found that the water absorption behavior obeys the Fick's laws of diffusion. In particular, the environment durability results demonstrate that ageing tests exerted varying degrees of influence on the mechanical properties of FFRCs, reflecting in the glass transition temperature, storage modulus, tensile modulus, Young's modulus and elongation at break, etc. Besides, three classes of damage events obtained from the AE monitoring, matrix cracking, fiber-matrix debonding, and fiber breakage/pull-out, were identified and assigned, which aided the analysis of mechanical and durability behaviors. Experiment results have proved that AE is very useful for detecting damage evolution and failure mechanism of composite materials. Besides, the mechanical and durability performance endows this composite the possibility as an external strengthening application.

3.1. Introduction

As a sustainable material, plant fibers have become the research hotspot in both academic and industrial fields to reinforce polymer composites due to the increasing environmental pressure. The manufacture of traditional synthetic materials and their usage is often considered a major cause of increased greenhouse gas emissions. On the contrary, natural reinforcing materials, such as flax fibers in this work, have a less environmental impact but possess specific mechanical properties compared with counterparts. Besides, they are cost-effective and low

in density, which makes them even more popular in the industry field [1,2]. From the point of application, the mechanical properties of composites are always important indicators, especially for those who serve as strengthening materials. There are some researches indicated that the specific tensile properties of natural fibers reinforced composites in some cases were even better than those of glass fibers [3-4]. Besides, they have other merits such as biodegradability, renewability, and lightweight, which proves their potential of natural fibers as reinforcement in many applications. These external strengthening materials create additional tensile forces on the surface of the original ones to resist deformation and provide an additional corrosion protection layer from the external environment.

However, the feasibility of natural fibers reinforced composites as strengthening materials also depends on their durability as they may be exposed to harsh environments such as extreme humidity or temperatures, and those service conditions have some inevitable effects on the physical changes and mechanical properties of composites. Among these, water ageing is the most aggressive degradation to natural fibers reinforced composites [5]. The sensitivity to humid environments is mainly related to the high hydrophilicity produced by the hydroxyl groups of natural fibers, resulting in poor hygroscopicity [6]. On the one hand, the water molecules can plasticize polymer matrices and interfere with van der Waals bonds in the polymer chain, causing matrix swelling, greater deformation, and reduced mechanical properties. On the other hand, flax fibers are highly hydrophilic because of the microscopic porous structures and the lignocellulosic component in the composition, which further leads to the incompatibility problem to the hydrophobic matrices. The high moisture uptake of flax fibers could affect the interfacial adhesion between fiber and matrix, which increases the strain at break and leads to a decrease in glass transition temperature and Young's modulus, then lower the composite durability, and thereby lower the mechanical performance of the composite [7].

In comparison, the effect of water molecules on the interfacial properties is much more severe than the matrix. This is mainly due to the plasticization caused by the uneven swelling of the material and the degradation of the fiber-matrix interface, thereby causing the occurrence of internal stress. The shrinkage and swelling of natural fibers caused by moisture may lead to the degradation of the fiber-matrix interface, resulting in a decrease in the mechanical properties of natural fiber-reinforced composite materials. Sodoke *et al.* conducted a wet-dry ageing experiment on flax reinforced epoxy composites, the mechanical characterization in their work was performed by tensile, flexural, and impulse excitation testing [8]. Results

showed that the hygrothermal effects on the static mechanical properties of the composite are obvious due to the cyclic ageing accelerates the dissolution of pectins, hemicelluloses, and some poorly crystallized celluloses to some extent. On the contrary, the cyanoethylation fiber treatment has a positive effect on the long-term durability of the composite. Moudood *et al*. studied the effect of the water content in the fiber on the performance of flax-epoxy biocomposites [9]. In their research, the composite board made of flax fiber was used in a 70% to 95% relative humidity environment and showed severe warpage. Due to the high moisture content in the fiber, the fiber-matrix interface became weaker and the porosity in the microstructure of the composite material increased. Although the fiber-matrix interface was affected, the best tensile strength was found in composites made with 50% relative humidity conditioning fabrics. Below and above this value, the tensile strength of the composite decreases. They showed that the water molecules in the fiber are plasticized and deformed, which increases the strain at break and reduces Young's modulus.

Natural fiber-reinforced composite materials are widely used in engineering fields, and the external environment exposed to them is also very different. Therefore, studying the mechanical performance and environment durability of FFRCs is of great significance for practical selection. This section discusses the effects of water saturation, freeze-thaw cycles, and dry-wet cycles on the mechanical properties of flax/bio-epoxy composites to understand the feasibility of bio-composites in different environments. They were subjected to monotonic tensile and load unloading tensile tests through AE recording. Finally, optiacal and scanning electron microscope (SEM) observations were performed to visualize the damage mechanism and confirm the AE results.

3.2. Materials and experiments

3.2.1. Materials and fabrication of composites

In this part, the thermoset resin system is designed for ambient and low-temperature cure. The biodegradable epoxy resin CHS-Epoxy G520 (viscosity=12.0-14.5Pa at 25℃) is a low molecular weight “green” epoxy prepolymer made from bio-based epichlorhydrine. The hardener is a solvent-free, low viscosity phenalkamine curing agent made through the Mannich reaction of cardanol from cashew nuts, formaldehyde, and amines as described in the previous chapter 2. The epoxy resin was prepared by blending the resin and the hardener at a weight ratio of 1.8:1, whose stoichiometric ratio between epoxy groups and amidogen is

1:1. The reinforcement of composite is a quasi-unidirectional flax fabric made of untwisted rovings. The weft and warp ratio is 9/91 and the areal density is 200 g/m^2.

In order to obtain a composite sample with the same moisture content in the fiber, a drying step was performed before the manufacturing job. The fabrics were dried in an oven at 60 ℃ for 4 hours, and then placed on a flat Teflon paper, the fabrics are in the same direction. Composite panels with a size of 250 mm ×250 mm were fabricated by wet hand layup method, as shown in Figure 3.1. The layup was done in a Teflon paper and was placed with less than 3.45 kPa (0.5 psi) of pressure to remove the air bubbles in the resin and create a relatively uniform surface on the top of the specimen sheet. The panels were cured at room temperature (RT) for at least 48 hours first, then post-cured at 90 ℃ for at least a week to obtain further cured in order to test the ageing of composite under severe environment without being disturbed by post-curing.

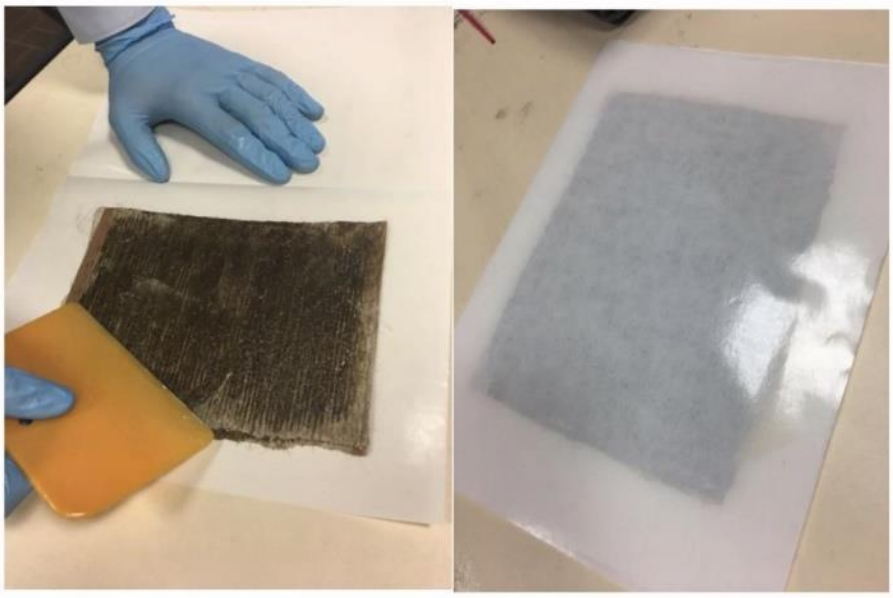

Figure 3.1 Manufacturing of composite plates.

The experiment samples were cut from the composite board into the required shape and size according to the relevant mechanical characterization standards (Figure 3.2). The average thickness of the composite sample in this experiment was about 2.5mm. The volume fiber content in the composite material is about 20%, estimated by the image J software.

Figure 3.2 Experiment samples for tensile and DMA tests.

3.2.2. Water absorption and water ageing experiments

The water absorption test was carried out by immersing the composite samples in distilled water at RT. Samples were removed from the water and wiped dry to remove surface moisture prior to weight and thickness measurements. The samples were then weighed periodically with an analytical scale accurate to 10μg. The sample's dimensions were precisely evaluated by a sliding digital caliper, and to the minimum the measuring error, sample thickness was measured at four different locations and the average thickness was determined. This part experiment lasted for 25 days. In order to analyze the influence of water ageing on the mechanical properties of flax-epoxy composites, both the DMA test and the monotonic tensile test was carried out after immersing in pure water for different periods.

3.2.3. Freeze-thaw (F-T) cycles

The composite samples were performed to F-T cycling tests according to the ASTM D7031-04 standard recommendations. The F-T cycling was performed on the totally cured specimens (cured at 90 ℃ for at least a week) based on the results of DSC test, for 1, 3, 5, 10 and 20 cycles. Before the test, all the composite samples were soaked into the water to make sure the water content in the samples at the quasi saturation level. Each cycle consists of two stages: firstly, the water-saturated specimens were placed in a freezer for 24 hours at a temperature

of -18 °C. Then, the samples were removed from the freezer and make them thaw in the water with a constant temperature of 40 ℃ for another 24 hours, as shown in Figure 3.3a. The following mechanical performance of the materials was conducted by DMA and tensile test to analyze their static and dynamic mechanical properties.

3.2.4. Wet-dry (W-D) cycles

The ageing study was also performed under "wet-dry" cycles, which adopts an oven and soaking in pure water for 8 consecutive weeks. It consisted of four cycles divided into wet and dry conditions. A single cycle had a total period of two weeks and the wet and dry conditions were alternated every week. In the wet condition, the samples were soaked into the water with a maintained temperature of 40 °C, while for the dry condition, specimens were taken out of the water and dry at a maintained temperature at 40 °C aided by an oven fan, as shown in Figure 3.3b. In order to distinguish the effects of water ageing and W-D cycle ageing, the composite samples were pre-soaked in the water at RT for 40 days until saturated before this W-D cycling study. The accelerated W-D ageing procedure in this section intends to simulate both hot/wet and hot/dry environmental conditions that might be experienced by the composites in either outdoor or indoor applications.

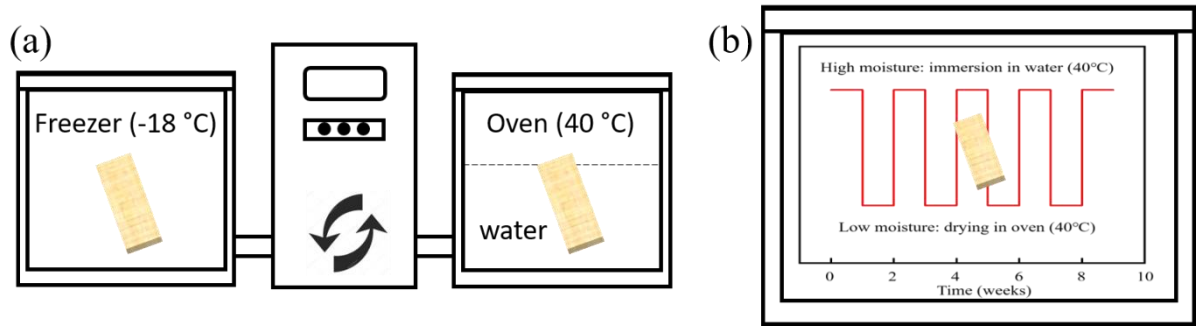

Figure 3.3 Schematic pictures for F-T cycles and W-D cycles.

3.2.5. Quasi-static and dynamic mechanical properties tests

The dynamic mechanical behaviors of FFRCs were analyzed by using DMA equipment (DMA50 from METRAVIB). The experiments were performed under tensile-compression mode. DMA technique allows the measurement of the storage moduli (E′), loss moduli (E″) as well as their ratio (E″/E′), tanδ named loss factor. Rectangular specimens of $20 \times 10 \times 3mm^3$ were prepared for the tests and aluminum tabs were bonded at the end of the sample in order to avoid damage in the jaw and spilling of the unidirectional UD samples.

The testing temperature ranged from RT to 200°C at a rate of 1 °C/min with different frequencies from 0.1 to 30 Hz.

Static tensile tests were performed on composite laminates until failure. They were carried out on a servo-hydraulic machine INSTRON-8516 equipped with a 30 kN load cell (Figure 3.4a). The tensile test machine was interfaced with an acquisition system for monitoring and data acquisition. The specimens were tested according to the standard test method ASTM D3039/D3039 M [4,8]. Three specimens were tested for each configuration sample in order to check the reproducibility. For the static tests, specimens were loaded with a displacement rate of 0.5mm/min at RT.

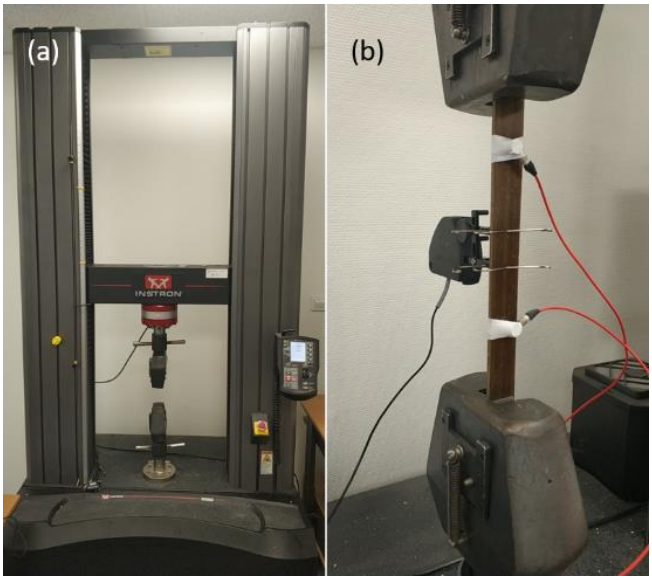

Figure 3.4 (a) The setup of tensile test and (b) tensile test monitored by AE.

3.2.6. Acoustic emission test

In order to obtain information on the damage evolution of the composite samples during the tensile test, the AE was used to continuously monitor the tensile process, as shown in Figure 3.4b. Two sensors with a bandwidth ranging from 100 kHz to 1MHz were fixed on the sample and connected to the European Physical Acoustics acquisition system. During the test, a 40dB gain preamplifier was used to amplify the signal received by the sensor at a sampling frequency of 5MHz, AE signals were acquired and processed with the AE acquisition and analyzing system AEwin for Mistras of Physical Acoustics Corp [10]. The AE signals during the tests were detected by two piezoelectric sensors (type R15) attached to the sample. In order to provide good acoustic coupling, silicone grease is used as a coupling agent between the sensor and the sample surface. To test the accuracy of the AE system when locating events,

100 dB events were generated on a marked specimen. The AE location map was then compared to the known location of the events. Two sources of errors have been identified: the velocity uncertainty and the repeatability of the acquisition system. The longitudinal wave velocity of our specimens is 2850 ±140 m/s measured using a pencil lead (2H) break test (Hsu-Nielsen source) [11].

3.3. Results and discussions

3.3.1 Moisture absorption

The operation of water absorption experiment was mentioned above, and the relative water absorption could be calculated using the following equation:

$$M_r(t) = \frac{M_t - M_0}{M_0} * 100\% \qquad \text{eq(1)}$$

Where $M_r(t)$ is the relative water uptake at time t, M_t is the weight at time t, M_0 is the initial weight of the composite specimens. This part of test lasted for 25 days.

In the case of natural fiber reinforced epoxy, water can act as a plasticizer of the matrix resin but also of the reinforcement. As introduced in the introduction part, the main components of flax fiber used in this experiment are cellulose, hemicellulose, pectin and lignin. Cellulose and hemicellulose contain a large number of hydroxyl (-OH) functional groups which have a strong possibility to interact with water molecules forming hydrogen bonding to the detriment of those between the macromolecules. Water is held within the fibers by adsorption force in amorphous zones. Hemicellulose which is fully amorphous plays a leading role in plasticizing effect of natural fibers. Cellulose is partially crystalline with a crystal rate in the range 60–70% [12]. Very compact cellulose crystalline zones are not affected by water molecules, which diffuse only through the amorphous regions. In parallel to the plasticization effect, the fiber swells until the cell walls are fully saturated with water (bound water) to the fiber saturation point (FSP) which is between 30 and 40% depending on structure and chemical compositions of the cell wall [13]. Beyond this FSP, the water is present in the cell lumen and voids as free water and the fiber may degrade.

The water absorption behavior and diffusion kinetics in FFRCs materials can be described by a variety of analytical models, and the Fick model is used in this section. When the composite sample has a uniform initial distribution of thickness and equal initial surface conditions, Fick's law can be expressed as the following equation: [9,14,15]

$$\frac{M_t}{M_m} = 1 - \frac{8}{\pi^2}\sum_{n=0}^{\infty}\frac{1}{(2n+1)^2}\exp\left(\frac{-(2n+1)^2\pi^2 Dt}{h^2}\right) \quad \text{eq(2)}$$

Where Mt is the water uptake at time t, Mm is the weight of water uptake when the sample is saturated, n is the summation index and D is the coefficient of diffusion in the composite, h is the thickness of the composite sample.

Shen and Springer [16] simplified this equation and identified into two cases. In the first case, when Mt/Mm is below 0.6, the correlation of the curve is

$$\frac{M_t}{M_m} = \frac{4}{h}\sqrt{\frac{Dt}{\pi}} \quad \text{eq(3)}$$

In the second case, when Mt/Mm is greater than 0.6, the equation describing the curve becomes:

$$\frac{M_t}{M_m} = 1 - \exp\left[-7.3 * \left(\frac{Dt}{h^2}\right)^{0.75}\right] \quad \text{eq(4)}$$

The diffusion coefficient (D) was calculated by the following equation:

$$D=\frac{\pi}{(4*M_m)^2} * \left(\frac{M_t * h}{\sqrt{t}}\right)^2=\pi\left(\frac{kh}{4M_m}\right)^2 \quad \text{eq(5)}$$

Where k is the initial slope of a plot of the Mt versus $\sqrt{t}$. Due to finite dimensions of the composite samples, diffusion through the edges should also be considered. Therefore, corrected diffusion coefficient D_c is calculated according to the following equation for the rectangular composite samples:

$$D_c = D\left(1 + \frac{h}{L} + \frac{h}{W}\right)^{-2} \quad \text{eq(6)}$$

Where L and W are the length and width of the soaked composite samples.

The results are as follow:

Table 3.1 the value of quasi saturated water absorption (Mm), the diffusion coefficient (D) and the corrected diffusion coefficient (D_c)

M_m	D ($*10^{-6}mm^2/s$)	D_C ($*10^{-6}mm^2/s$)
4.51%	1.845	1.325

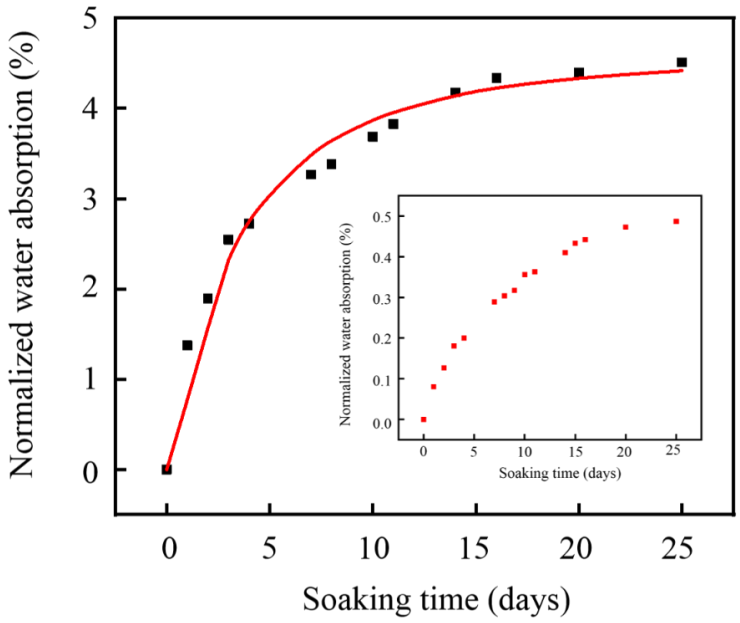

Figure 3.5 Water uptake curve obtained by experimental tests and analytical modeling for composites, and for bio-epoxy resin (inner figure).

Figure 3.5 shows the comparison of experimental and analytical water absorption behavior of FFRCs underwater immersion conditions. The equation of the Fick model as discussed above was used to draw a curve representing the theoretically predicted water absorption. The results show that the water absorption performance of the composite material obviously obeys the Fick's diffusion behavior: a linear increase in the initial stage, then the absorption rate decreases, and finally reaches a quasi-saturated state (about 5%) with a slowly increased state. In comparison, the water absorption content for pure bio-epoxy is much smaller, which is about 0.5% when reaching saturated.

3.3.2. Mechanical performances of composites under different ageing conditions

This chapter focuses on the engineering structural applicability of FFRCs under different environmental conditions. Evaluating the durability of bio-composites is the main motivation for this research. The composite laminates were exposed to different environmental conditions: water immersion, F-T cycles and W-D cycles. In order to analyze the tensile experiment and to monitor the damage evolution, the AE was applied. The AE classification method has been widely used to identify and analyze the damage mechanism inside the composite [17,18]. Five temporal parameters were selected to classify the AE signal in this section: amplitude, rise time, duration, number of peaks, and energy, which are described below in Figure 3.6.

Threshold: the level set to distinguish signal from noise.

Amplitude: the peak value reached by the signal in an AE event which covers the range from 40 dB to 100 dB.

Rise time: the time required for the signal to reach the amplitude after crossing the threshold.

Duration: the time difference between the first and last threshold crossings with the event signal.

Number of counts to peak: the number of times the signal crosses the threshold between the peak amplitude and the threshold.

Energy: the area under the curve of amplitude versus time for an event.

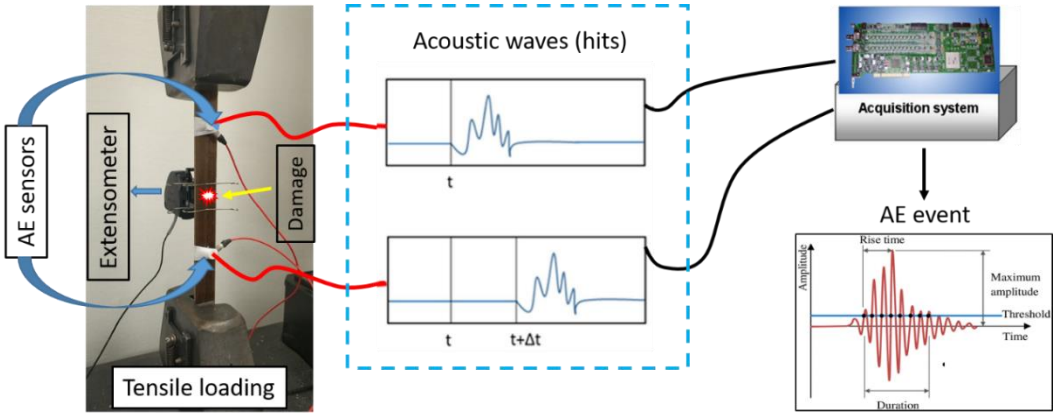

Figure 3.6 Diagram of the AE test as well as the typical AE waveform and its parameters.

3.3.2.1 Water immersion ageing

The dynamic mechanical results of FFRCs at different aged levels (0, 2 weeks, 3 months and 7 months at RT) are given as followed**.**

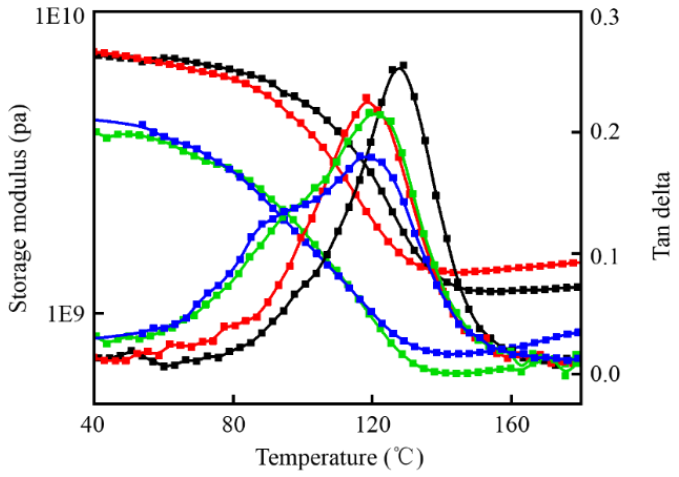

Figure 3.7 DMA results of composites with different ageing levels (black, red, green and blue curves represent the water soaking time of 0, 2 weeks, 3 months and 7 months) frequency 1 Hz.

This Figure shows typical graphs of storage modulus (E') and loss factor (tan δ) versus temperature for composites with different ageing degrees at 1 Hz. In the range of temperature studied, the tan δ spectra of unaged material (soaking for 0 day, black curve) shows one peak (127 ℃ with 1Hz). The peak is concurrent in a large drop in the storage modulus (near 1 decade) from glassy to rubbery state. The relaxation, named α-relaxation is associated with the glass transition of the polymer and corresponded to the coordinated motion of relatively long-chain segments by debonding of low energy bonds. It is well known that the measurement of α-relaxation temperature which is associated with Tg can be used as an accurate indication of the cross-link density of a thermosetting material.

It can be observed that with increasing ageing periods, the onset of the storage modulus drops (from 7.35E+09 to 4.37E+09) and the maximum of tan δ associated with α-relaxation are shifted towards low temperatures with a broadening of the tan δ peak and even the occurrence of a double relaxation peak for the highest period of ageing (soaking for 3 and 7 months, green and blue curves). Moreover, for all the aged materials a slight increase of E' is observed in the rubbery plateau region. The glass-rubber transition, which is associated to the cooperative thermal motion of individual chain segments along the polymer backbone is affected by water as the presence of water increase the free volume between the polymer segments allowing them to move easily. As a consequence of this plasticizing effect of water, a decrease in Tg and therefore in α-relaxation is observed. The volatility of the water during DMA test is responsible for the broadening and the splitting of the peak but also of the slight increase of the storage modulus at high temperature, as for unaged material this last phenomenon doesn't occur.

For the highest periods of ageing, an overall decrease in modulus over the whole test temperature range is observed. As previously mentioned, absorbed water acts as a plasticizer for the fibers and even for highly severe environment may degrade. Moreover, water molecules can be transported at the interfaces which may further cause the interface between flax fibers and the resin matrix to debond. These phenomena probably decrease the reinforcement effect of the fibers with increasing ageing periods in water.

3.3.2.2. Quasi-static mechanical studies of FFRCs with different aged levels

FFRCs under different ageing times in water at RT (0 to 24 weeks) were tensile tested up to failure with 0.5 mm/min. The elongation was measured using an extensometer. The

comparison of Young's modulus, tensile strength, and elongation at break of flax/bio-epoxy composites with different ageing levels is shown in Figure 3.8 and the corresponding data is in Table 3.2.

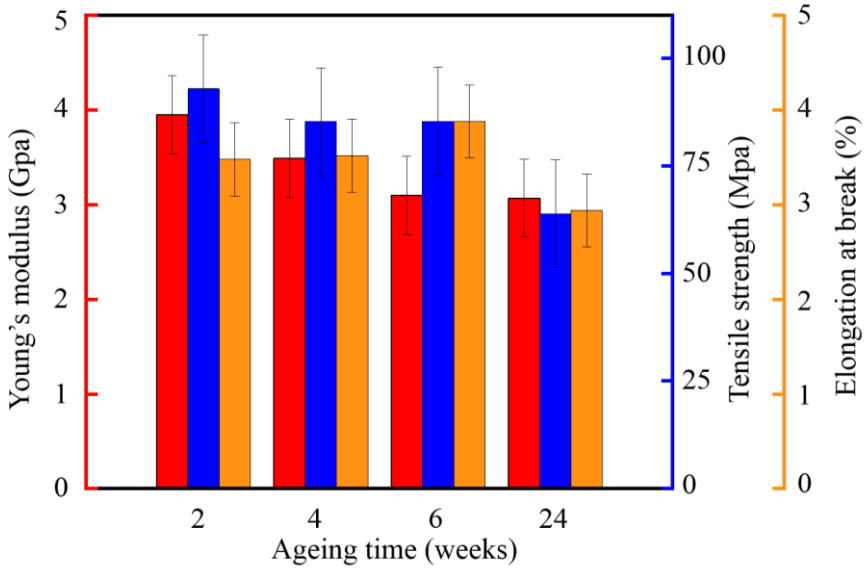

Figure 3.8 Tensile behavior of flax/bio-epoxy composites with different ageing time.

As it can be observed, Young's modulus gradually decreases after increasing exposure time to humid atmospheres (from 4.17% at 2 weeks to 6.55% at 24 weeks). The tensile strength decreases dramatically by 40% after ageing in water for six months. In contrast, the elongation at break is gradually increasing during this period.

Table 3.2 Mechanical test results of FFRCs.

Water ageing (weeks)	Young's modulus (Gpa)	tensile strength (Mpa)	elongation at break (%)	Water absorption (%)
2	3.95	92.97	3.48	4.17
4	3.49	85.32	3.52	4.52
6	3.10	85.4	3.88	4.71
24	3.07	63.93	3.00	6.55
SD	0.412098	12.50882	0.361294	1.065407

The performance of reinforced composites depends on many variables: fiber, matrix, interface bonding, fiber volume content and different flaws which exist before any loading (usually related to the manufacturing method), such as porosities, matrix zones, misalignment of the fibers (in plane or out of plane), defects at the interfaces, matrix or fiber microcracks and in some cases undercuring. The longitudinal modulus of 0 °-UD homogeneously reinforced composite material follows well the laws of mixing. In the case of 0 °-UD homogeneously carbon or glass-reinforced composite materials, the longitudinal modulus shows no or very little effect of moisture as long as the fiber content is sufficiently high (vf > 0.40), the axial reinforcement modulus being not affected by moisture.

Moisture is more detrimental to the modulus of composites made by wet hand lay-up method due to plasticization of the matrix. This manufacturing process produces lower quality materials. The matrix content is generally high (v_m is around 0.85 to 0.75), with the presence of porosities and inhomogeneous distribution of the matrix. Marouani *et al*. showed for example on EP/carbon samples (vm = 0.75) made by this type of process and aged in water at 20 ℃ for several weeks that the longitudinal modulus may fell by nearly 20% [19].

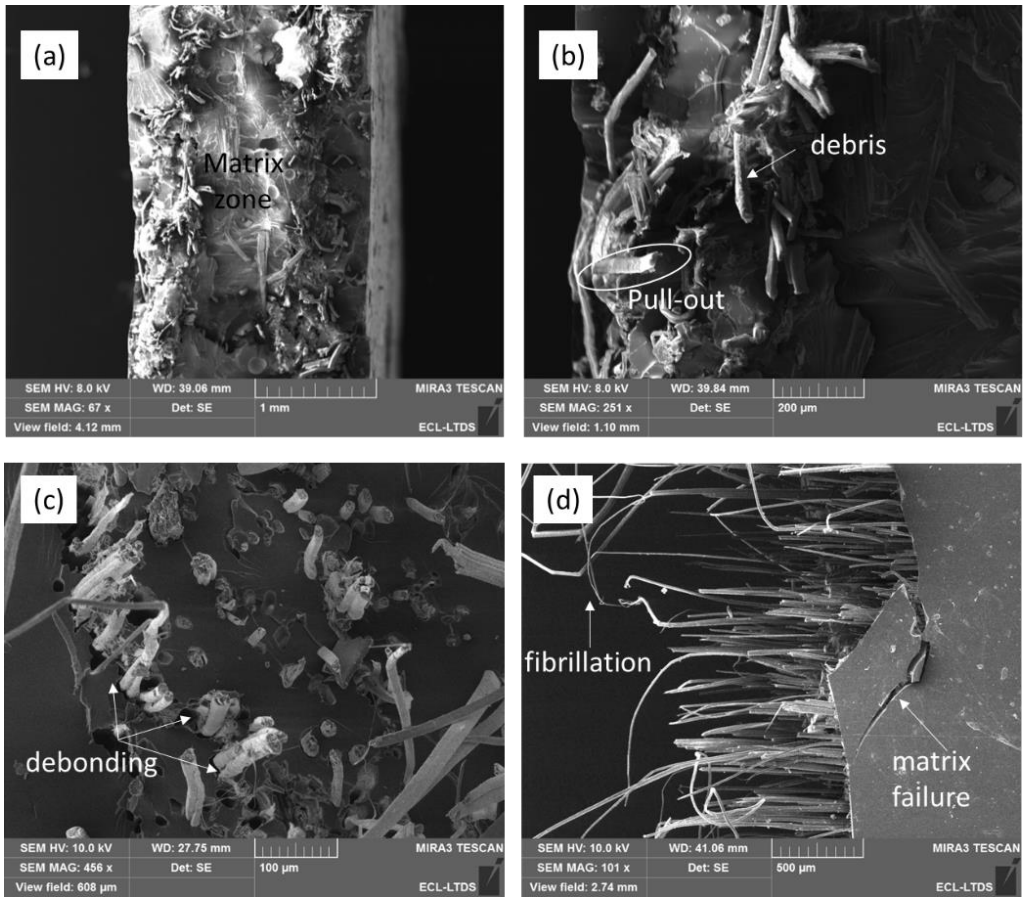

Figure 3.9 SEM fracture feature view of the 2-week aged sample (a, b) and the 24-week aged sample (c, d).

In this case, the matrix volume fraction is of the order of 0.80 with, as can be seen on the SEM picture of the composite fracture feature a large matrix area in the center of the composite (Figure 3.9a). In addition, unlike inorganic fibers, the modulus of flax fibers is sensitive to moisture due to the plasticization of these constituents, which leads to a loss of rigidity [20]. Therefore, the combination of the plasticization effect of the two main parts of the composite may explain the gradual drop in modulus with exposure time.

For 0 °-UD composites, tensile performance is mainly determined by the properties of the fiber-(stress and strain at failure, statistical behavior of the fibers (fibers have not all the same ultimate strength)). Unlike the modulus, the quality of the interface plays also a role in the final breakdown process as load transfer occurs at first fiber break through the interface by shear. Too strong fiber-matrix bond can make a composite with a brittle matrix (as epoxy) more brittle, because the strong fiber-matrix bond causes cracks to propagate straight through the composite leading to a sudden brittle failure (Figure 3.10a). Conversely, if the interfacial bonding strength is too low and not sufficient for the load to be transferred from the matrix to fibers, cracks do propagate along the length of the fibers. Extensive debonding at fiber/matrix interfaces and long fiber pull-out take place leading to low performance at break (Figure 3.10b). The extreme situation (very weak fiber/matrix interface) consists of debonding along the entire length of the fibers and a composite behaving as a bundle of fibers. As the interfacial condition controls the propagation of cracks at the fiber first failure, an optimum interface for a given matrix/fiber system should involve a relatively strong strength but not necessarily maximized to allow, at the same time, some toughening damage mode with interface debonding over moderate length (pull-out), good load transfer and resistance to crack propagation (Figure 3.10c-d).

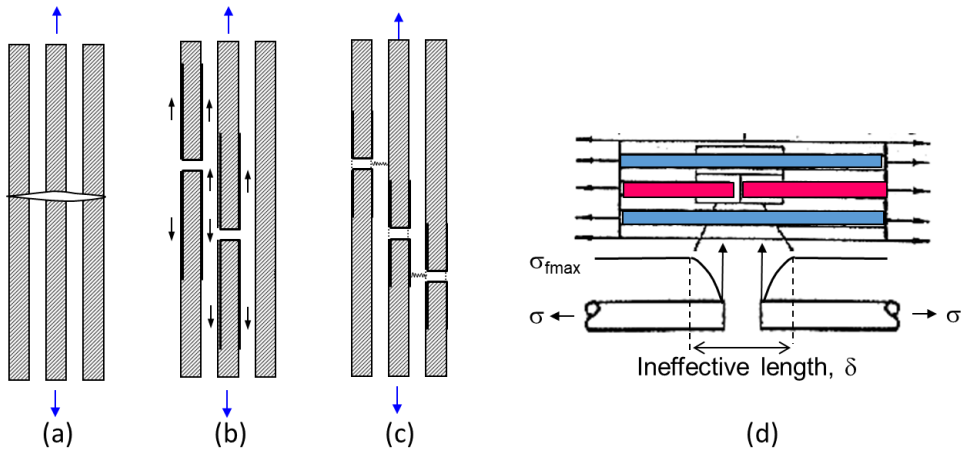

Figure 3.10 (a) strong interface; (b) weak interface; (c) optimized interface; (d) load transfer mechanism principle.

It is commonly known that the carbon and E- glass fibers, if they are well protected from water by an optimized sizing, are resistant to moisture absorption and therefore should remain dimensionally and mechanically stable in water. When composites reinforced with such fibers are subjected to a humid environment, irreversible degradation phenomena may occur at the fiber/matrix interface by diffusion, absorption and capillary condensation and differential swelling as the matrix only plasticized. This can result in macroscopic defects within the composite, mainly interfacial cracking and debonding, affecting the mechanical strength of the interfaces through load transfer and resistance to crack propagation and therefore the performance of inorganic reinforced composites.

Unlike carbon and E-glass, natural fibers are sensitive to water. Their performance at break, as the modulus, is dependent on moisture content. Several authors reported that the flax fiber tensile strength decrease (slightly) and strain at failure (significantly) increase with moisture rise [20-22]. This was explained by the plasticizing effect of water on cell wall constituents. Moreover, a less detrimental effect on the fiber-matrix interface of the humidity may be observed in the case of natural fiber-reinforced composites due to moisture swelling of the fibers [23].

The reason for the gradual increase in elongation at failure with the moisture content of our composites, up to 6 weeks, lies in the joint plasticization of the resin and the fiber. The significant decrease of tensile strength (30%) and slightly lower for the elongation at failure (20%) observed on 24 week aged composites is associated with degradation at the interface. This is supported by the SEM analysis of the fracture surfaces for composites after 2- and 24-week ageing (Figure 3.9). This Figure shows voids at the interface between the fiber and the matrix for the longest aged composite, highlighting the separation of the fiber from the matrix and long pull-out length associated to fibrillation, resulting to a splitting of the fiber in the longitudinal way. This Figure also shows a brittle failure whatever the ageing time.

Study the damage evolution by monitoring AE

In order to highlight the damage trends, both fractography analysis and AE were used. The AE was used to monitor during the tensile test up to failure. AE is an efficient technique for in-situ health monitoring of composite materials. This is achieved by monitoring the cumulative number of events and the analysis of AE parameters of the signal emitted by a failure event signature waveform (hit) like the amplitude, the energy or the duration of the event. The amplitude of the signal is often used because it is independent on the detection

threshold. Several authors have shown on different fiber reinforced composites that events with low amplitude (between 40-50 dB) are correlated with matrix micro-cracking, intermediate amplitude with delamination and micro-cracking coalescence (50 dB to 60dB) and with matrix/fiber debonding (60 dB-70 dB) and high amplitude with fiber/matrix friction associated with pull-out (70 dB-85 dB) and fiber breakages (>85 dB) [24,25].

In this chapter, for the sake of simplifying the categories in amplitude were reduced to three: category A associated to matrix: breakages and matrix/matrix interface (delamination) [40-60 dB]; category B: matrix/fiber debonding [60-70 dB]; finally, category C, associated with fiber pull-out and fiber breakages is [70-100 dB].

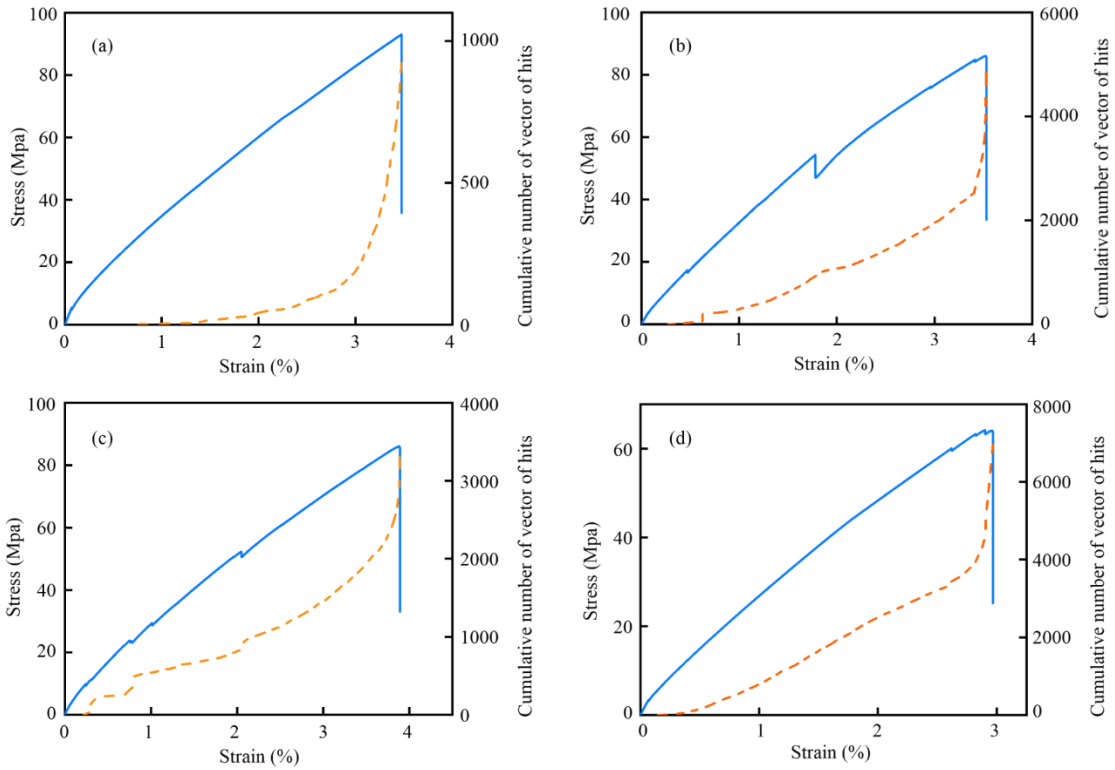

Figure 3.11 Correlation between the evolution of acoustic activity of all samples and the law of stress-strain behavior: (a) soaking in water for 2 weeks, (b) soaking in water for 4 weeks, (c) soaking in water for 6 weeks, (d) soaking in water for 24 weeks.

Figure 3.11 shows the correlation between the typical evolution of acoustic activity and tensile behavior of each composite specimen with different water ageing test. The evolution of acoustic activity and load occurred in the following stages:

First stage: the linear elastic stage, which is characterized by no detection of AE activity. At this phase, the loading would not affect the integrity of the sample.

Second stage: The beginning of this phase coincides with the deviation from linearity of the load-time (deflection) which is associated with the onset of AE signals which reflects the beginning of damage of composites. In all the cases, a near exponential type curve is obtained for the AE response according to time indicating a strong acoustic activity. The threshold elongation at which the first acoustic signal appears considerably lowered when the moisture level increase (from 1% of the strain to 0.17% after 6 weeks), except for the highest level of aging (at which the composite has reached water saturation) for which the value is intermediate between that of two-week aged composite and the other aged materials.

The third stage: The maximum of the load corresponds to the occurrence of a macro-crack resulting in the coalescence of microcracks. As compared with ageing at two weeks, the number of events is much higher for the other aging states, especially for the ageing at 4 weeks.

In order to further understand the failure mechanism of composites appearing with time until failure, the distribution of the amplitude of the AE signal (Figure 3.12) and the cumulative hits (Figure 3.13) were compared with the changes in the applied load versus time (elongation) using clustering method. In addition, the typical failure features (optical) observed on composites with different ageing are presented in Figure 3.14.

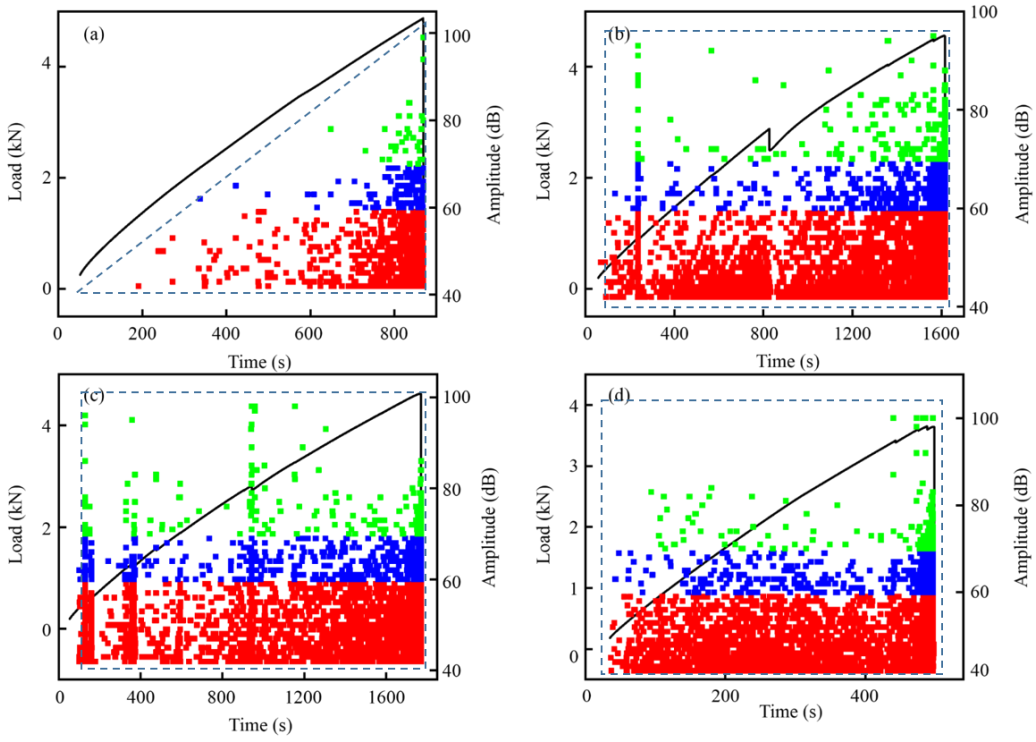

Figure 3.12 Distribution of amplitude versus time of AE signals under tensile tests for all specimens: (a) soaking in water for 2 weeks, (b) soaking in water for 4 weeks, (c) soaking in water for 6 weeks, (d) soaking in water for 24 weeks.

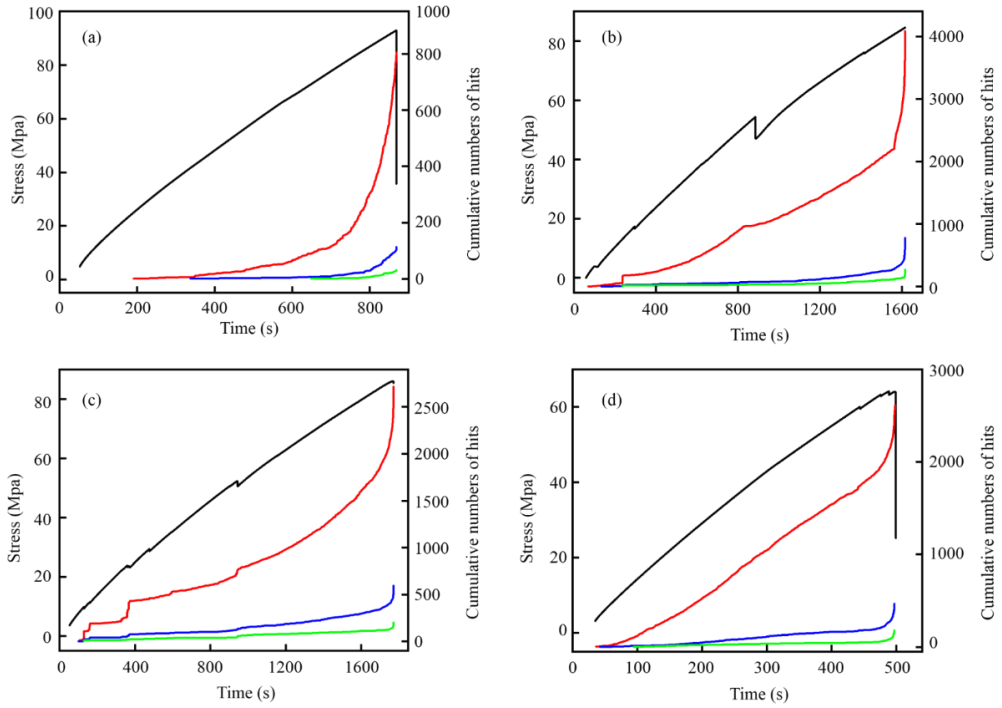

Figure 3.13 Time dependency of different classes of damage mechanisms identified under tensile tests for all specimens: (a) soaking in water for 2 weeks, (b) soaking in water for 4 weeks, (c) soaking in water for 6 weeks, (d) soaking in water for 24 weeks.

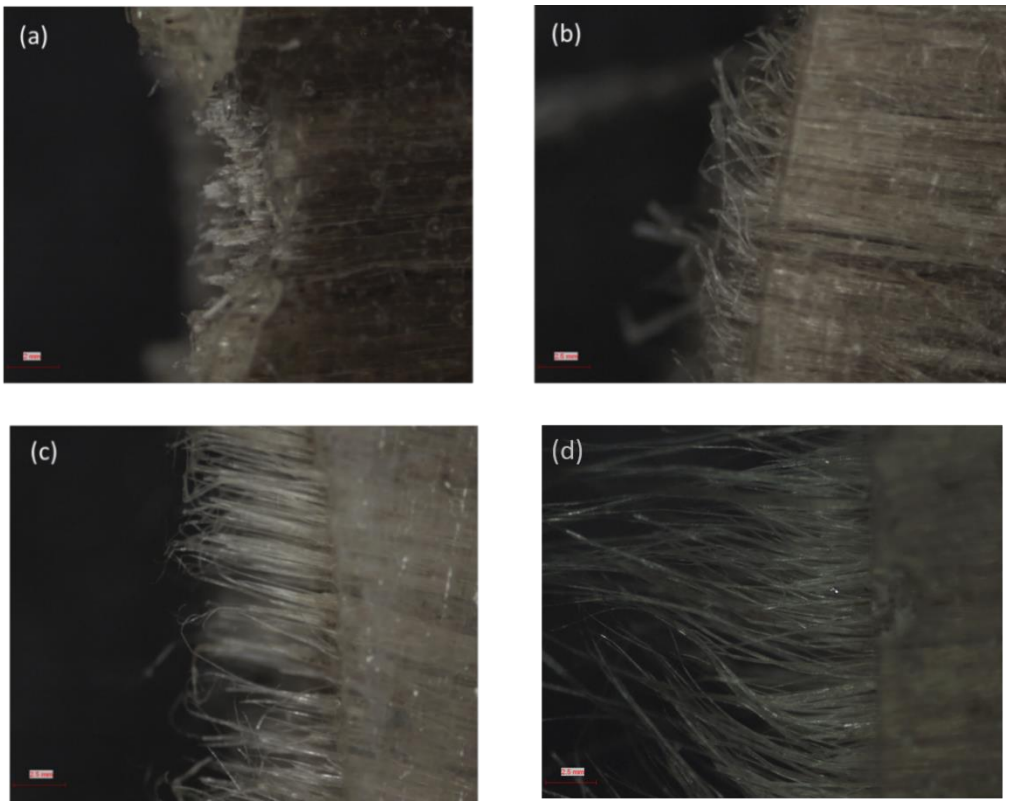

Figure 3.14 Optical observation of the composite fracture after tensile test under different ageing period: a) soaking in water for 2 weeks, (b) soaking in water for 4 weeks, (c) soaking in water for 6 weeks, (d) soaking in water for 24 weeks.

The amplitude of AE events versus time shows a triangular-shaped appearance for the 2 weeks of ageing, whereas it shows a rectangular shaped appearance for the samples aged for 4, 6 and 24 weeks, as shown in Figure 3.12. This indicates that for the last three ageing states (4, 6 and 24) all defect categories appear almost at the same time whereas for the first state (2), class A damage, associated mainly to matrix breakages is the first mechanism to appear.

For the samples aged for two weeks (Figure 3-12a & 3-13a), class A acoustic activity started at 200 seconds (approximately 1% of the strain), increased in a gradual manner, and then increased suddenly near the end of the tensile test (820s (elongation of 3.19%)) until the sample was completely broken. Class B (debonding at the interface) and class C (involving pull-out and flax fiber failures), occurred at about 400s (the elongation of 1.52%). There is a very slight increase up to 820s at which a sudden increase was observed, as for class A damage. These results tend to show that the interface fiber/matrix is strong enough to transfer stresses from matrix to fiber but enough tough to avoid cracks to propagate straight through the composite. Indeed, for epoxy reinforced with natural fibers, the quality of the interface is associated with two main processes: (i) hydrogen bondings between hydroxyl (OH) groups in the backbone chain of the epoxy resin and the flax fibers, which also contain OH groups (cellulose) and (ii) mechanical interlocking due mainly to roughness of the fiber and friction. These results are in agreement with SEM and optical pictures (Figure 3.9 and 3.14). The pull-out phenomenon can be observed for this samples (Figure 3.9a and 3.14a). It consists of small extracted fiber with matrix debris on the fiber surface (Figure 3.9), thus indicating that the stress transfer was well governed by mechanical interlocking and friction.

The composite samples aged for 4, 6 and 24 weeks (Figures 3.12b-d & 3.13b-d), show different behavior than the previous composite. The acoustic activity appeared just after the beginning of stretching, (65s, with an elongation of 0.098%) with the appearance of B and C classes at the same time than class A damage. All the kind of damage took place throughout the life of the sample in a gradual manner. This may suggest fiber/matrix interface and matrix weakening due to increase in water in composite and possibly degradation of the fibers by the water absorption. The fibers were more easily extracted as fiber/matrix interfaces are becoming weaker. These results are consistent with microscopy analyses. The optical failure feature micrograph displays pull-out lengths greater (Figure 3.14b-d) than those observed on 2 week-aged composite and a greater length on the sample with the longest ageing period. Moreover, for the severer ageing condition (24 weeks) fibrillation of the flax fiber occurred (Figure 3.14d), as shown previously.

3.3.3. Freeze-thaw cycles

In the northern climate, external infrastructures like concrete would withstand harsh environmental conditions and extreme temperature fluctuations. When using FFRC as a reinforcement and refurbishment material, it has to withstand all those harsh external situations. The effects of long-term water immersion have been studied above; however, the research of repeated F-T cycle exposure, a common phenomenon in outdoor conditions, on structural alterations is also necessary. In this part, FFRC is subjected to repeated F-T cycles to confirm its performance, both the dynamic and the quasi-static mechanical analysis were conducted, AE was applied to aid the tensile test.

In order to distinguish between pure water ageing and F-T ageing, the composite samples in this experiment were immersed in water for 40 days and have reached the water saturation state at RT. Moreover, a constant temperature water bath is used when thawing, so as to avoid the influence of uneven water content in the composite material during the experiment. The freezing temperature (-18 ℃) and thawing temperature (40 ℃) in the experiment are more extreme than the temperature in most areas, and they have a good outdoor simulation. Besides, the composite material under real conditions is also in a water-saturated state when outdoors, but the saturated water content would vary with the alternating of the rainy and dry seasons.

Each F-T cycle includes placing a water-saturated composite material in the freezer for 24 hours and then thawing in 40 ℃ in the water for another 24 hours. The whole experiment lasted 4 months of 20 F-T cycle in the temperature range of +40 ℃ to -18 ℃.

3.3.3.1. Dynamic mechanical study of FFRCs with different aged levels

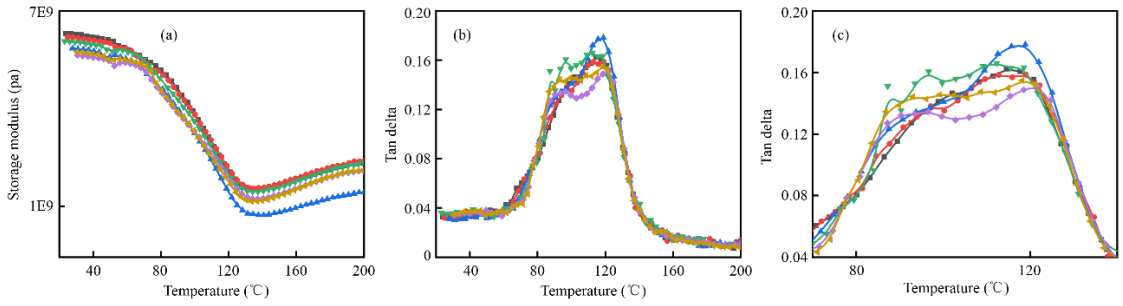

Figure 3.15 DMA results of composites with different ageing levels: (a) storage modulus vs. temperature, (b) tanδ vs. temperature, and (c) partial enlarged view of tanδ vs. temperature from 60℃ to 160℃ (black, red, blue, green, blown and purple curves represent the 1,2,3,5,10 and 20 F-T cycles at 1 Hz).

Figure 3.15 shows typical graphs of storage modulus (a) tanδ (b and c) versus temperature (RT-200 ℃) for composite samples under different F-T cycles at 1 Hz.

The slight increase of E' in the rubbery plateau region and the tan δ double peaks are associated, as shown previously, with a progressive removing, during DMA test, of water from the materials, which were initially water-saturated. It can be observed that the trends of these curves for all the aged materials have many similarities in the tested temperature range, even if at glassy a slight decrease in modulus with cycles is observed. It seems that the -18 ℃ to 40 ℃ cycle does not significantly strengthen the water absorption rate or total amount, so the water content is controlled and kept basically unchanged. Judging from the data of dynamic mechanical performance analysis, the F-T test seemed not to affect the structure of composite materials.

3.3.3.2. Quasi-static mechanical studies of FFRCs with different aged levels

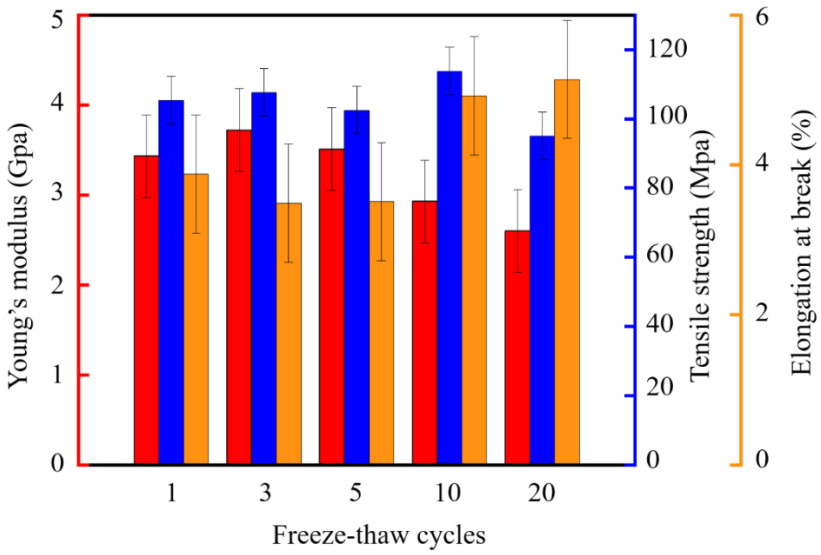

Figure 3.16 Tensile behavior of flax/bio-epoxy composites under different F-T cycles.

Comparison curves of Young's modulus, tensile strength, and elongation at break of flax/bio-epoxy composites through different F-T cycles are shown in Figure 3.16. Young's modulus did not change significantly up to 5 F-T (around 3.5 GPa) after which it decreased (- 24 % at 20 F-T cycles). The tensile strength of the material fluctuates obviously and does not appear to be significantly affected by F-T cycling with, however, a slight decrease of around 9% observed after 20 cycles. As for Young's modulus, the elongation at break did not change

significantly up to the first 5 cycles (+ 9%) after which it increased more deeply (+ 32 % at 20 F-T cycles). The specific experimental data are shown in Table 3.3.

Table 3.3 Mechanical test results of FFRCs undergone different F-T cycles.

F-T cycles	Young's modulus (Gpa)	tensile strength (Mpa)	elongation at break (%)
1	3.43	105.38	3.88
3	3.72	107.9	3.49
5	3.51	102.46	3.51
10	2.93	113.78	4.92
20	2.6	95.06	5.14
SD	0.459641	6.877934	0.788016

The typical failure features (optical, SEM) observed on composites under different F-T cycles are presented in Figure 3.17 & 3.18.

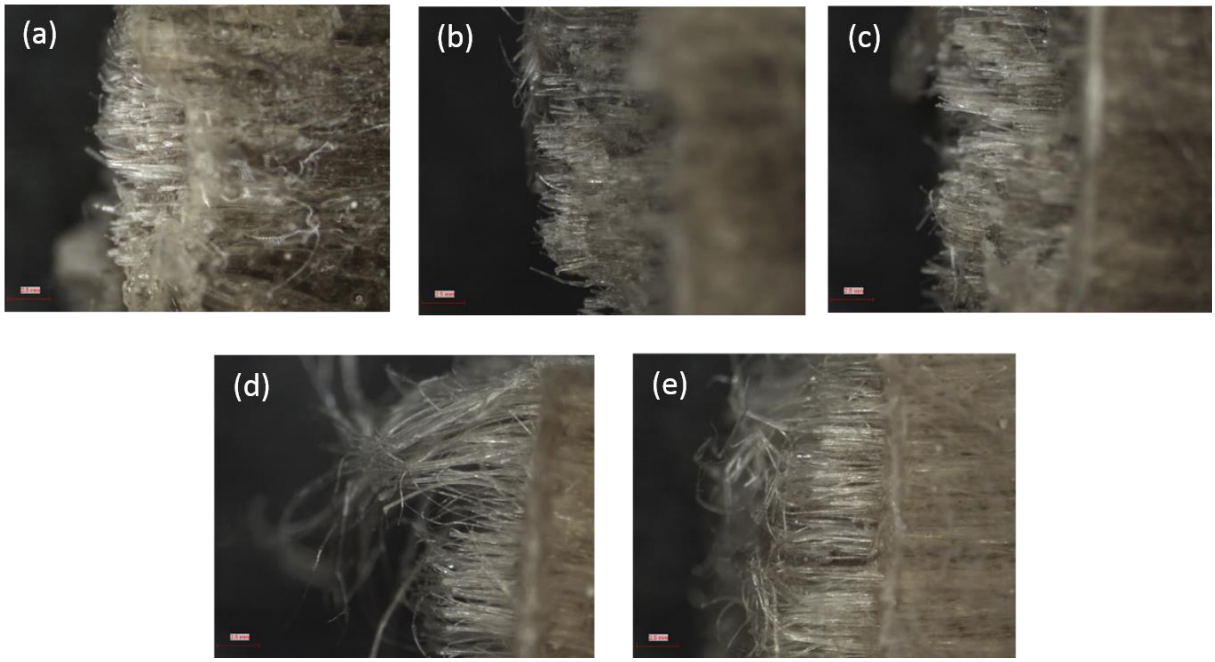

Figure 3.17 Optical view of the composite fracture under different F-T cycles, (Figure a-e represent 1, 3, 5, 10 and 20 cycles respectively).

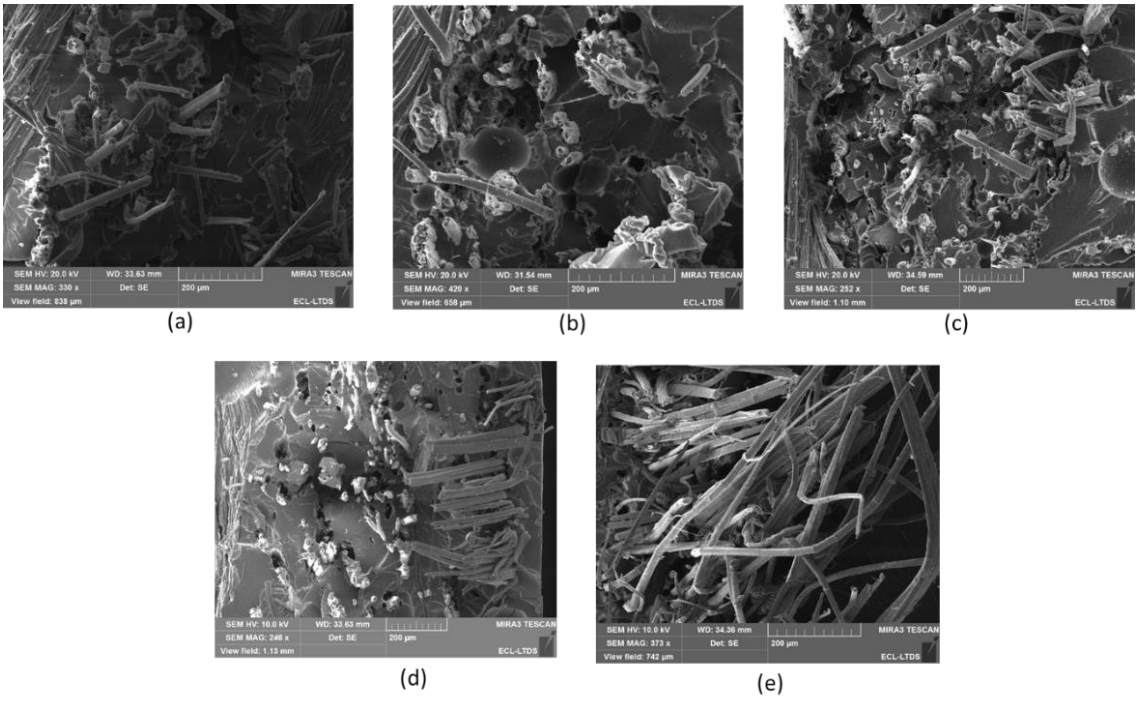

Figure 3.18 SEM observation of the composite fracture under different F-T cycles, (Figure a-e represent 1, 3, 5, 10 and 20 cycles respectively).

The micrographic analyses are consistent with the previous results. The figure 3.17a-c shows that there are no major differences in pull-out lengths and fiber appearance up to the 5th cycle. It consists of small extracted fiber with matrix debris on the fiber surface (Figure 3.18a-c), thus indicating enough good stress transfer. As previously mentioned, the quality of the interface is associated with hydrogen bonding and mechanical interlocking. For F-T experiments, the material is at water saturation state and it was shown that in this case the mechanical anchoring is improved due to fiber swelling making the effect of water less detrimental than at lower humidity levels.

Beyond the 5th cycle, there is an increase in the length of the pull-out associated with fibrillation of the fibers (Figure 3.17d-e & Figure 3.18d-e), in some areas after 10 F-T cycles and on the entire fracture surface for the 20th cycles. During F-T, humidity cycling generates breakage phenomena associated with the alternating swelling and contraction of the composite's constituents (fiber and matrix). This type of stress plays the same role as mechanical fatigue and leads to crackings and failures at the interface. It is, then, for the fibers disconnected from the matrix to deform and fibrillate. Consequently, the differences in mechanical properties are due to a progressive degradation at the interface of the fibers, which become more significant with the cycles. This is highlighted on the SEM views (Figure 3.18d-e), where debonding at the interfaces are clearly visible as holes between fiber and matrix and

the occurrence especially for the 20th cycle. Moreover, as for the water ageing, the matrix exhibits, in all the cases a relatively smooth fracture surface with river and ribbon patterns which means that no large-scale plastic deformation occurred during the fracturing process.

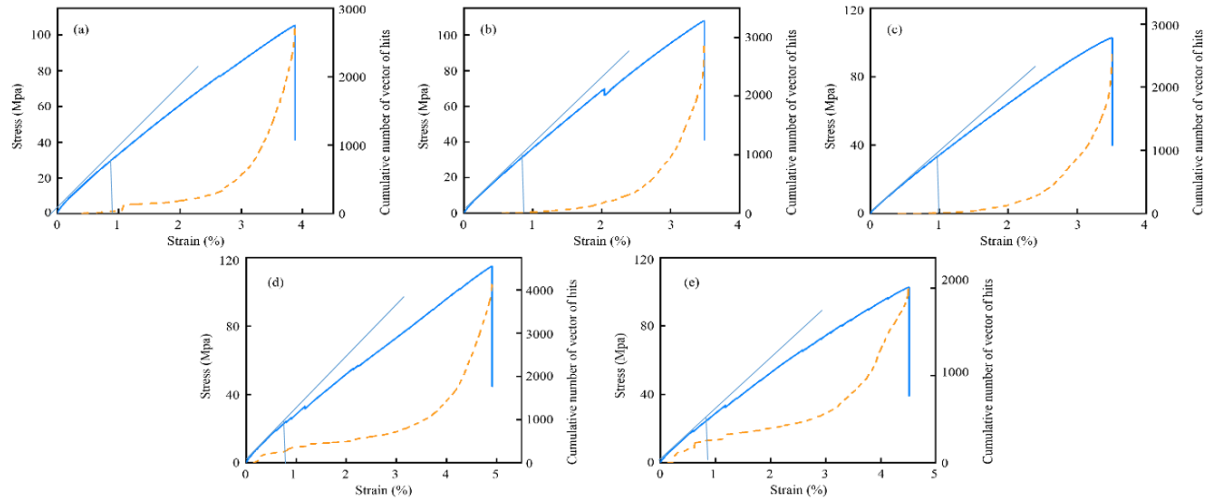

Figure 3.19 Correlation between the evolution of acoustic activity of all samples and the law of stress-strain behavior:

(a) F-T 1 cycle, (b) F-T 3 cycles, (c) F-T 5 cycles, (d) F-T 10 cycles, (e) F-T 20 cycles.

The acoustic signals in Figure 3.19a-c have a certain similarity, corresponding to the test results after 1, 3, and 5 F-T cycles of the composite, respectively. The onset of AE occurrence is almost identical (1 %) and the cumulative hit curves according of strain show, in all cases, an exponential shape. Figure 3.19d and 3.19e show the mechanical and acoustic response of the composite specimens after 10 and 20 F-T cycles. Compared with the previous trend, it can found that the stage with no acoustic response reduces, and the second stage appears earlier. In addition, it can be further observed that as the higher cycles, (10 and 20) the second-stage acoustic response shows a stabilization before an exponential increase until the material fails.

Figure 3.20 and 3.21 are acoustic signal diagrams of composite specimens that have undergone F-T cycles, using the clustering method. By analyzing the AE signals during the quasi-static tensile test, the failure mechanisms which are involved in the fracture process can be understood. As shown in those pictures, the acoustic signal corresponding to debonding at the interface (class B) and pull-out (class C) is detected from the beginning of stretching, which consistent and SEM pictures and the degradation of the interface with F-T cycles. It can be also observed that the stabilization for the highest cycles, appears for all three classes of damage. This may due to the fact that the occurrence of early cracks can slow the propagation of cracks by defection mechanism and blunting effect. For the composite having

undergone 20 cycles, it was observed a decrease in the acoustic activity of the classes when compared to the other composites. This kind of result is associated to a decrease of the quality of the load transfer. These analyses provide an understanding of the quasi-stability of the mechanical properties of the composite for low cycles and the more significant changes in particular for composites that have been subjected to 20 F-T cycles.

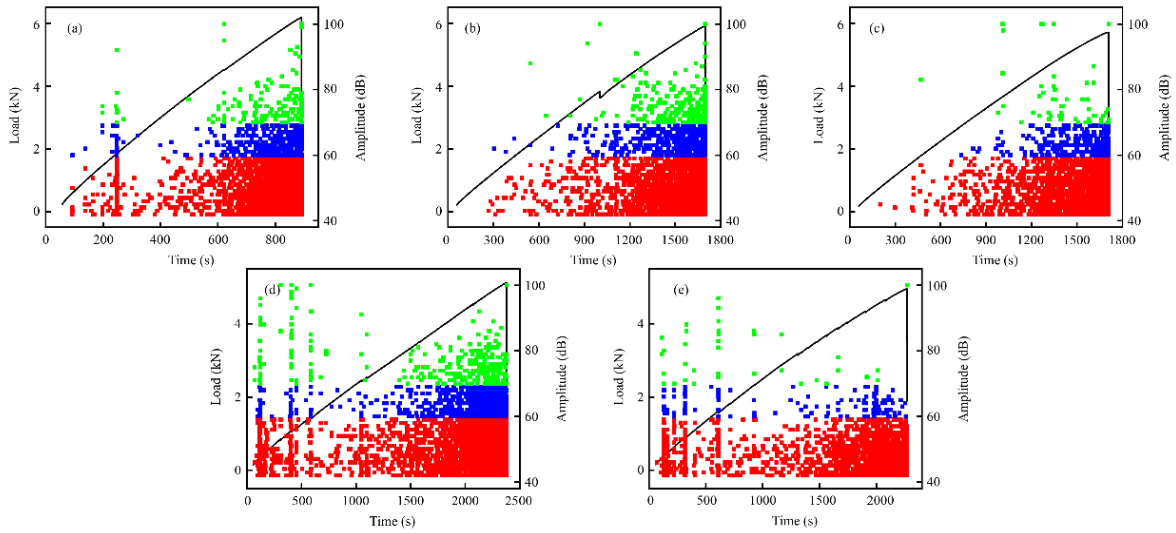

Figure 3.20 Distribution of amplitude versus time of AE signals under tensile tests for all specimens: (a) F-T 1 cycle, (b) F-T 3 cycles, (c) F-T 5 cycles, (d) F-T 10 cycles, (e) F-T 20 cycles.

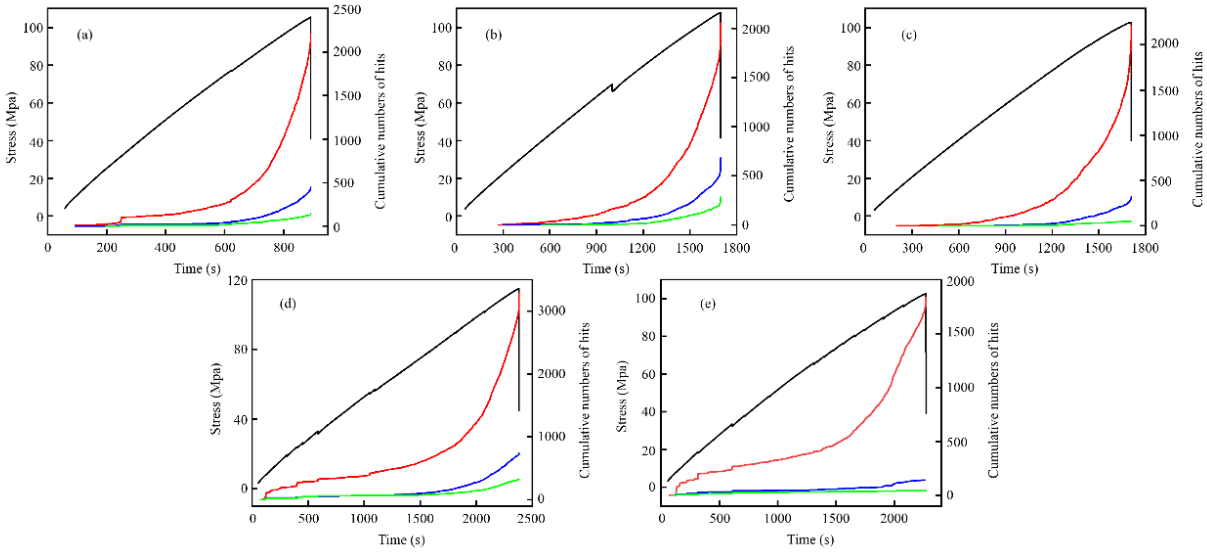

Figure 3.21 Time dependency of different classes of damage mechanisms identified under tensile tests for all specimens: (a) F-T 1 cycle, (b) F-T 3 cycles, (c) F-T 5 cycles, (d) F-T 10 cycles, (e) F-T 20 cycles.

3.3.4. Wet-dry cycles

This part studies the changing process of the tensile properties of FFRCs under long-term W-D cycles. The ageing study was performed under "wet-dry" cycles at constant temperature: the samples (water quasi-saturated) were soaked into the water with a maintained temperature of 40 °C for a week, then dried at 40 °C in an oven for another week. Unfortunately, due to external reason for pandemic lockdown, only 4 sorption-desorption cycles were done.

3.3.4.1. Dynamic mechanical study of FFRCs with different aged levels

Regarding the dynamic experiment of FFRCs under through W-D cycles, the typical curves of storage modulus and tan delta versus temperature at 1 Hz are shown below (Figure 3.22). Among them, the black, red, blue, and green curves represent the composite samples after one, two, three, and four W-D cycles, respectively.

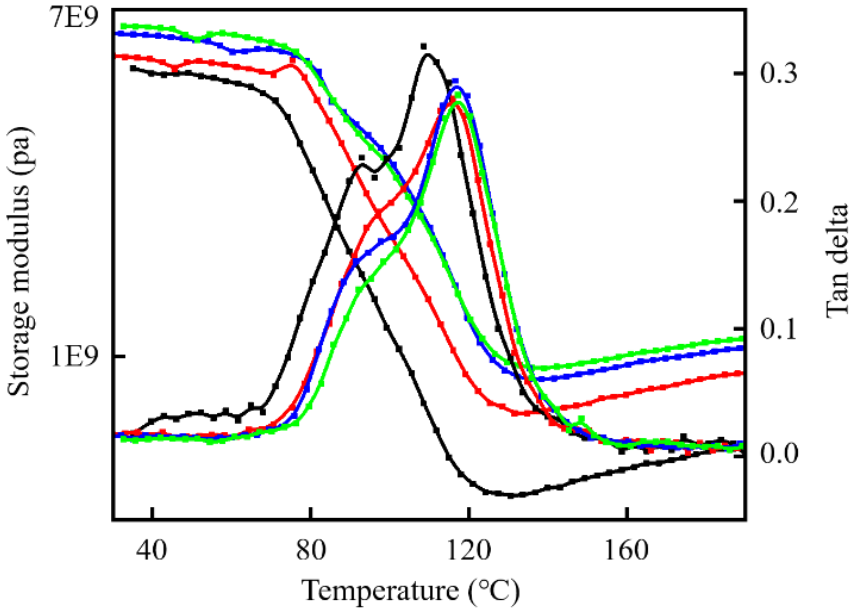

Figure 3.22 DMA results of composites under different cycles (the black, red, green and blue curves represent the composites through 1,2,3,4 W-D cycles) at 1Hz.

It can be observed that, as the number of cycles increases, the storage modulus of the composite material increases in both the glassy state and the rubbery state, and the magnitude of the increase gradually decreases. A double tan δ peak (located at 90 ℃ and 120 ℃) is always seen whatever the number of cycles that the composite has undergone. The reason for this double peak is the plasticization to the composite laminates by moisture, and the progressive drying of the material during test, as shown previously. As the experiment progresses, the bimodal trend gradually fades. This indicates that the moisture is partially removed during the

W-D cycles from the matrix. The damping of the fibers plays practically no importance on the overall damping of the composite because it is very low (around 10^{-2}) [26] and the fiber volume rate is small, around 0.20. The global increase of the tan δ is associated to the progressive loss of water in the matrix but also in the fibers. As for the loss factor, the progressive drying of the fibers must play a role in the global increase of the modulus, as their Young's modulus is much higher than that of the matrix.

3.3.4.2. Quasi-Static mechanical studies of FFRCs with different aged levels

The typical comparison of Young's modulus, tensile strength, and elongation at break of FFRC with different W-D cycles is shown in Figure 3.23.

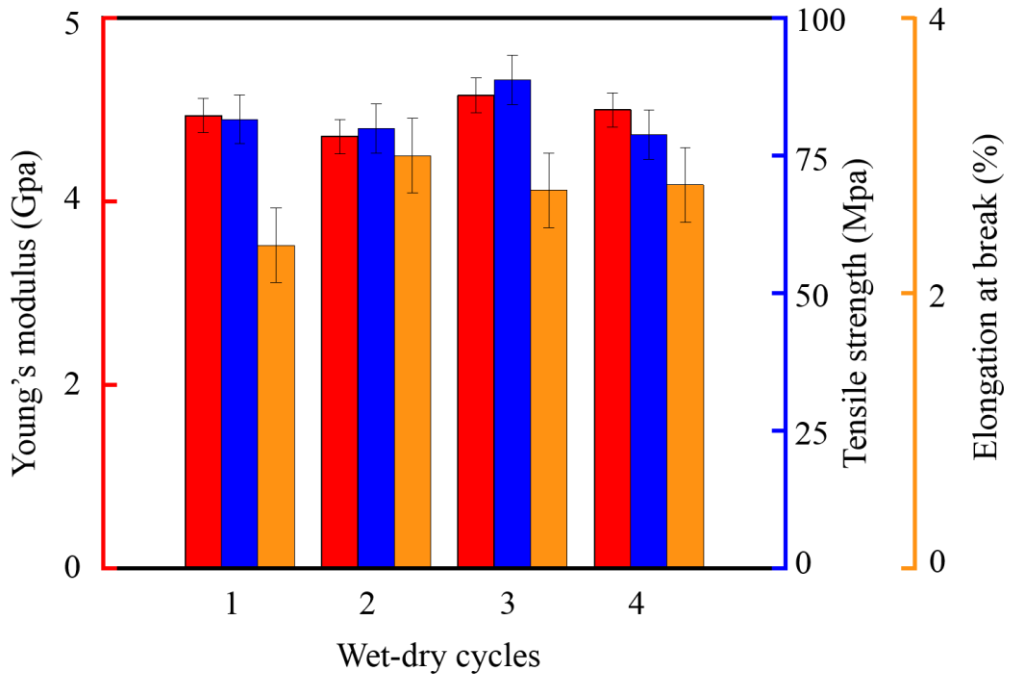

Figure 3.23 Tensile behavior of FFRCs under different W-D cycles.

According to the number of cycles, the average mechanical properties seem less affected than for the other ageing types and the changing trend of these values is not very obvious, with fluctuations. This is probably partly due to the low number of cycles. The number of cycles has a very slightly positive effect on Young's modulus of this material (≈+1%). Unlike the modulus, after 4 cycles' exposure, the ultimate strength of the composite decreased, but also very slightly (- 3%). The tensile strength is determined mainly by the tensile strength of the fibers and the properties at the interface fiber/matrix, but as previously mentioned many sample-dependent defects (fiber misalignment, distribution of the components, etc.) have

some importance. Therefore, this variation is not significant. The elongation at break also fluctuates with an overall increase. The average experimental data are shown in Table 3.4.

Table 3.4 Mechanical test results of FFRC under different W-D cycles

WD cycles	Young's modulus (Gpa)	tensile strength (Mpa)	elongation at break (%)
1	4.94	81.63	2.35
2	4.71	80	3
3	5.16	88.78	2.75
4	5	78.82	2.79
SD	0.186436	4.46615	0.271462

Fracture features seen under the Optical Microscope are presented in Figure 3.24. Unlike for water ageing and F-T cycles, there are no significant differences between composites in terms of pull-out length and fiber appearance with cycles. This result suggests no major influence of sorption-desorption cycles in the range of number of cycles studied on the quality of interfaces. Optical microscopy pictures also reveal the presence of surface cracks at the fracture level, which seems to indicate the presence of matrix embrittlement. SEM photos (Figure 3.25) confirm that pull-out lengths do not change significantly with cycles. It is also shown in this figure that the matrix has a brittle behavior whatever the cycling and that matrix cracks mainly occur in the external region, near the edge of the sample.

The action of water (in a stage of non-degradation) on polymers is similar to that of temperature. Water adsorption causes the epoxy resin and the fiber swollen and they shrink when the composite is dried that may lead to matrix microcracks and debonding at the interface, as for mechanical fatigue. Unlike for water ageing and F-T cycles there are no significant differences between composites in terms of pull-out length, which suggests a low degradation of the interfaces, probably due to the low number of cycle. On the other hand, the W-T cycles seem to be more drastic than F-T cycling, with regard to matrix cracking in the external region. In fact, the desorption-absorption process is mainly located in the external zone as the advancement of water inside the sample is lower than air.

The small evolution of the mechanical properties at failure with the cycles shows that the matrix cracks have little influence on them, conversely the properties at the interfaces.

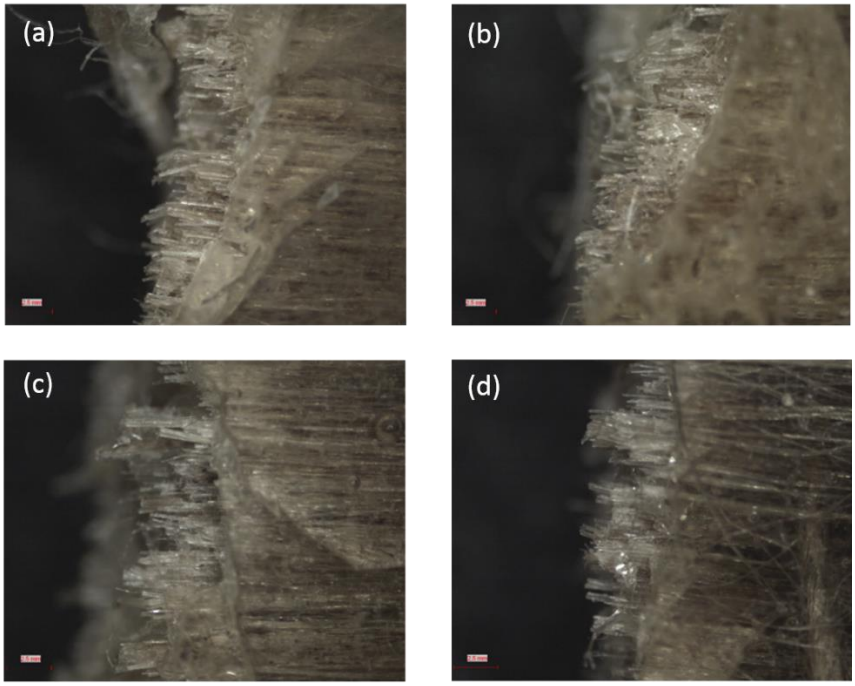

Figure 3.24 Optical view of the composite fracture under different W-D cycles, (Figure a-d represent 1, 2, 3 and 4 cycles respectively).

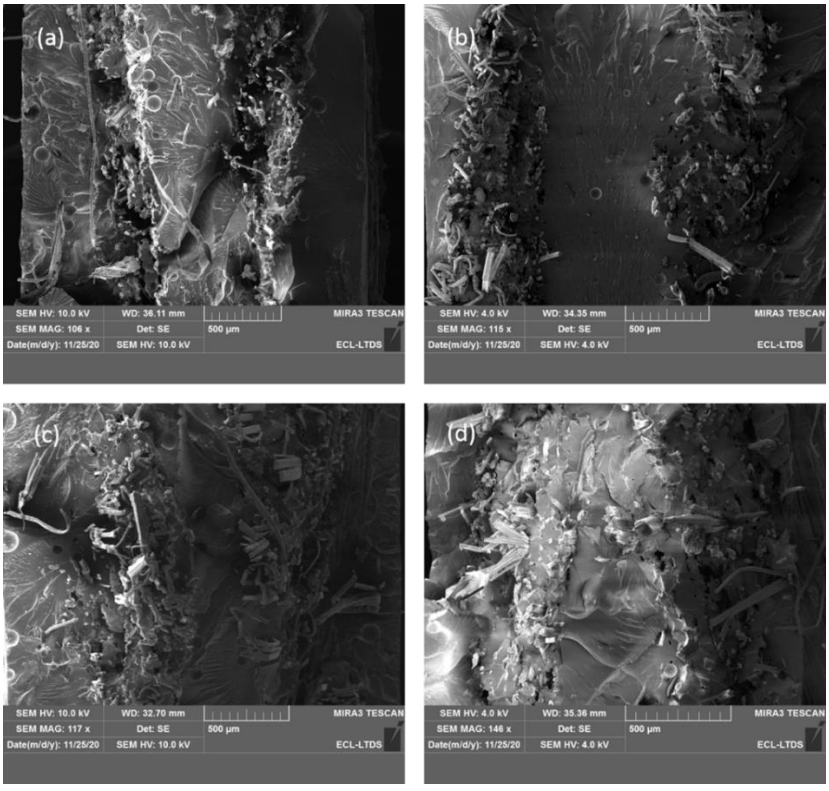

Figure 3.25 SEM observation of the composite fracture under different W-D cycles, (Figure a-d represent 1, 2, 3 and 4 cycles respectively).

Study the evolution of damage by monitoring AE activity

Like previous ageing analysis, the quasi-static tensile experiments of the composite laminates that have undergone W-D cycles were also monitored and analyzed by AE, and its activity was expressed by the evolution of the cumulative number of hit carriers, as shown in Figure 3.26.

The stress-strain curves in Figure 3.26 have the same trend: a linear part (stage I), a deviation from linearity associated with the beginning of the AE (onset of the stage II) and finally the coalescence of the different defects with a sudden break (stage III). However, the tendencies of the acoustic activities in the four graphs show some differences. The almost-zero acoustic events phase in Figures 3.26a and 3.26c lasted for a long time, until about 1.5% of the strain after which there is an exponential increase of AE. The period without acoustic events in Figures 3.26b and 3.26d is shorter. After that, the cumulative events versus elongation curve shows an upward trend and then a stabilization before an exponential increase until the material fails. This effect is much more significant for the material that has undergone the most W-D cycles. This behavior was yet observed in the case of F-T cycled samples and was assigned to the occurrence of micro-failures that can act as barriers to crack propagation and can reduce the stress at the tip of the large cracks.

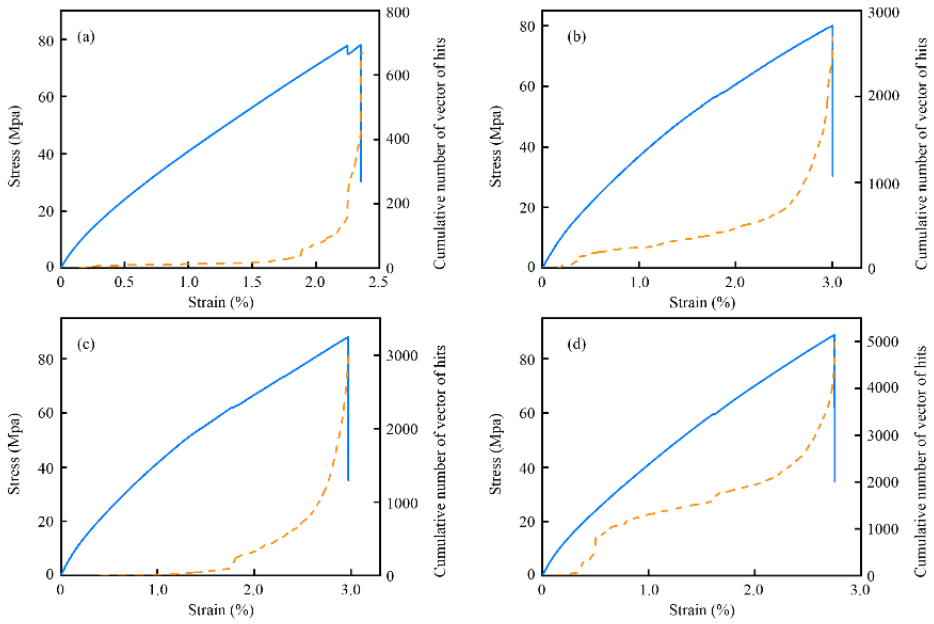

Figure 3.26 Correlation between the evolution of acoustic activity of all samples and the law of stress-strain behavior: (a) W-D for 1 cycle, (b) W-D for 2 cycles, (c) W-D for 3 cycles, (d) W-D for 4 cycles.

Figure 3.27 and Figure 3.28 show the time dependence of the different types of damage mechanisms under the tensile test according to the clustering method. For the number of W-D cycles, high-amplitude damage events such as Class B (debonding at the interface) or Class C (fiber breakage/pull-out) are gradually detected in advance. As few changes were observed in both fracture behavior and fracture features, this result highlights the importance of AE in the monitoring and control of composite materials and structures.

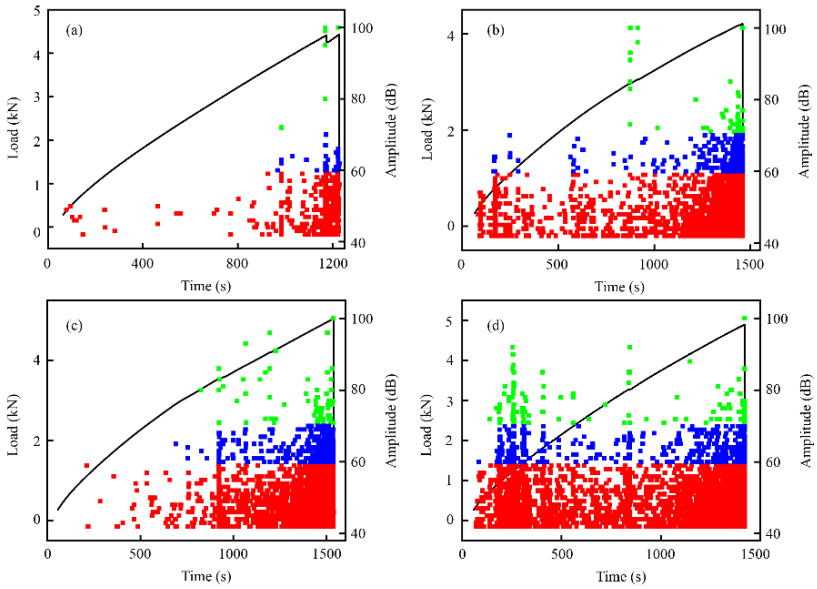

Figure 3.27 Distribution of amplitude versus times of AE signals under tensile tests for all specimens: (a) W-D for 1 cycle, (b) W-D for 2 cycles, (c) W-D for 3 cycles, (d) W-D for 4 cycles.

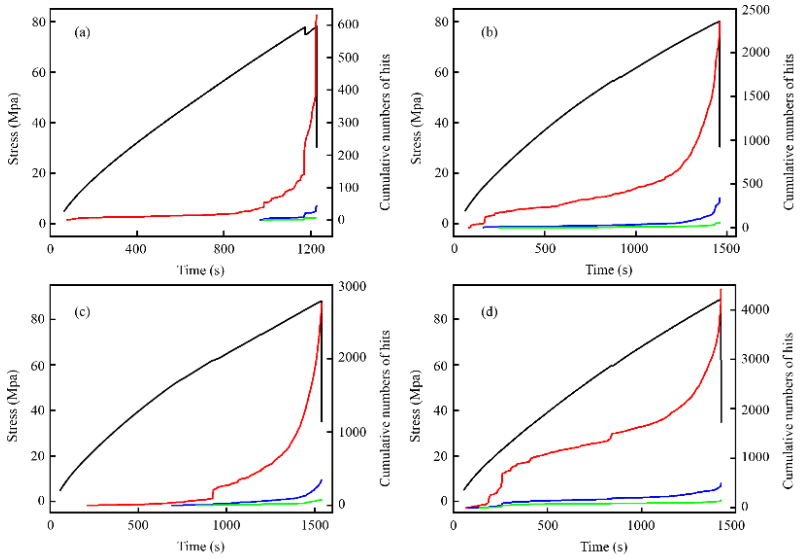

Figure 3.28 Time dependency of different classes of damage mechanisms identified under tensile tests for all specimens: (a) W-D for 1 cycle, (b) W-D for 2 cycles, (c) W-D for 3 cycles, (d) W-D for 4 cycles.

3.4. Chapter summary

Flax/bio-epoxy composites are increasingly extensively used in different engineering applications, requiring a thorough understanding of their mechanical properties and durability resistance during service. Extreme environmental conditions could reduce their mechanical properties or even shorten their service life. This chapter focuses on the engineering structural applicability of FFRCs under different environmental conditions. Evaluating the durability of bio-composites is the main motivation for this section. The composite laminates were exposed to different environmental conditions: water immersion, freeze-thaw cycles and wet-dry cycles. For those composite specimens with different ageing degrees, dynamic mechanical performance analysis and static tensile experiments under AE monitoring were used to understand their overall performance and the adverse effects of different exposure conditions. The results show that for the samples immersed in water at room temperature, the water absorption obeys Fick's laws of diffusion. Ware immersion ageing causes fiber and resin plasticization, and further leads to composite material structure damage and mechanical performance degradation. For the freeze-thaw cycles, due to the shrinkage/swelling process of the components the effective bond with the matrix is lost, and a gap is created between the fiber and the matrix, and this gap becomes a new source of micro damages. For the wet-dry cycles, the overall mechanical performance of composite materials has not been significantly affected compared with other ageing modes, even if the AE shows that high amplitude damages occur at lower stress levels after 4 cycles.

3.5. References

1. Matykiewicz D, Barczewski M. On the impact of flax fibers as an internal layer on the properties of basalt-epoxy composites modified with silanized basalt powder[J]. Composites Communications, 2020: 100360.
2. Fiore V, Calabrese L, Scalici T, et al. Experimental design of the bearing performances of flax fiber reinforced epoxy composites by a failure map[J]. Composites Part B: Engineering, 2018, 148: 40-48.
3. Wambua P, Ivens J, Verpoest I. Natural fibres: can they replace glass in fibre reinforced plastics?[J]. Composites science and technology, 2003, 63(9): 1259-1264.
4. Joshi S V, Drzal L T, Mohanty A K, et al. Are natural fiber composites environmentally superior to glass fiber reinforced composites?[J]. Composites Part A: Applied science and manufacturing, 2004, 35(3): 371-376.
5. Assarar M, Scida D, El Mahi A, et al. Influence of water ageing on mechanical properties and damage events of two reinforced composite materials: Flax–fibres and glass–fibres[J]. Materials & Design, 2011, 32(2): 788-795.

6. Hallonet A, Ferrier E, Michel L, et al. Durability and tensile characterization of wet lay-up flax/epoxy composites used for external strengthening of RC structures[J]. Construction and Building Materials, 2019, 205: 679-698.
7. Cuinat-Guerraz N, Dumont M J, Hubert P. Environmental resistance of flax/bio-based epoxy and flax/polyurethane composites manufactured by resin transfer moulding[J]. Composites Part A: Applied Science and Manufacturing, 2016, 88: 140-147.
8. Sodoke F K, Toubal L, Laperrière L. Wetting/drying cyclic effects on mechanical and physicochemical properties of quasi-isotopic flax/epoxy composites[J]. Polymer degradation and stability, 2019, 161: 121-130.
9. Moudood A, Rahman A, Khanlou H M, et al. Environmental effects on the durability and the mechanical performance of flax fiber/bio-epoxy composites[J]. Composites Part B: Engineering, 2019, 171: 284-293.
10. Ameur M B, El Mahi A, Rebiere J L, et al. Investigation and identification of damage mechanisms of unidirectional carbon/flax hybrid composites using acoustic emission[J]. Engineering Fracture Mechanics, 2019, 216: 106511.
11. Rindorf H J. Acoustic emission source location in theory and in practice[M]. Brüel & Kjær, 1981.
12. Advanced high strength natural fibre composites in construction[M]. Woodhead Publishing, 2016.
13. Jiang Y, Lawrence M, Hussain A, et al. Comparative moisture and heat sorption properties of fibre and shiv derived from hemp and flax[J]. Cellulose, 2019, 26(2): 823-843.
14. Wang A, Wang X, Xian G. Mechanical, low-velocity impact, and hydrothermal aging properties of flax/carbon hybrid composite plates[J]. Polymer Testing, 2020: 106759.
15. Cheour K, Assarar M, Scida D, et al. Effect of water ageing on the mechanical and damping properties of flax-fibre reinforced composite materials[J]. Composite Structures, 2016, 152: 259-266.
16. Shen C H, Springer G S. Moisture absorption and desorption of composite materials[J]. Journal of composite materials, 1976, 10(1): 2-20.
17. R, Touchard F, Chocinski-Arnault L, et al. Influence of moisture and drying on fatigue damage mechanisms in a woven hemp/epoxy composite: Acoustic emission and micro-CT analysis[J]. International Journal of Fatigue, 2020, 136: 105593.
18. W, El Mahi A, El Gharad A, et al. Acoustic emission monitoring of damage progression in glass/epoxy composites during static and fatigue tensile tests[J]. Applied Acoustics, 2018, 132: 124-134.
19. Marouani S, Curtil L, Hamelin P. Ageing of carbon/epoxy and carbon/vinylester composites used in the reinforcement and/or the repair of civil engineering structures[J]. Composites Part B: Engineering, 2012, 43(4): 2020-2030.
20. Stamboulis A, Baillie C A, Peijs T. Effects of environmental conditions on mechanical and physical properties of flax fibers[J]. Composites Part A: Applied Science and Manufacturing, 2001, 32(8): 1105-1115.
21. Chen H, Miao M, Ding X. Influence of moisture absorption on the interfacial strength of bamboo/vinyl ester composites[J]. Composites Part A: Applied Science and Manufacturing, 2009, 40(12): 2013-2019.

22. Joffe R, Andersons J, Wallström L. Strength and adhesion characteristics of elementary flax fibres with different surface treatments[J]. Composites Part A: Applied Science and Manufacturing, 2003, 34(7): 603-612.
23. Masoodi R, El-Hajjar R F, Pillai K M, et al. Mechanical characterization of cellulose nanofiber and bio-based epoxy composite[J]. Materials & Design (1980-2015), 2012, 36: 570-576.
24. Barré S, Benzeggagh M L. On the use of acoustic emission to investigate damage mechanisms in glass-fibre-reinforced polypropylene[J]. Composites Science and Technology, 1994, 52(3): 369-376.
25. Ceysson O, Salvia M, Vincent L. Damage mechanisms characterization of carbon fiber/epoxy composite laminates by both electrical resistance measurements and acoustic emission analysis[J]. Scripta Materialia, 1996, 34(8).
26. Kelley S S, Rials T G, Glasser W G. Relaxation behaviour of the amorphous components of wood[J]. Journal of materials science, 1987, 22(2): 617-624.

Chapter 4. Cure and Damage Monitoring of Flax Fiber-Reinforced Epoxy Composite Repairs for Civil Engineering Structures Using Embedded Piezo Micro-Patches

In recent years, high interests of the repair of civil engineering structures were concentrated on the fiber-reinforced thermosets as a structural component for repairing applications. The properties of the resulting mechanical composites are directly in relation to the reinforcement type but also to viscoelastic matrix properties. During this part of the research, it proposes to in-situ follow-up the cure mechanism of a flax reinforced bio-epoxy-amine resin as repairing patches using piezoelectric elements embedded in the composite structure. After curing, the sensors remain in the part and were used as a damage detector for structural health monitoring (SHM). Curing results compared to DMA analysis show that embedded piezoelectric cells are well suited to in-situ monitor the reaction progress. Moreover, this technique was found to be reliable for detecting preliminary signals of critical state for the composite by comparison with Acoustic Emission (AE) and Digital Image Correlation (DIC).

4.1. Introduction

The built heritage in France is wide but often aged. Many civil engineering structures have defects that need to be repaired in a more or less short-term period to prevent the rapid development of structural disorders that may lead to tragedies such as the Morandi Bridge (Italy) collapse. Recently, increasing interests of the maintenance and repair to civil structures have concentrated on the fiber-reinforced thermosets as structural components for repairing applications. They are expected as a repair and/or reinforcement method for structural rehabilitation for their high specific stiffness, specific strength and chemical resistance compared to traditional materials such as steel and concrete. Those composite patches are usually fabricated by hand lay-up manufacturing process and then bonded on the cracked structures to prevent the growth of the failures. Among the thermosets, room temperature curing epoxies get the most attention due to their merits for fabrication and easy to control. The properties of composites are directly in relation to reinforcement type, stacking sequence but also to viscoelastic matrix properties and reinforcement/matrix interactions. The most important factor, which controls the properties of the matrix and of the reinforcement-matrix

interface, is in particular the cross-linking density. The cross-linking density is influenced by manufacturing processes, and it is linked to the degree of cure. However, the cure of thermosets is a complex process to form a three-dimensional (3D) macromolecular network, and the final morphology of this particular 3D network determines the properties and applications of the final material.

That is, how to monitor and control the curing process of thermosets to the desired level is an essential issue. As a result, there is a growing interest in utilizing the sensors which can be embedded within a structural material and provide real-time, performance feedback. In previous, several systems with a sensing function, which could be embedded within the composite material to analyze, were used to evaluate the different phenomena during on-line polymerization of thermoset materials, as for instance dielectric sensor, optical fibers, or piezoelectric sensors. These sensors can be used to monitor the health state of composites, from their curing process to the end of their life cycle.

Dielectrics sensors consist of interdigitated electrodes deposited on an insulating substrate. They are used to measure the sample complex permittivity ($\varepsilon^* = \varepsilon' + j\varepsilon''$) and conductivity ($\sigma$) changes during curing. From these measurements, it is possible to follow the progress of chemical reactions and to obtain information on relevant phenomena in terms of different levels of polymerization [1-2]. Implantation of optical fibers in composite structure during cure, helps to follow the progress of chemical reaction in terms of degree of conversion using for example the variation of its density by refractive index measurements (intensity-based sensors) [3] or by the use of Bragg gratings sensors (wavelength based sensors) that measure the local strain changes associated to thermoset shrinkage [4]. The embedding of small piezoelectric inserts through the material to be monitored overcomes coupling reproducibility with conventional ultrasonic non-destructive testing (NDT) technique. These inserts can be used to have in-situ information about material states from the matrix liquid state to the end of their life cycle [2-5].

This study, in the frame of a collaborative research (MICRO ANR project), proposes to use flax reinforced bio-epoxy-amine resin as repairing patches. Up to now continuous carbon fiber reinforced epoxy composites (CFRP) are mainly used especially due to their lightness and durability to repair existing infrastructures and to increase their life-span. Indeed, the density of carbon fibers (1.77 g/cm^3 for the high strength carbon fiber which is the mostly used) is

significantly lower than that of E-glass fibers (GF) (2.6 g/cm^3), and alkaline environment of concrete can cause degradation to the latter.

Natural fiber reinforcements especially flax fibers, show interesting characteristics for civil engineering applications for which the reduction of carbon emissions is becoming one of the main challenges [6]. They are environmentally friendly, relatively cheap to produce and renewable. The stiffness (E) and strength (σ_{ult}) along the axis of the fiber are in the range (45-55 GPa) and (800–1000 MPa) respectively, and due to their lightness (density = 1.4-1.5 g/cm^3), their specific properties are comparable to those of the E-glass fiber (E= 73 GPa ; σ_{ult} = 2000 MPa) [7].

Small PZT piezoelectric discs fully embedded in the composite were chosen as sensors. These sensors have high sensitivity and are well suited for monitoring composite repairs. They are manufactured directly on site. They are indeed more easily embeddable than optical sensors for which precautions must be taken: (i) to prevent excessive bending during handling, (ii) to embed them parallel to the reinforcing fibers to avoid the occurrence of large resin pockets. These kinds of flaws can have a detrimental effect on the durability of the composite repair.

The change in the impedance spectrum, which is linked to the changes of matrix viscoelastic properties as cure progressed, was used to analyse the different steps of the epoxy cure and their consequences on the mechanical properties of the material. Moreover, after curing, this sensor could be used as structural health monitoring (SHM) sensor for the composite material. Indeed, during their use, the composite patches could be subjected to different damages, such as ageing processes or debonding from the concrete structure. The SHM capability of such a system is based on the existence, during the damaging processes of acoustic emission, which can be registered by piezoelectric sensors in a passive or active way.

4.2. Materials

The thermoset resin system is designed for ambient and low temperature cure, and it is the same than used in previous chapters. The DGEBA epoxy prepolymer is a low molecular weight “green” epoxy resin made from bio-based epichlorhydrine (EnviPOXY®530 from SPOLCHEMIE) (28% bio-based carbon). The bio-hardener is a solvent-free, low viscosity phenalkamine curing agent made through the Mannich reaction of cardanol from cashew nuts, formaldehyde, and amines (Cardolite NX5619) (100 % bio-based carbon). Resin and hardener were mixed in stoichiometric ratio. The glass transition temperature (Tg) of the reactive

mixture, T_{g0} was -39 ℃ determined from DSC heat flow curves (midpoint), recorded at a heating rate of 10 K/min *(*DSC1 device from METTLER-TOLEDO). In this work, the curing was carried out at room conditions (T = 23 ℃; HR = 40%). The reinforcement is a *quasi*-unidirectional flax fabric made of untwisted rovings (LINCORE® FF FLAX FABRIC) supplied by DEPESTELE Group. The weft and warp ratio is 9/91 and the areal density is 200 g/m^2. The relative moisture content of the fabric is about 5-6 % under ambient-condition storage and it was used as received, without any preliminary treatment. In this work, the curing was carried out at room conditions (T = 23 ℃; HR = 40%). The PZT discs sensors are 0.2 mm thick disk with a diameter of 7 mm from STEMINC® working in radial vibration mode (resonant frequency is about 300 kHz). The Curie temperature of the ceramics is around 250 ℃. Ag electrodes are deposited on each side of the ceramic and the electrical wires for connection were soldered on one side.

4.3. Experimental

4.3.1. In situ curing monitoring method

The technique used in this work was based on the measurement of the electrical impedance of a piezoelectric PZT ceramic disc embedded in the composite materials as its impedance is linked to the characteristics (stiffness, damping) of the surrounding medium, which vary as cure progresses. Indeed, the curing process is the transition that thermosettings change from viscous liquid state to infusible cross-linked solid (3D-network) [8-9]. This transformation may involve two main transitions: gelation when the viscous liquid prepolymer is transformed in an infusible, insoluble gel or rubber-like material and vitrification, which corresponds to rubber-glass transition. At vitrification, the rate of the cure reaction may be reduced due to molecular mobility. This phenomenon occurs only if the reactive mixture is cured at a temperature lower than the infinite Tg of completely cross-linked system. This takes place when the Tg equals the cure temperature.

The composites were fabricated using wet hand lay-up to be representative of materials used in the rehabilitation of civil engineering structures. A first UD fabric layer was arranged on a wooden mold coated with release agent. The resin was then applied by using a squeegee and a paint roller to ensure enough infiltration of the reinforcement with the resin and removing excess resin and entrapped air. Once the first layer was fully impregnated, the second reinforcement ply in which two piezoelectric discs were placed is applied and impregnated. Figure 4.1 shows the plate after manufacturing. To ensure the wetting of the outer ply and to a

minimize air pocket rate, careful roll-out was done again. Indeed, poor wet-out and large amount of porosities can induce a structural weakness of the composite repairs and affect their long-time behavior [10]. In civil engineering rehabilitation field, skilled labor is required, but due to difficult workability environment conditions, composites may exhibit some defects originating from manufacturing processes. This justifies the need for in-situ control in this procedure.

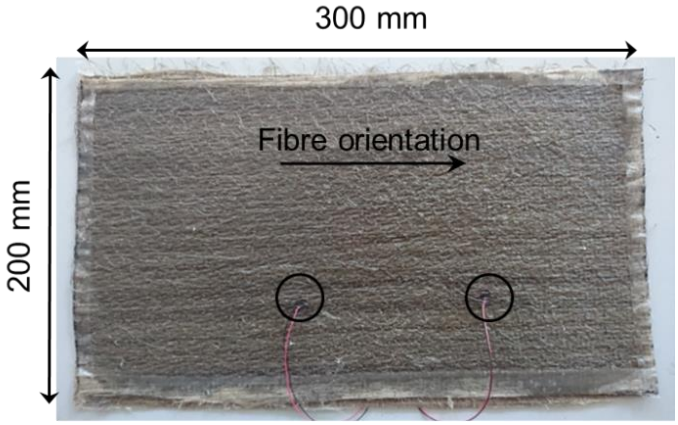

Figure 4.1 Flax reinforced epoxy composite material with embedded PZT discs; the position of the sensors is given by the black circles.

The purpose of embedding two piezo-cells between the two layers of the flax fabric was to ensure a way to perform an analysis of the composite material integrity, by signal transmission through the plate. However, it was here used to confirm the recorded signal shape by comparison with one another. The PZT sensors were connected to an impedance analyser and the impedance was monitored as a function of time at room temperature (RT) at 4 kHz. The principle of the measurement was to record the voltage at the poles of the electrical resistor which is mounted in series with the piezo-disc. The ratio of this voltage to the voltage supplied to the two elements (piezo + resistor) gives the value of the piezo's electrical impedance. Due to the electromechanical properties of the piezo-component, this electrical impedance is linked to the mechanical ones and therefore to the level of curing for the matrix. The choice of the signal frequency is led by the signal-to-noise ratio of the mounted electromechanical system. The choice of the resistor's value is made in order to have the same order of magnitude as the expected piezo impedance. The recorded signal is the time-dependent electrical impedance of the piezo-disc. They confirmed the efficiency and the reliability of the method when compared to conventional methods as shown further in the chapter in section 4.2.

4.3.2. Dynamical mechanical analysis

Dynamical mechanical analysis (DMA) was performed for a better understanding on piezoelectric results. This technique provides convenient and sensitive determination of thermo-mechanical properties of polymers and reinforced polymers at solid or liquid state as a function of frequency and temperature [11]. The dynamic mechanical characteristics (complex modulus, E* and loss factor, Tan δ) were determined using a DMA50 of 01dB METRAVIB in tension-compression mode on rectangular specimens (30x10x2 mm^3) with fibers aligned perpendicular to the load axis. Tests were carried out at controlled dynamic displacement (±5 μm) in the linear viscoelasticity domain within a temperature range of -50 at 150 ℃ (heating rate = 1 K/min) at a constant frequency of 1 Hz.

4.3.3. Tensile test and damage monitoring

Experimental investigations on SHM capability of the piezoelectric sensor were performed using tensile test. In this case, the sensor's time DC voltage was directly measured. The purpose of integrating two sensors was initially to address the capability of analysing the composite material's level of wear by signal transmission from one piezo to the other: one piezo would have been used as an emitter and the other as a receiver. This strategy was harder to implement than expected since the choice of the frequency range can change significantly the vibration's interaction with the singularities and the breaks. The idea has not been abandoned, just postponed at this stage. However, integrating a couple of sensors was here used to confirm the recorded signal shape by comparison with one-another.

After curing and aging at room conditions during 12 months, samples for tensile tests with the fibers oriented at 0 ℃ to the main specimen axis were cut at LMC2 laboratory in the area where the sensors were embedded. Specimen dimensions were 200 mm long, 25 mm wide and 2 mm thick. Composite end-tabs (50 mm-long) were bonded on the ends of the tested specimens in order to minimize the stress concentration due to the tightening of grips. The gage length is 140 mm. The volume fraction of flax fiber for the composite samples is about 0.20 (Image analysis using Image J).

Monotonic tensile tests (Figure 4.2) were performed using an INSTRON tester equipped with a load cell of 30 kN at a cross-head speed of 2 mm/min and digital image stereo correlation (DISC or 3D-DIC) was used to determine in and out of displacements and strain maps on deformed surfaces [12]. For this purpose, the samples were painted with aerosol white and black

spray paint on one face to create a speckle pattern with adequate contrast. A region of interest (ROI) was defined on the specimen surface. The correlation algorithm compared gray level of each pixel in subset defined in the ROI. Once the matching was done, the displacement components of the center of the reference and deformed subset can be determined. In this study, strain computation was carried out by Vic3D® software developed by Correlated Solutions®.

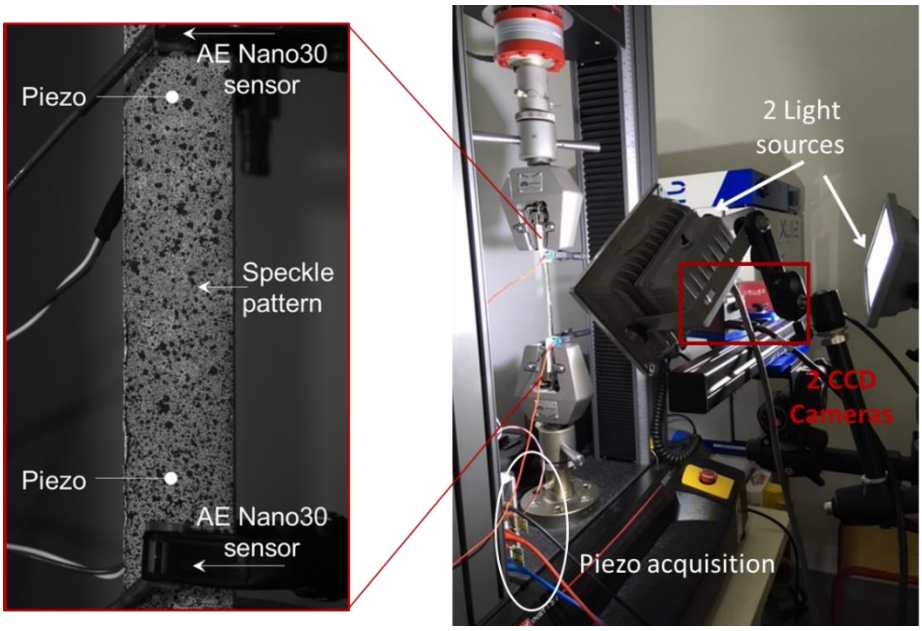

Figure 4.2 (a) Position of the PZT piezoelectric and AE sensors and the speckle pattern; (b) Tensile test Configuration.

In order to better analyse piezoelectric insert response, conventional acoustic emission (AE) signals were monitored during tests using Mistras 2001 system from Physical Acoustics Corporation (PAC). The AE sensor (Nano30) were attached to the sample by silicon grease and a mechanical specific device. The detection threshold of AE was fixed at 40dB.

4.4 Results and discussion

4.4.1. In situ curing monitoring

Once the impregnation process was completed, the impedance was monitored at 4 kHz every 10 min at room temperature (23 ℃). A comparison of normalized change in impedance vs. time obtained on two different plates manufactured two weeks apart, shows the high reproducibility that was achieved (Figure 4.3).

The variation of impedance versus time had a sigmoidal shape. At the very early beginning, a slight increase in impedance appeared. Beyond this lag-time, the impedance increased sharply, then levelled off until it reached a quasi-asymptotic value. At the very beginning, the thermoset

mixture was composed of low-molecular pre-polymers. As the reaction proceeded, chain extension occurred to produce relatively high molecular weight reaction products resulting in an increase in impedance. Gelation which corresponded to the first appearance of an infinite cross-linked network may be associated to the time at which the first significant increase in stiffness. As mentioned previously, vitrification was associated with the transition from a rubbery modulus to a glassy modulus. Above vitrification, the mobility of the reacting groups was restricted with the reduction of free volume. Thereby, this phenomenon led to an extremely slow reaction, as the reaction became diffusion-controlled. Therefore, vitrification was associated to the instant at which the impedance reached an almost constant value. Beyond, the impedance continued to increase slowly long after the vitrification: the reaction dramatically slowed, since the cure mechanism was controlled by the molecular diffusivity, but did not come to end.

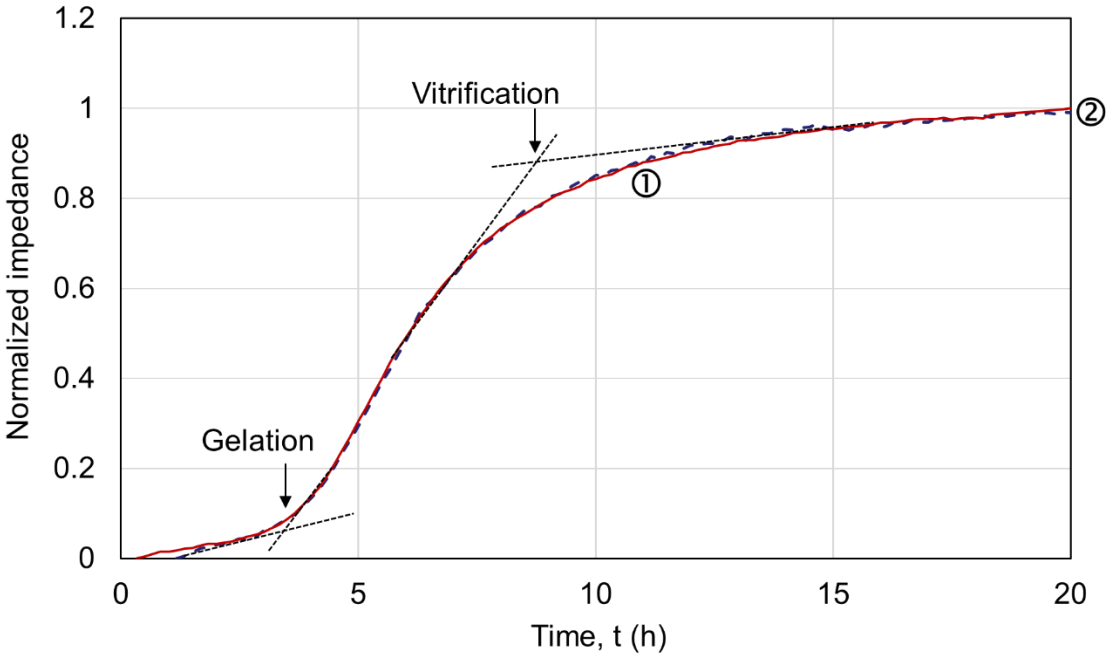

Figure 4.3 Normalized impedance vs time during cure at RT of two different plates (arrows indicate gelation and vitrification).

The influence of the curing time on the progress of polymerization at ambient conditions (23 ℃, 50% HR) was also investigated by DMA analysis, on samples cut in transverse directions with respect to the fiber direction in a plate after curing at various cure times (12 hours (sample 1), 2 days (sample 2), 8 days (sample 3)).

Typical plots of the loss factor tan δ and the storage modulus E' versus temperature were given in Figure 4.4a and 4.4b respectively. In the range of temperature studied, the tan δ spectra

showed two peaks whatever the sample. The highest temperature peak is concurrent in a large drop in the storage modulus (near 2 decades); this relaxation, named α-relaxation is associated with the glass transition and corresponded to the coordinated motion of relatively long chain segments by debonding of low energy bonds (hydrogen bonds). It is well known that the measurement of α-relaxation temperature which is associated with Tg can be used as an accurate indication of cross-link density of a thermosetting. The small process occurring just below the α-relaxation, so called α-relaxation was attributed to different mechanisms: the presence of water in the material, physical aging [13], and to unreacted chain segments in the network [14].

As shown in Figure 4.4, the onset of the storage modulus drops and the maximum of tan δ associated with α-relaxation were shifted towards high temperatures and the area under the curve of loss factor was reduced when the curing time increases from 12h (sample 1) to 24h (sample 2), and the magnitude of the α-relaxation decreased. These results were consistent with a progressive decrease in chain motion due to *a* degree of crosslink increase during curing. Conversely, the α-relaxation temperature is similar for the samples cured during 2 (sample 2) or 8 (sample 3) days. But, it is interesting to note that from sample 2 to 3, the height of the tan δ peak associated with the glass transition decreased slightly, and the intensity of the α-relaxation dropped sharply. These observations show that the crosslinking density can continue to increase slightly long after the vitrification.

The joint analysis of the impedance (Figure 4.3) and DMA (Figure 4.4) results shows that the in-situ measurement of impedance of PZT insert embedded in a composite provides a powerful tool for monitoring the changes in physical properties of thermoset during cure.

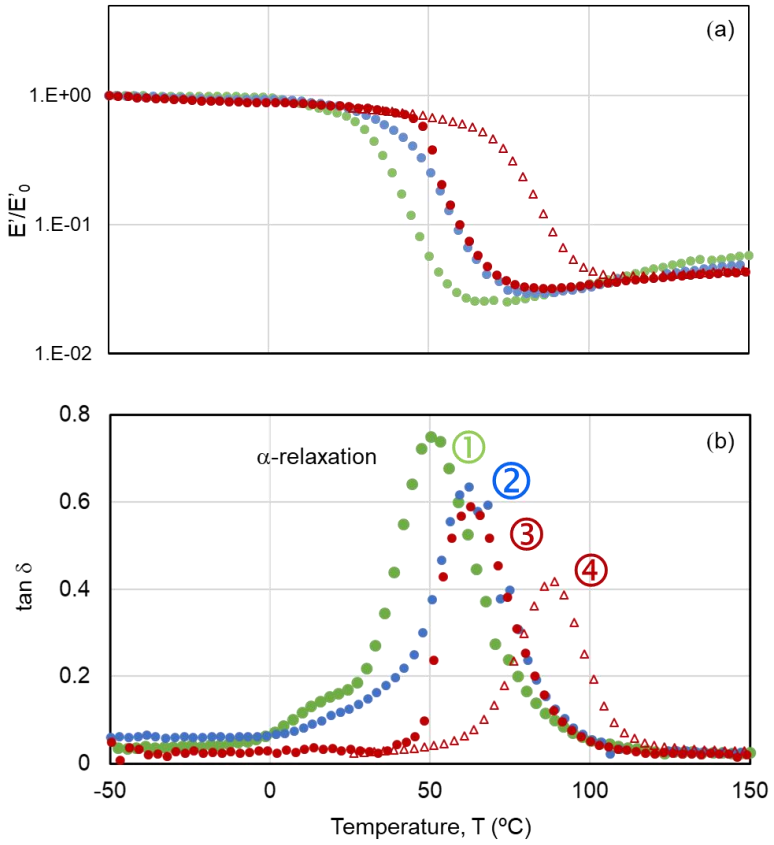

Figure 4.4 Temperature dependence of (a) tan δ and (b) E'/E_0' response at F=1 Hz for flax reinforced composites at various curing states: (●) 12 hours; (●) 2 days; (●) 8 days; (△) 8 days + sweep until 150 ℃.

4.4.2. Damage monitoring

At the end of the curing process, the sensors remain in the part and could be used as damage or aging sensors during all the life of the composite patches. The monitoring of the structural integrity of the repairing patches is of particular interest. Indeed, due to their manufacturing process (in situ hand lay-up, cold-curing resin), as previously mentioned, it is difficult to obtain very high quality composites:

- The curing conditions lead to a slight incomplete matrix cure. Indeed, as can be observed from Figure 4.4, the α-relaxation of the epoxy composite, after 8 days at room conditions, was about (61 ℃), and increases by about 25 ℃ after a second DMA scan (sample 4). Moreover, a slight and continuous increase in the rubbery modulus is observed above the α-relaxation temperature for samples cured at RT (samples 1 to 3). This also confirms that the curing at RT led to a partially cured network, and underwent a post-curing during DMA test. Indeed, it is well known that the rubbery modulus of networked structures is inversely proportional to the average mass of the segments between

crosslinking nodes (concept of rubber elasticity [15]) which decreases with the degree of cure, up to the completion of curing. When exposed to a temperature higher than Tg, residual reactions occurred as the mobility of the residual reactive epoxy and amine groups is increased.

- SEM micrographs of a polished cross-section observed perpendicular to the axis of fibers (Figure 4.5a) and of a post-mortem failure feature after tensile test (Figure 4.5b) of the flax reinforced bio-epoxy composite, show different defects: voids due to air trapped, large resin-rich zone between the two reinforcement layers and around the bundles. Figure 4.5c shows a magnified view of the fracture feature. In this figure, it can be observed, even if the fibers were not treated, that bonding between flax fibers and matrix was strong enough. Indeed, the process of failure mainly involved cohesive phenomena with fracture of the surrounding matrix shown by the presence of matrix debris on the fibers. Probably, the adhesion is associated with two main processes: (i) fiber surface roughness resulting in mechanical anchoring, (ii) hygrogen bondings between hydroxyl (OH) groups in the backbone chain of the epoxy resin and the flax fibers, which also contain OH groups (cellulose), as previously mentioned [16].

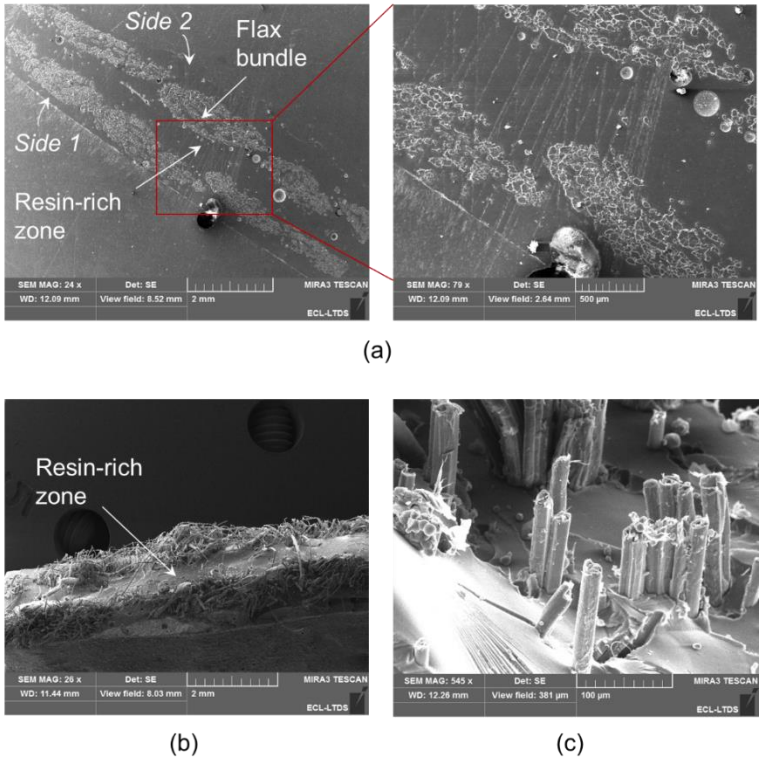

Figure 4.5 (a) Polished cross-section of flax reinforced epoxy composite; (b) and (c) Post-mortem scanning electron micrograph after tensile test up to failure.

These defects may be responsible for different damages and aging processes which could affect the behavior of the final patches during service. In the aim to evaluate the capability of the embedded sensors for detecting and assessing damage in flax reinforced epoxy composite under load, tensile tests were performed. The results from the PZT sensors were compared to conventional AE, force sensor (unfiltered) results and digital image correlation analysis (VIC3D).

Figures 4.6a to 4.6c show the results obtained on one specimen. Unfiltered Force, sensor voltage, and cumulative AE hits vs. time (or displacement) are given in Figure 4.6a. Figure 4.6b gives the amplitude of the AE signals according to time. The strain distribution observed in the region of interest (ROI) for different times t_1, t_2 and t_3 is shown in Figure 4.6c.

The most relevant contribution of the piezo-sensor was at the early stage of the damage evolution. Indeed, as visible in Figure 4.6a, the voltage exhibits a sharper and stronger evolution than the acoustic counting. At a low level of stress, it is more sensitive than acoustic sensors bonded on the surface of the sample. A correlation between sensor voltage measurement and the other results can be exhibited in a specific phase of the damage evolution (framed area in Figures 4.6a and 4.6b). On both the force and the cumulative acoustic counting records, there is a change in the intensity of the damage processes. This change is perceived by a change on the slope of the cumulative acoustic counting and the occurrence of disturbances on the uniform increase of the force. The measurement of the force is unfiltered on purpose.

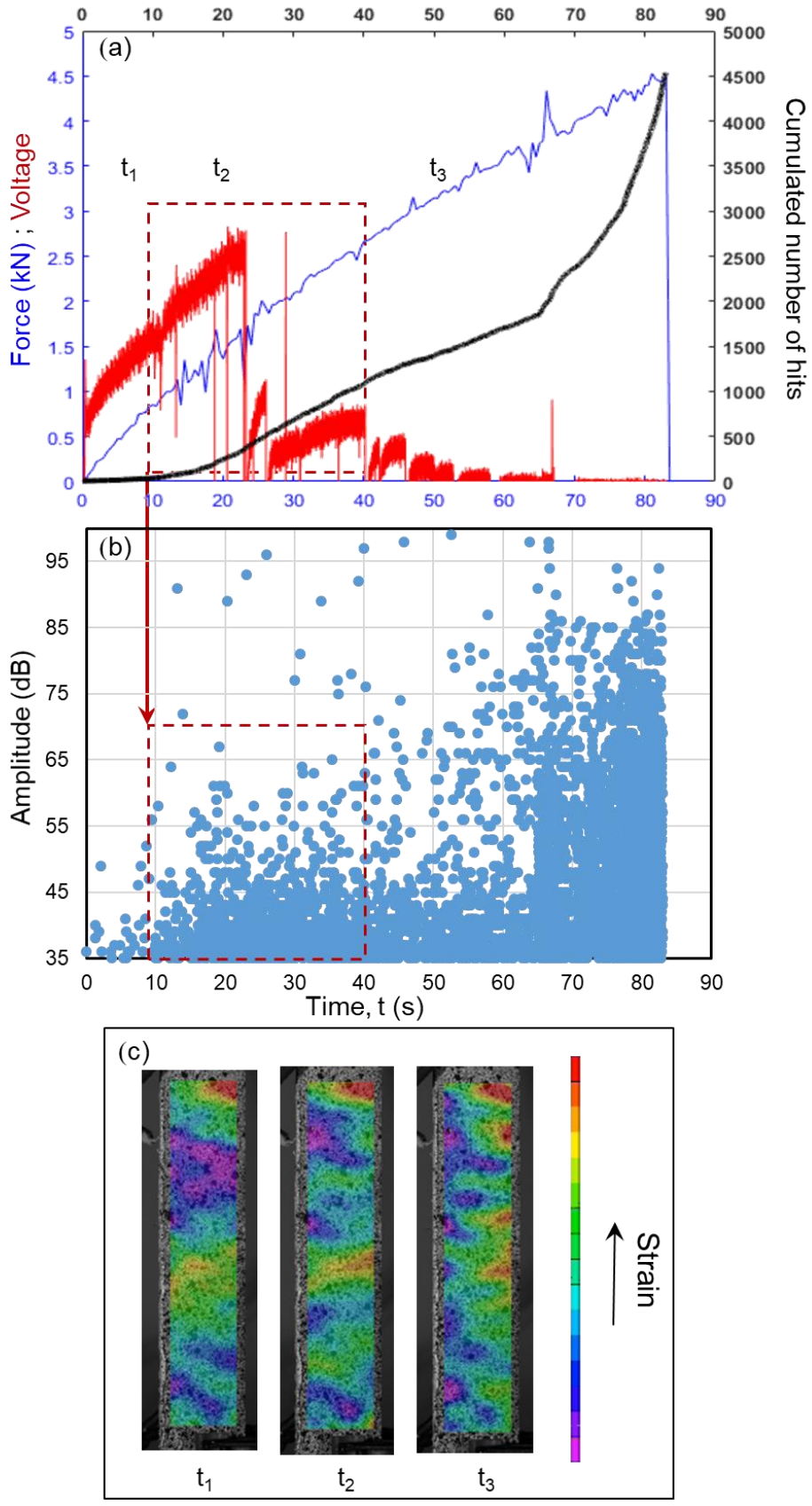

Figure 4.6 (a) Unfiltered Force, sensor voltage, and cumulative AE hits vs. time; (b) Amplitude of the AE signals vs. time; (c) Strain distribution at different times.

However, it seems that the piezo-sensor is inoperative during the last phase of the testing. Yet, the setting of the sensor, inside the composite material, is the key element to explain such behavior. Indeed, the piezo sensor is placed inside the matrix-rich zone between the two fiber layers (Figure 4.5). Hence, it is only sensitive to events occurring in this zone. Whether the matrix is broken or is debonding from the plies, a vibrational signal is recorded. However, once the separation between the ply and the matrix is locally initiated, the sensor is less loaded. This loss of efficiency of the sensor is a sharp and preliminary signal that the material is entering a critical state, not yet breaking, but prone to do so in the short term.

Still, it is coherent with the acoustic emission and DIC results which show damages associated with matrix breakages and delamination in the same time-range:

- AE signals are detected very early and until the specimen fails (Figure 4.6b). In the first phase, up to 16% of the maximum force (Figure 4.6a), events of small amplitude (between 35–50 dB) occur. These events are often related to matrix cracking [17]. In the second phase, events of low to average amplitude are measured. These aspects combined could indicate, in addition of resin failures, friction due to matrix–matrix debonding (delamination), microcracking coalescence (50 dB to 60dB) and matrix/fiber debonding (60 dB-70 dB). The third phase is when a failure occurs: multiple high amplitude events indicate fiber/matrix friction associated with pull-out (70 dB-85 dB) and multiple fiber breakages (>85 dB).
- As shown Figure 4.6c, at the very beginning (t_1), the axial strain distribution is layer distributed in the height of the specimen, associated with local morphological differences (fiber distribution, matrix layer thickness, thickness) along the specimen axis due to the manual manufacturing method. This distribution tends to change in the second phase (t_2), and the strain distribution is no longer axisymmetrical in the last phase (t_3) which may be related to a large extent of the damage especially on one side of the specimen.

The fact that AE is able to give information up the failure of the sample is related to the fact that its sensors are directly in contact with the fabric layer, on the surface of the sample. This ensures a permanent transmission of the breaks vibration signal, throughout the different components of the layer.

4.5. Conclusion

A novel PZT ceramic/flax-reinforced epoxy resin composite was fabricated by a hand lay-up manufacturing method for the purpose to be used as smart repairing patches for civil engineering structures.

The curing behavior of this system was investigated by means of piezoelectric impedance. The variation tendency in the impedance spectrum is in accordance with the transitions of matrix viscoelastic properties as cure progressed. The results showed that the piezoelectric transducers are well suited to in-situ monitor the reaction progress during isothermal curing of flax reinforced epoxy materials.

Besides, after curing, the sensor may be further applied as SHM sensor for the composite material. In order to assess the efficiency of such a system for health monitoring, tensile tests were performed with conventional AE and optical deformation system associated with scanning electron microscope analysis. The results show that the sensor is a sharp and preliminary signal that the material is entering a critical state, not yet breaking, but prone to do so in the short term.

4.6. References

1. A. A. Skordos, P. I. Karkanas, I. K. Partridge, A dielectric sensor for measuring flow in resin transfer moulding, Meas. Sci. Technol., 11 (2000), 25-31. http://dx.doi.org/10.1088/0957-0233/11/1/304.
2. E. Chailleux, M. Salvia, N. Jaffrezic-Renault, Y. Jayet, A Mazzouz, G. Seytre, In situ multidetection cure monitoring of an epoxy-amine system, J. Adv. Sci., 12 (2000), 291-297. http://*doi*.org/10.2978/jsas.12.291.
3. E. Chailleux, M. Salvia, N, Jaffrezic-Renault, V. Matejec, I. Kasik, In situ study of the epoxy cure process using a fiber optic sensor, Smart Mater Struct., 10 (2001), 1-9. https://doi.org/10.1088/0964-1726/10/2/304.
4. U. Sampath, H. Kim, D. G. Kim, Y. C. Kim, M. Song, In-Situ Cure Monitoring of Wind Turbine Blades by Using Fiber Bragg Grating Sensors and Fresnel Reflection Measurement, Sensors, 15 (2015), 18229-18238. https://*doi*.org/10.3390/s150818229.
5. M. Scheerer, Z. Simon, M. Marischler, B. Rittenschober, A Multifunctional Piezo and Temperature Sensor for Process and Structural Health Monitoring of CFRP Structures Made by Resin Transfer Molding, In: International Workshop on Structural Health Monitoring Volume 1, Stanford, 2017. *doi:* 10.12783/shm2017/14155.
6. K. T. Lau, P. Y. Hung, M. H. Zhu, D. Hui, Properties of natural fiber composites for structural engineering applications, Compos. Part B-Eng., 136 (2018), 222-233. https://doi.org/10.1016/j.compositesb.2017.10.038.

7. A. Lefeuvre, A. Bourmaud, C. Morvan, C. Baley, Elementary flax fiber tensile properties: Correlation between stress–strain behaviour and fiber composition, Ind. Crops Prod. 52 (2014) 762– 769. https://doi.org/10.1016/j.indcrop.2013.11.043.
8. C. Billotte, F. M. Bernard, E. Ruiz, Chemical shrinkage and thermomechanical characterization of an epoxy resin during cure by a novel in situ measurement method, Eur. Polym. J., 49 (2013), 3548-3560. https://doi.org/ 10.1016/j.eurpolymj.2013.07.013.
9. J.Enns, J. Gillham, Time-temperature-transformation (TTT) cure diagram: modeling the cure behaviour of thermoset, J. Appl. Polym. Sci., 28 (1983), 2567-2591 https://doi.org/10.1002/app.1983.070280810.
10. M. Mehdikhani, L. Gorbatikh, I. Verpoest, S. V Lomov, Voids in fiber-reinforced polymer composites: A review on their formation, characteristics, and effects on mechanical performance, J. Compos. Mater. 53 (2019), 1579–1669. https://doi.org/10.1177/0021998318772152.
11. J. D. Ferry, Viscoelastic Properties of Polymers, 3rd Ed, Wiley, New York, 1980.
12. Camille Flament, Michelle Salvia, Bruno Berthel, Gérard Crosland, Local strain and damage measurements on a composite with digital image correlation and acoustic emission, J. Compos. Mater. 50 (2016), 1989-1996. https:///doi.org/10.1177/0021998315597993.
13. D. Colombini, J.J. Martinez-Vega, G. Merle, Dynamic mechanical investigations of the effects of water sorption and physical ageing on an epoxy resin system, Polymer 43 (2002) 4479-4485, https://doi.org/10.1016/S0032-3861(02)00272-0.
14. J. P. Foreman, D. Porter, S. Behzadi, K.P. Travis. F. R. Jones, Thermodynamic and mechanical properties of amine-cured epoxy resins using group interaction modelling, J Mater Sci. 41 (2006), 6631-6638. https://doi.org/10.1007/s10853-006-0202-9.
15. J.P. Pascault, H. Sautereau, J. Verdu, R.J.J. Williams, Thermosetting Polymers, 1st *edition*, Marcel Dekker, New York, 2002.
16. A. K. Mohanty, M. Misra, L. T. Drzal, Natural Fibers, Biopolymers, and Biocomposites, Boca Raton, FL: Taylor & Francis/CRC Press, 2005.
17. S. Barre, M. L. Benzeggagh, On the use of acoustic emission to investigate damage mechanisms in glass fiber-reinforced polypropylene, Compos Sci Technol, 52 (1994), 369-376. https://*doi*.org/10.1016/0266-3538(94)90171-6

Chapter 5. The application of FFRCs as reinforcement laminate on concretes

5.1. Reinforcing laminates interests

In the past decades, the world's infrastructure deficit has continued to increase, and some existing infrastructures need to be renovated or repaired to avoid collapses in a short term [1,2]. Apparently, the complete demolition and reconstruction will obviously cause a great waste of resources. At the same time, the public's awareness of environmental protection has increased sharply, which has put forward requirements for environmental sustainability and renewable material sources. Maintaining existing buildings in qualified stage in order to extend their life span requiring solutions to fix cracks and slow down the damage propagation. For that purpose, a popular method to solve this is to use externally bonded fiber-reinforced polymers. Compared to traditional repairing strategies, this method has shown significant advantages, which mainly lays in its easy processing and application of composite laminates, the high strength-to-weight ratio, its corrosion resistance, and its excellent mechanical properties [3]. Although these composite patches are more cost-effective, the materials used are usually synthesized from petroleum and are not environmentally friendly and sustainable [4-6]. This is the main reason why people are paying more and more attention to the development and use of biological compounds to replace synthetic variants, such as flax fibers and bio-epoxy materials. This is also the purpose of the present study.

Due to the gradual improvement in the performance of FFRCs, such as mechanical properties, corrosion resistance, environmental durability and inherent customization, its application has gradually expanded to the repair of damaged buildings. They have actually been extended in a long term in the construction of infrastructure and new facilities [7]. We can hence quote the reinforcement of masonry walls, the seismic reinforcement of bridges and buildings, the repair and reinforcement of concrete structures, metal and wooden beams, girders and floor slabs, and the restoration of unique structures such as chimneys, historical monuments and offshore platform. Fiber-reinforced polymer composites (FFRC) have been common applied in structural reinforcement and repair applications. Many studies have confirmed that externally bonded FFRC patches can be used to strengthen the concrete beams because they can significantly increase the bending and shearing capabilities of the element [5,7,8].

Recently, the construction industry has become one of the world's largest consumers of polymer composites [8]. Adhesive composite reinforced materials are increasingly used in civil engineering structures, and the factors that affect its final industrial application are their mechanical properties. As mentioned before, the mechanical properties of FFRCs depend on many factors, such as the type of reinforcement, the characteristics of the matrix, the relative volume fraction. Behinds these characteristics, the shape, the size and the organization of reinforcing phases also play an important role. Moreover, the application in the field of civil engineering reinforcement depends largely on the reinforcement/matrix interfacial shear strength [9-11]. The use of FFRCs to reinforce civil components has become a potential solution to the problem of limited strength. However, due to the separation or debonding of the composite material from the component, the refurbished component usually exhibits a brittle failure mode [12]. In order to effectively transfer the applied load, a relatively strong interfacial bonding force is required, since a weaker interface may cause premature failure of the reinforcement effect of the composite material.

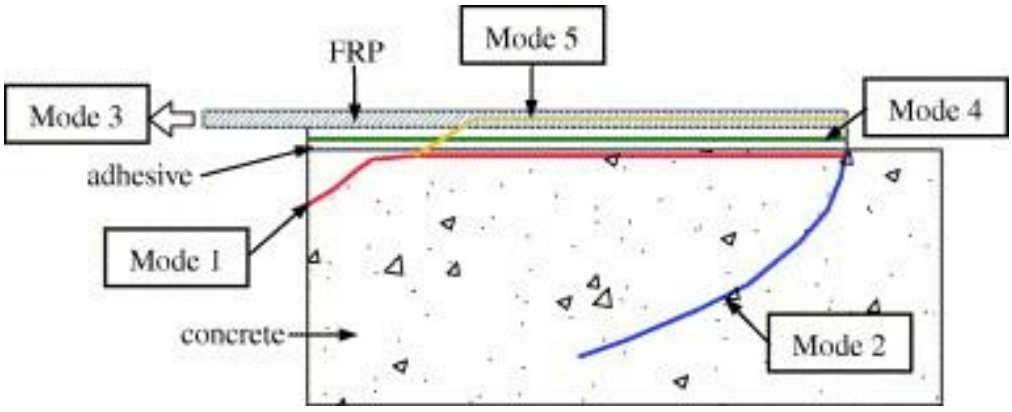

Figure 5.1 Failure modes observed in shear-lap tests.

About the failure modes between the bonded FFRC and the concrete, there are several, as shown in Figure 5.1 [13,14]. Mode 1 is the most common fracture which is called interface debonding failure. The failure surface is a few millimeters below the interface between the concrete and the adhesive, and the concrete can also be pulled out near the stressed end. Mode 2 is shear tension failure, in which the main crack propagates from the end of the FFRC into the concrete block. This pattern tends to appear only when the laminate is relatively thick. For modes 3, 4, and 5, damages correspond to occurrences in laminate and adhesive materials, respectively. If the cross-sectional area of FFRC is very small, mode 3 tensile fracture may occur. It may also be Mode 4, which is the cohesive failure of the adhesive. Composite materials can also be layered according to Mode 5, and the layered path may cross the

adhesive layer and penetrate into the concrete. The latter three modes are relatively rare, especially for ordinary-strength concrete, whose shear strength is much lower than that of binders and FFRC.

5.2. Experimental devices and operations

In order to take full advantage of this external bonding technology, a better understanding of the stress transfer mechanisms between the bonded joints and concrete is required. To evaluate the bonding methods between FFRC and concrete matrices, there are mainly the following three common settings: double pull–pull test, single pull-push test, and bending test, as shown in Figure 5.2 [13]. For the double pull–pull test, composite laminates are bonded on both sides of the two pieces of concrete to connect them together. There is a small gap between the concrete matrices. The bonding force is applied by pulling the steel bars poured in the concrete block, and the tension can be applied by two steel plates bonded to the sides of the concrete block or by hydraulic actuators placed between the concrete blocks. In a single push-pull test, the composite material is only bonded to one side of the concrete, and the load is directly applied to the FFRC composite from the free end. The concrete is fixed in place with a supporting structure that abuts the concrete surface near the load end. The main advantage of this test configuration is that it can reduce the use of FFRC and concrete materials. However, a relatively complicated loading device is required. In the third type of test, FFRC is bonded to the serrations in the middle of the beam, and the surface tension of the FFRC is caused by the bending of the beam. Compared with the previous two pasting methods, this method requires a more complicated loading platform.

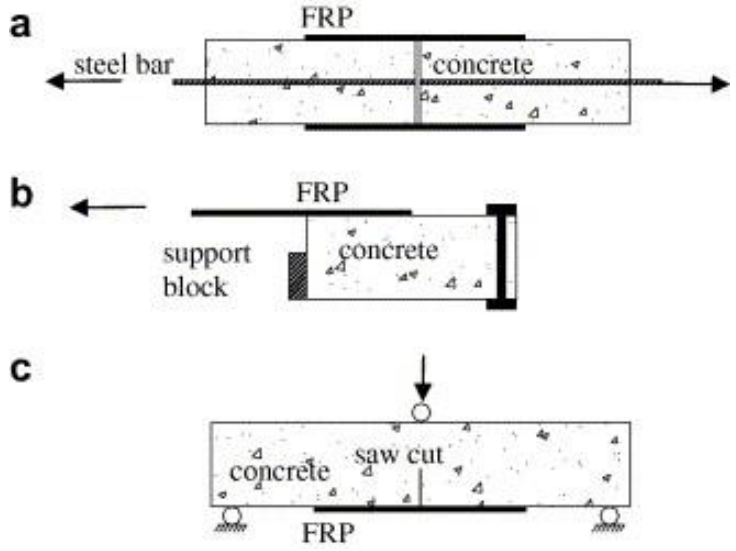

Figure 5.2 Experimental set-ups for shear-lap tests: (a) double pull–pull test; (b) single pull–push test and (c) bending test.

To aware of the enhancing efficiency of FFRCs, a new experimental set-up to perform single-lap shear debonding tests on FFRC reinforcements bonded to concrete will be considered. In this experimental setting, the single pull-push test is applied, the backsides of both FFRC laminates and concrete specimen are fixed to an external restraining system and the force is applied to the other side of FFRC reinforcement.

5.2.1. Samples preparation for the shear-lap test

As a preliminary testing of the reinforcement's reliability, the adhesivity limit of FFRC is here tested. The experimental procedure in this section uses a single pull procedure. As shown in Figure 5.3, the size of the concrete block is $100 \times 100 \times 50$ mm^3.

The concrete strength reported in the literature is 3-4 Mpa [15,16], while the tensile strength of the FFRC used in this experiment is about 120 MPa with a thickness about 3.0 mm.

The process of pasting FFRC on concrete involves two main steps: surface preparation and bonding. A high-pressure water jet (4000 psi or 28 MPa) was adopted to sand the concrete surface in order to remove the paste and exposing the coarse aggregate [17]. The bonding operation is to directly paste the prepared composite material to a specified place, and the curing time at room temperature is one month, the specific manufacturing stage for the composite is mentioned before in chapter 3.

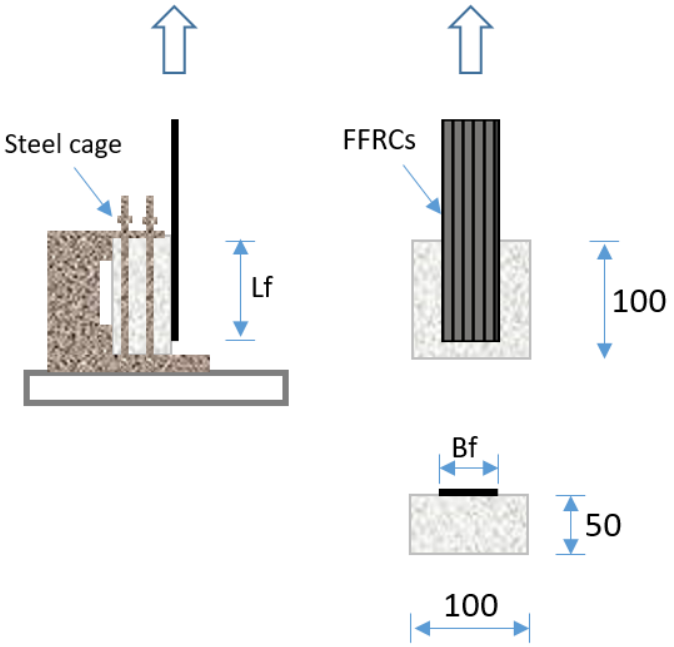

Figure 5.3 Diagram of the experimental components.

5.2.2. Experimental setup

The photos of the FFRC-concrete bonding interfacial shear-lap experiment device are shown in Figures 5. 4. The backside of the concrete sample was fixed on the external fixing system with a steel cage, and at the same time, an external force was applied by grasping the free end of the composite laminate with a stretching rate of 0.5mm/min. The shearing experiment device includes upper top plate, lower bottom plate, lower bottom plate chuck, baffle plate, bolt, composite material patch, concrete block. The upper and lower plates are placed horizontally and parallel, while the concrete is placed in the middle. Moreover, the upper top plate and the lower bottom plate are provided with holes at corresponding positions, and bolts pass through. The lower base plate is fixed on the test bench by the lower base plate clamp. There is an L-shaped opening on one side of the upper roof. The side of the concrete material is aligned with the concave surface of the concave opening. The FFRC extends above the upper roof on the side of the material and along the vertical direction of the concrete bonding concave opening. The top of the FFRC is connected with a tension clip.

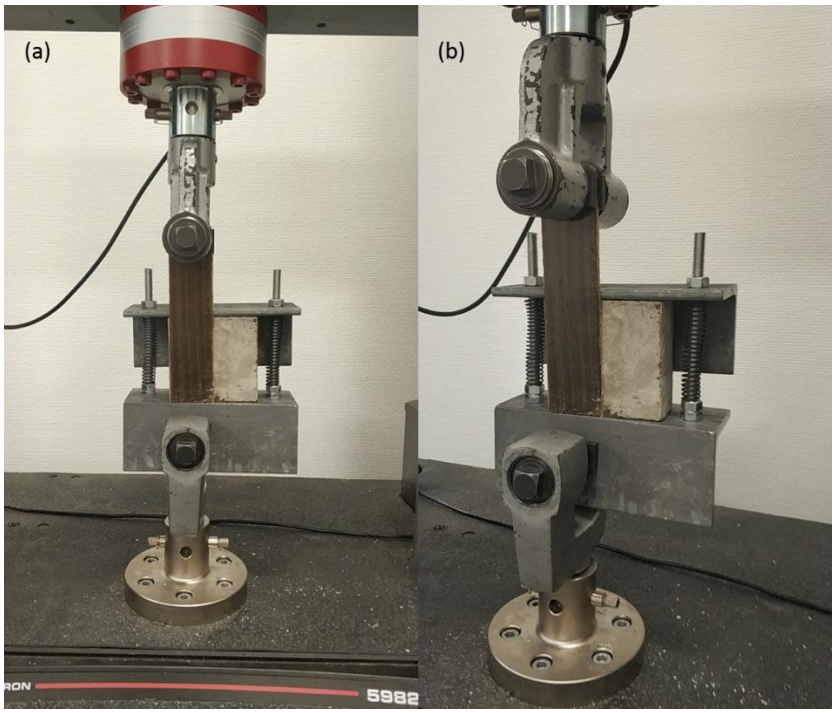

Figure 5.4 Photos of the experiment setup.

5.3. Results and discussions about the shear-lap testing

In order to determine the relationship between the applied force and the grip displacement, and to analyze the shear-lap results, the typical force versus displacement of this experiment

is given in Figure 5.5. These results highlight some of the mechanical events that occurred during the test, from which four different stages can be clearly identified.

The first phase is the clamping of the fixture, which depends more on the test setup than the performance of the joint (A). After gripping the clamp, the second stage illustrates the elastic behavior of the bonded joint (B). Once the applied force reaches the corresponding value, the stiffness of the joint seems to decrease, indicating that irreversible deformation has occurred (C). Eventually, a load plateau is reached, indicating that the failure propagates along the bonded joint (D). This figure has lots of differences with the typical stress-strain curves in section 3. First of all, there is an obvious duration of clamping fixtures. It is an inevitable stage in the shear lap test, which is affected by the system error of the experiment setup. Besides, instead of brittle fracture of the composite tensile test, the final failure of the shear lap joint is progressive. During stage D, the displacement increased dramatically under a constant force. Compared with the tensile results of composite materials in chapter 3, it can be clearly observed that the tensile strength of the composite is about two orders of magnitude higher than that of the shear-lap strength. The stress value that causes the failure of the composite material and concrete interface is about 3Mpa, and this value is similar to the tensile modulus of concrete in the literature. That is to say, the tensile weak point of the composite material patch reinforced concrete structure is the concrete matrix, not the composite material or the interface between the two phases.

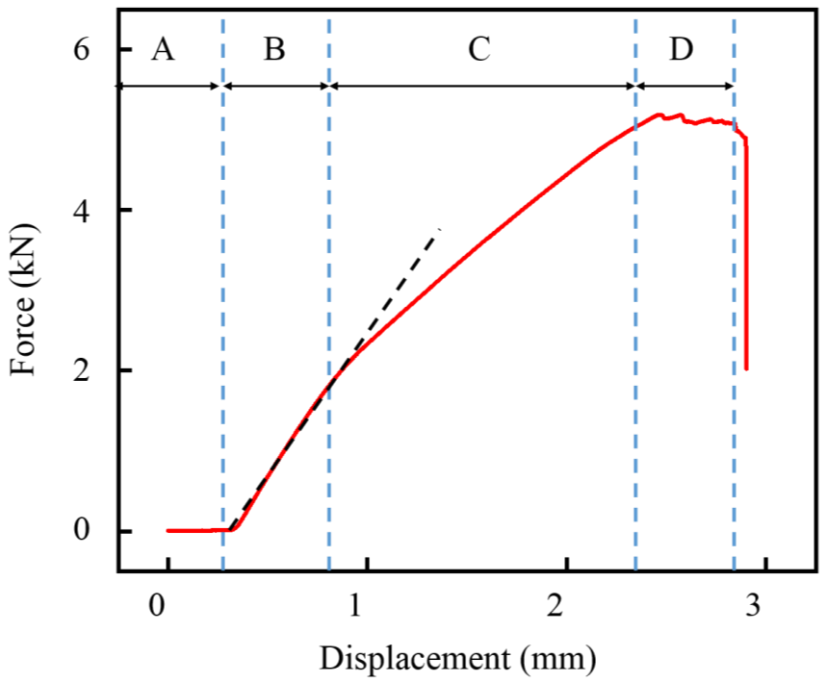

Figure 5.5 Applied force versus displacement of the grips.

Regarding the location of bonding failure, it always occurs inside the concrete near the interface, at 1-4mm, and fiber damage is rarely observed, as shown in Figure 5.6. The concrete below the bonding interface breaks under the shear force, while a thin concrete base layer remains to the laminate. During the bonding process, epoxy resin penetrates into the rough surface of the concrete. The interfacial shear strength is mainly provided by the interlocking between the epoxy resin and concrete surface irregularities. When the shear stress increases to a very high value, these irregularities begin to crack, and the cracks propagate through the cement slurry and aggregate at the same time [18].

Figure 5.6 Picture of a specimen after failure.

5.4. Chapter summary

This chapter discusses the feasibility of FFRC serves as concrete-reinforced sheets, and builds an FFRC-concrete bonding interface shear test device, which can perform direct shear experiments on FFRC-concrete single-sided lap joints to test. Those results of bonding strength and enhancing efficiency of FFRC on concrete would in turn to provide a reference for the engineering application of FFRC patches. The experiment results reveal that, in all the testing processes, the cohesive failure inside the concrete is the main cause of the interface failure, which also shows that the concrete is the weak link of the assembly. Besides, the results show that degumming is a quasi-brittle phenomenon, and under load levels that are

significantly lower than the bending or shear resistance of reinforced components, there is often no visible warning.

5.5. References

1. Henderson S R. Outer metropolitan areas and infrastructure deficits: Policy dynamics on the edge of Melbourne, Australia[J]. Cities, 2019, 90: 24-31.
2. Ray D, Ing L Y. Addressing Indonesia's infrastructure deficit[J]. Bulletin of Indonesian Economic Studies, 2016, 52(1): 1-25.
3. Mathijsen D. Using innovative composites technology to reduce the cost of bridge building and help fix the US infrastructure deficit[J]. Reinforced Plastics, 2019, 63(3): 151-155.
4. Kulkarni P, Mali K D, Singh S. An Overview of The Formation of Fibre Waviness and Its Effect on The Mechanical Performance of Fibre Reinforced Polymer Composites[J]. Composites Part A: Applied Science and Manufacturing, 2020: 106013.
5. Jirawattanasomkul T, Likitlersuang S, Wuttiwannasak N, et al. Behaviour of Pre-damaged Reinforced Concrete Beams Strengthened with Natural Fibre Reinforced Polymer Composites[J]. Composite Structures, 2020: 112309.
6. Singh T, Gangil B, Singh B, et al. Natural-synthetic fiber reinforced homogeneous and functionally graded vinylester composites: Effect of bagasse-Kevlar hybridization on wear behavior[J]. Journal of Materials Research and Technology, 2019, 8(6): 5961-5971.
7. Naser M Z, Hawileh R A, Abdalla J A. Fiber-reinforced polymer composites in strengthening reinforced concrete structures: A critical review[J]. Engineering Structures, 2019, 198: 109542.
8. Napoli A, Realfonzo R. Reinforced concrete beams strengthened with SRP/SRG systems: experimental investigation[J]. Construction and Building Materials, 2015, 93: 654-677.
9. Mohamad M E, Ibrahim I S, Abdullah R, et al. Friction and cohesion coefficients of composite concrete-to-concrete bond[J]. Cement and Concrete Composites, 2015, 56: 1-14.
10. Santos P, Júlio E N B S. Interface Shear Transfer on Composite Concrete Members[J]. ACI Structural Journal, 2014, 111(1).
11. Soltani M, Ross B E. Database Evaluation of Interface Shear Transfer in Reinforced Concrete Members[J]. ACI Structural Journal, 2017, 114(2).
12. Yuan F, Pan J, Xu Z, et al. A comparison of engineered cementitious composites versus normal concrete in beam-column joints under reversed cyclic loading[J]. Materials and structures, 2013, 46(1-2): 145-159.
13. Pham H B, Al-Mahaidi R. Modelling of CFRP-concrete shear-lap tests[J]. Construction and Building Materials, 2007, 21(4): 727-735.
14. Yao J, Teng J G, Chen J F. Experimental study on FRP-to-concrete bonded joints[J]. Composites Part B: Engineering, 2005, 36(2): 99-113.
15. Chassib S M, Zemam S K, Madhi M J. New approach of concrete tensile strength test[J]. Case Studies in Construction Materials, 2020, 12: e00347.

16. Khan M I. Direct tensile strength measurement of concrete[C]//Applied mechanics and materials. Trans Tech Publications Ltd, 2012, 117: 9-14.
17. Mazzotti C, Savoia M, Ferracuti B. A new single-shear set-up for stable debonding of FRP–concrete joints[J]. Construction and Building Materials, 2009, 23(4): 1529-1537.
18. Chataigner S, Caron J F, Benzarti K, et al. Use of a single lap shear test to characterize composite-to-concrete or composite-to-steel bonded interfaces[J]. Construction and building materials, 2011, 25(2): 468-478.

General conclusion

For cost-effective considerations, the externally bonded composite reinforcement system has gradually become an interesting attempt for strengthening and refurbishing those aged or damaged infrastructures. Compared to the complete dismantling and rebuilding, which is obviously against environmentally friendly and sustainability, it is a better choice to re-meet the requirements for bearing capacity and safe use, then to extend their service life. In this research, a novel composite was fabricated with flax fibers and bio-epoxy resin made from environmentally renewable resources. Those composite patches are implemented via the hand layup method, which endows it good adaptability for any damaged structures, and then attached on the surface to protect the infrastructure from the inner stress and external erosion and to limit crack growth.

The strengthening efficiency of FFRCs is determined by several conditions. First of all, the mechanical properties of the composite materials, which determine the upper limit of the reinforcing effect. Higher mechanical performance tends to endows the damaged infrastructures more enhancing efficiency. Then, the interfacial bonding determines whether the component interface can effectively transfer stress from one side to another of the damaged area, which would decide the lower limit of the enhancement effect. Some researches indicate that the bonding interface between the composite reinforcement sheet and the infrastructure is the weak link of the entire reinforced component. Interfacial delamination is a fragile fracture that occurs suddenly without obvious warning signs. In addition, the smoothness of the surface and environmental ageing will also affect the actual application of composite patches.

The core content of this research is to verify the feasibility of the composite reinforcement system to enhance the damaged infrastructures, and how to improve the strengthening efficiency. To obtain a comprehensive and profound acknowledgment about this study, the curing mechanism of epoxy resin, the mechanical performance of FFRC, the environmental durability behaviors of FFRC, and the shear-lap test between FFRC and concrete were the exploration emphases.

1. Curing study of the bio-epoxy resin,

The bio-epoxy resin in this research contains two different hardeners, DSC jobs were adopted to optimize the curing conditions, which consists of curing temperature and curing time. The exothermic curves show that this is a typical dual-stage curing system. Based on the epoxy curing mechanism and the existing laboratory operating conditions (temperature range of the oven), the fully curing condition is room temperature for 48 hours, 90 ℃ for a week (the first curing stage), and 140 ℃ for another 12 hours (post-cure). Besides, the reaction mechanisms of the two curing stages are different, the first stage is Kamal autocatalytic model and the activation energies in this part are 45.48 KJ/mol and 33.23 KJ/mol, which correspond to the uncatalyzed and catalyzed reactions in the system, respectively. The overall reaction order is 1.6. The second obeys the autocatalytic mechanism, the apparent activation energy, and overall reaction order in this period are 76.78 KJ/mol and 1.66.

2, The mechanical properties and environmental durability of FFRC

Serving as a reinforced patch, the mechanical property of FFRC is always a key factor, as its strength will determine the enhancing effect on the damaged infrastructures. Since the application surroundings of FFRCs is outdoor, the impact of environmental ageing on its mechanical properties need to be paid extra attention. Considering the highly hydrophilic characteristic of flax fiber as well as the temperature and humidity difference in the actual application circumstance, the specific experiments are water immersion, freeze-thaw cycle, and wet-dry cycle. The aged FFRCs was conducted to the tensile test to analyze the impact of each ageing model. Acoustic emission was used to monitor the specific fracture sound inside the composite during the tensile procedure.

The FFRC was fabricated by a hand-layup method with 2 layers of flax fiber and bio-epoxy resin, whose fiber volume fraction is about 20%. The strength modulus of FFRCs is 120Mpa. The durability results show that for the samples immersed in water at room temperature, the water absorption obeys Fick's laws of diffusion. Ware immersion ageing causes fiber and resin plasticization and further leads to composite material structure damage and mechanical performance degradation. For the freeze-thaw cycles, due to the shrinkage/swelling process of the components the effective bond with the matrix is lost, and a gap is created between the fiber and the matrix, and this gap becomes a new source of micro damages. For the wet-dry cycles, almost no performance of composite specimens seems less affected than by the other modes of ageing.

3, Fracture monitoring experiments

In this part, PZT sensors were inserted inside the FFRCs material by hand lay-up method, serving as an intelligent repair material for civil engineering structures. The PZT sensor was used to study the curing performance of the system through piezoelectric impedance in the first place. Experiment results point out that the changing trend of impedance spectrum is related to the transition of matrix viscoelasticity during curing, which indicates the effectiveness of piezoelectric transducer for on-site monitoring of the reaction progress during the isothermal curing of flax-reinforced epoxy composites. In addition, after curing, the sensor was further used as a structural health monitoring sensor for composite materials. In order to evaluate the efficiency of this system for health monitoring, a tensile test was conducted using conventional AE and an optical deformation system related to SEM analysis. The results show that the sensor is a clear and preliminary signal, indicating that the material is entering a critical state and has not yet broken, but it is easy to break in a short time.

4, The application of FFRCs on concrete

The final application of FFRCs in this research, serving as external reinforcement sheets on concrete. In this part, the shear-lap test was used to testify the mechanical feasibility of this idea. The tensile test in chapter 3 reveals that the strength modulus of FFRCs is about 120Mpa, and those seriously aged samples still possess a strength modulus of 60Mpa, far greater than the shear strength between composite and concrete, which is about 4Mpa. The failure occurred inside the concrete and a thin layer of concrete attached to composite laminate, which proves that the FFRC patch is strong enough to enhance the concrete materials and the concrete is the weak point in the shear-lap test experiment.

Appendix

Publications and conference communications during PhD:

1. **Mingfa Zhang**, Olivier Bareille*, Michelle Salvia "Cure and damage monitoring of flax fiber-reinforced epoxy composite repairs for civil engineering structures using embedded piezo micro-patches" Construction and Building Materials 225 (2019) 196-203.
2. Zhenxin Jia†, **Mingfa Zhang**†, Bin Liu, Fucheng Wang, Gang Wei*, and Zhiqiang Su* graphene foams for electromagnetic interference shielding: a review, ACS Appl. Nano Mater. 2020, 3, 7, 6140–6155.
3. **Mingfa Zhang**, Olivier Bareille and Michelle Salvia* "Synthesis and Characterization of Natural Fibers Reinforced Epoxy Composite". 3rd Euro-Mediterranean Conference on Structural Dynamics and Vibroacoustics, 17-19 Feb 2020 Napoli (Italy)
4. **Mingfa Zhang**, Olivier Bareille and Michelle Salvia*, Natural fiber-reinforced epoxy for civil engineering repairs: cure monitoring and damage monitoring using embedded piezoelectric micro-sensors" ICCE-27 July 14-20, 2019 in Granada, Spain.
5. **Mingfa Zhang**, Xiaopeng Cui, Michelle Salvia*, Olivier Bareille. "Embedded sensing micro-components for fibre reinforced composite material syntheses and monitoring". Surveillance, Vishno and AVE conferences, INSA-Lyon, Université de Lyon, Jul 2019, Lyon, France. hal-02189227.
6. Olivier Bareille, Michelle Salvia*, **Mingfa Zhang** "Embedded Piezo Micro-Patches for cure monitoring of fiber reinforced epoxy in civil engineering repairs", 9 th International Conference on Fibre-Reinforced Polymer Composites in Civil Engineering CICE 2018 – Paris – July 17-19.
7. Olivier Bareille, Michelle Salvia*, **Mingfa Zhang**, "Embedded curing and life-time monitoring of fiber-reinforced epoxy in civil engineering repairs by distributed piezo sensors" 9th european workshop on structural health monitoring (ewshm 2018), july 10-13, 2018 in manchester, uk (ewshm 2018)

N°d'ordre NNT: 2020LYSEC49

THESE de DOCTORAT DE L'UNIVERSITE DE LYON
opérée au sein de
L'Ecole centrale de Lyon

Ecole Doctorale N°34
Ecole Doctorale Matériaux de Lyon

Spécialité/Discipline de doctorat : Matériaux

Soutenue publiquement le 18/12/2020, par :

Mingfa ZHANG

Composite reinforcement system for enhancing application on civil infrastructures

Devant le jury composé de :

Karim Benzarti,	Directeur de Recherche, Université Gustave Eiffel,	Rapporteur
Emmanuel Foltête,	Directeur de Recherche, ENSMM,	Rapporteur
Mohamed Ichchou,	Ecole Centrale de Lyon,	Examinateur
Laurence Curtil,	Université Claude Bernard Lyon 1,	Examinateur
Michelle Salvia,	Ecole Centrale de Lyon,	Directrice de thèse
Olivier Bareille,	Ecole Centrale de Lyon,	Co-directeur de thèse
Bruno Berthel,	Ecole Centrale de Lyon,	Co-directeur de thèse